Title
Dielectric Actuation of Polymers

Author
Niu, Xiaofan

Publication Date
2013

Peer reviewed|Thesis/dissertation

UNIVERSITY OF CALIFORNIA

Los Angeles

Dielectric Actuation of Polymers

A dissertation submitted in partial satisfaction of the requirements for the degree Doctor of Philosophy in Materials Science and Engineering

by

Xiaofan Niu

2013

ABSTRACT OF THE DISSERTATIOIN

Dielectric Actuation of Polymers

by

Xiaofan Niu

Doctor of Philosophy in Materials Science and Engineering

University of California, Los Angeles, 2013

Professor Qibing Pei, Chair

Dielectric polymers are widely used in a plurality of applications, such as electrical insulation, dielectric capacitors, and electromechanical actuators. Dielectric polymers with large strain deformations under an electric field are named dielectric elastomers (DE), because of their relative low modulus, high elongation at break, and outstanding resilience. Dielectric elastomer actuators (DEA) are superior to traditional transducers as a muscle-like technology: large strains, high energy densities, high coupling efficiency, quiet operation, and light weight.

One focus of this dissertation is on the design of DE materials with high performance and easy processing. UV radiation curing of reactive species is studied as a generic synthesis methodology to provide a platform for material scientists to customize their own DE materials. Oligomers/monomers, crosslinkers, and other additives are mixed and cured at appropriate ratios to control the stress-strain response, suppress electromechanical instability of the resulting polymers, and provide stable actuation strains larger than 100% and energy densities higher than

1 J/g. The processing is largely simplified in the new material system by removal of the prestretching step. Multilayer stack actuators with 11% linear strain are demonstrated in a procedure fully compatible with industrial production.

A multifunctional DE derivative material, bistable electroactive polymer (BSEP), is invented enabling repeatable rigid-to-rigid deformation without bulky external structures. Bistable actuation allows the polymer actuator to have two distinct states that can support external load without device failure. Plasticizers are used to lower the glass transition temperature to 45 ^{o}C. Interpenetrating polymer network structure is established inside the BSEP to suppress electromechanical instability, providing a breakdown field of 194 MV/m and a stable bistable strain as large as 228% with a 97% strain fixity.

The application of BSEP in tactile display is investigated by the prototyping of a large scale refreshable Braille display device. Braille is a critical way for the vision impaired community to learn literacy and improve life quality. Current piezoelectrics-based refreshable Braille display technologies are limited to up to 1 line of Braille text, due to the bulky size of bimorph actuators. Based on the unique actuation feature of BSEP, refreshable Braille display devices up to smartphone-size have been demonstrated by polymer sheet laminates. Dots in the devices can be individually controlled via incorporated field-driven BSEP actuators and Joule heater units.

A composite material consisting of silver nanowires (AgNW) embedded in a polymer substrate is brought up as a compliant electrode candidate for BSEP application. The AgNW composite is highly conductive (R_s: 10 Ω/sq) and remains conductive at strains as high as 140% (R_s: $<10^3$ Ω/sq). The baseline conductivity has only small changes up to 90% strain, which makes it low enough for both field driving and stretchable Joule heating. An out-of-plane bistable area strain up to 68% under Joule heating is achieved.

The dissertation of Xiaofan Niu is approved.

Yu Huang

Suneel Kodambaka

Christopher S. Lynch

Qibing Pei, Committee Chair

University of California, Los Angeles

2013

To

my beloved, bright, and brilliant wife

Chenhong Fang,

and my always supportive parents and parents-in-law

Liwei Niu and Luyun Xu,

Xue Fang and Bo Chen

for their encouragement and patience to make this dissertation possible.

Table of Contents

LIST OF FIGURES ..... **IX**

LIST OF TABLES ..... **XIV**

ACKNOWLEDGEMENTS ..... **XV**

CHAPTER 1 INTRODUCTION **1**

1.1 OVERVIEW 1

1.1.1 Background and mechanisms of dielectric elastomers 1
1.1.2 Materials and compliant electrodes 4
1.1.3 Advantages and applications 6

1.2 MOTIVATION OF THE THESIS RESEARCH 9

1.3 SCOPE AND LAYOUT OF THE DISSERTATION 12

CHAPTER 2 NEW PRESTRAIN-FREE DE WITH TUNABLE ELECTROMECHANICAL PROPERTIES **14**

2.1 BACKGROUND OF THE STUDY 14

2.1.1 Materials 14
2.1.2 Prestretching process 15
2.1.3 Electromechanical instability and analysis 16
2.1.4 Scope 18

2.2 EXPERIMENTAL 19

2.2.1 Chemicals and Prepolymer Solutions 19
2.2.2 Elastomer Film Preparation 19
2.2.3 Mechanical Tests 20
2.2.4 Actuation Tests 21
2.2.5 Permittivity Measurement 22

2.3 DESIGN GUIDELINES 22

2.4 EFFECT OF CROSSLINKER 24

2.5 EFFECT OF PLASTICIZERS 32

2.6 ENERGY DENSITY 38

2.7 MULTILAYER ACTUATOR DEMONSTRATION 39

2.8 CONCLUSIONS 41

CHAPTER 3 PERFORMANCE IMPROVEMENT OF BI-STABLE ELECTROACTIVE POLYMERS 42

3.1 BACKGROUND OF THE STUDY 42
3.1.1 Mechanism 42
3.1.2 Material improvements 44
3.1.3 Scopes 45
3.2 EXPERIMENTAL 46
3.2.1 Chemicals 46
3.2.2 Film Preparation 47
3.2.3 Mechanical Tests 48
3.2.4 Actuation Tests 48
3.2.5 Dielectric Tests 49
3.3 THERMOPLASTIC LINEAR POLYMERS WITH PLASTICIZERS 49
3.3.1 Mechanical property 49
3.3.2 Field-Strain 50
3.4 BSEP INTERPENETRATING NETWORKS 51
3.4.1 Methodology 51
3.4.2 Swelling Characterization 53
3.4.3 Shape Memory Behavior 55
3.4.4 Mechanical Property 55
3.4.5 Field-Strain 58
3.4.6 Actuation current 59
3.4.7 Energy density 60
3.5 CONCLUSIONS 61

CHAPTER 4 DESIGN OF A REFRESHABLE BRAILLE ELECTRONIC READER BASED ON BSEP POLYMERS 63

4.1 BACKGROUND 63
4.1.1 Urgent need of large scale refreshable Braille display device 63
4.1.2 Current technologies and their limitations 64
4.1.3 Advantages of BSEP 64
4.2 PROTOTYPING AND CHARACTERIZATION 65
4.3 ACTUATOR UNIT 66
4.4 HEATER UNIT 69
4.5 SCALING-UP 72

4.6 CONCLUSIONS 74

CHAPTER 5 SILVER NANOWIRES AS COMPLIANT ELECTRODES FOR ACTUATION AND JOULE-HEATING 76

5.1 BACKGROUND 76
5.2 EXPERIMENTAL 77
5.3 RESULTS 78
5.4 CONCLUSIONS 88

CHAPTER 6 FUTURE RESEARCHES 89

6.1 FURTHER STUDY IN PRESTRAIN-FREE DIELECTRIC ELASTOMERS 89
6.2 NEW BSEP FORMULATIONS 90
6.3 FULL-PAGE REFRESHABLE BRAILLE DISPLAY 90

CHAPTER 7 CONCLUSIONS 92

REFERENCES 94

LIST OF FIGURES

Figure 1-1. Mechanism of actuation in dielectric elastomers. 3

Figure 1-2. Commercialized dielectric elastomer products: (a) roll-to-roll manufactured DEAP™ films made by Danfoss Polypower; (b) electronically tunable lens made by Optotune AG, Switzerland; (c) illustration of Vivitouch™ haptic feedback module made by AMI; (d) Mophie Pulse™ haptic feedback accessory using Vivitouch™ technology; (e) illustration of 4D haptic feedback headphones using Vivitouch™ technology. 8

Figure 1-3. Prototypes based on dielectric elastomers that are under development: (a) a walking robot built by SRI International; (b) a cell stretcher; (c) an arm-wrestling machine; (d) a remote control of music player with tactile feedback; (e) a 3-cell refreshable Braille device. 9

Figure 1-4. (a) A prestretching machine built in EMPA, Switzerland; (b) a prestretched VHB film attached to a rigid plastic frame (MIT). 11

Figure 2-1. Three types of dielectrics described in Suo's model. 18

Figure 2-2. Auto drawdown machine and UV curing conveyer used in fabrication of UV-DE material. 20

Figure 2-3. Experimental setup for actuation tests. 22

Figure 2-4. (a) Swelling ratio Q (□) and gel fraction (■) and (b) nominal stress versus stretch ratio relationship of UV-DE with different crosslinker concentrations. 26

Figure 2-5. (*Top*) Storage modulus and (*Bottom*) loss factor of UV-DE with different crosslinker concentrations, compared to the reference VHB4905 and IPN4905 materials. 27

Figure 2-6. (*Top*) Electromechanical strain versus applied electric field relationships of UV-DE with different crosslinker concentrations; (*Bottom*) Pictures of the actuated elastomer films. 28

Figure 2-7. (a) Maximum electromechanical strain (□) and breakdown field (■) and (b) permittivity of UV-DE with different crosslinker concentrations. 29

Figure 2-8. (a) Voltage versus stretch $\Phi\lambda$ curves and (b) intersection of $\Phi\lambda$ and breakdown field versus stretch $\Phi B\lambda$ curves of UV-DE with different crosslinker concentrations. 31

Figure 2-9. (a) Swelling ratio Q (□) and gel fraction (■) and (b) nominal stress versus stretch ratio relationship of UV-DE with different plasticizer concentrations. 33

Figure 2-10. (*Top*) Storage modulus and (*Bottom*) loss factor of UV-DE with different plasticizer concentrations. 34

Figure 2-11. (a) Electromechanical strain versus applied electric field relationships, (b) maximum electromechanical strain (□) and breakdown field (■), and (c) permittivity of UV-DE with different plasticizer concentrations. 36

Figure 2-12. Modulus and loss factor change of C5-P20 along with frequency. 37

Figure 2-13. Energy density of UV-DE with different (a) crosslinker (no plasticizer) and (b) plasticizer (HDDA kept at 5%) concentrations. 38

Figure 2-14. A typical multilayer stack linear actuator. The device is attached to a piece of adhesive tape to keep freestanding during the actuation strain measurement. 39

Figure 2-15. (a) Vertical displacement versus time of a 10-layer linear actuator. Tested at 5000 V, 0.1 Hz. The overall thickness of the device is measured 1.08 mm; (b) Vertical displacement versus driving voltage, 5th cycle tested at 0.1 Hz. 41

Figure 3-1. BSEP Mechanism..... 43

Figure 3-2. DMA results of plasticized PTBA: (A) 0%, (B) 2%, (C) 5%, (D) 10%. Solid lines show Young's moduli and dash dot lines show loss factors of various samples..... 50

Figure 3-3. (*Left*) When heated up above Tg, the BSEP film with 10% DBEF plasticizer (73μm thick) can be actuated to 580% strain at 1600V (*bottom*) from initial state (*up*) and maintain that shape after sequentially cooling the film to ambient temperature and removing the actuation voltage. When reheated to above Tg, the thin film recovers its originally shape.; (*Right*) Dielectric actuation of DBEF plasticized PTBA thin films at 45 ℃: (A) 0%, (B) 2%, (C) 5%, (D) 10%. Solid lines show parabolic fittings of experimental results. 51

Figure 3-4. Schematic illustration of fabrication process of a PTBA-IPN membrane. The first UV-cured PTBA network is swollen in a second monomer solution with solvent. The second monomer is then UV cured, followed by thermal annealing on a glass substrate. 52

Figure 3-5. (a) Thickness and area of a PTBA-IPN-50 membrane during the various fabrication stages; (b) Thicknesses of PTBA-IPN membranes after annealing as a function of the volume fraction of toluene in the swelling solvents. Solid line is derived from Equation (1). 54

Figure 3-6. (a) A PTBA-IPN-50 membrane freshly made (distance between the blue markers are 25 mm) , (b) heated at 70°C, (c) stretched by 100% in the horizontal direction and then cooled to room temperature, and (d) reheated for 10s at 70°C. 55

Figure 3-7. (a) Storage modulus versus temperature and (b) loss factor versus temperature of PTBA and PTBA-IPN-50 membranes. 56

Figure 3-8. Tensile stress-strain response of PTBA and PTBA-IPN membranes till break at 70°C. 58
Figure 3-9. Actuation strain vs applied field for PTBA and PTBA-IPN-50 membranes at 70°C. 59
Figure 3-10. Actuation current and area strain during continuous actuation at constant voltages. 60
Figure 4-1. Braille Lite M40, a refreshable Braille display capable of displaying one line of text (*Left*) and the transducers (8 piezoelectric bimorphs) under a Braille cell (*Right*)..... 64
Figure 4-2. Device structure and characterization. For illustration only and scale is not accurate. 66
Figure 4-3. (a) Braille 1 dot; (b) Raised height and temperature of a Braille dot as a function of time during a bistable actuation cycle. 100MV/m 67
Figure 4-4. (*Left*) Raised height of a Braille dot during 1001^{st}-1010^{th} cycles during a repeated actuation cycle test at 70°C; (*Right*) Raised height of a Braille dot with the number of actuation cycles during the cycle test..... 68
Figure 4-5. Supported force of a Braille dot actuator at the ON state as a function of the amount of height reduced as a result of the applied force. 69
Figure 4-6. Relationship between heating time t_h and actuator vertical displacement. 70
Figure 4-7. Relationship between cooling time t_c and actuator vertical displacement. 71
Figure 4-8. (*Up*) 1-cell and (*Down*) 2-cell Braille cell with custom-made control system. 73
Figure 4-9. Photograph of a refreshable Braille display panel made of PTBA-IPN-50, the blow-up of one cell with 3 left dots raised to display the letter “L”. 74
Figure 5-1. Fabrication method and structure of the AgNW/polymer composite electrode material. 79

Figure 5-2. Transmittance and general look of AgNW/polymer composite electrodes with different AgNW loadings. 80
Figure 5-3. Effect of acrylic acid in the composite material to sheet resistance while stretching. 80
Figure 5-4. Effect of AgNW loading to sheet resistance while stretching. 83
Figure 5-5. Joule heating with AgNW/polymer composite. 84
Figure 5-6. AgNW/polymer composite as Joule-heating and actuation electrodes 86
Figure 5-7. Bistable actuation under Joule heating. 87
Figure 6-1. Tablet-size Braille cell with custom-made combination control system. 91

LIST OF TABLES

Table 1-1. Electrical-mechanical transducer technology summary 6

Table 2-1. Formulations (parts of weight) and nomenclature of prepolymer solutions and corresponding elastomer films. 23

Table 3-1. Material properties of PTBA-IPN in comparison with common dielectric elastomers 61

ACKNOWLEDGEMENTS

I would like to give my honest thanks and acknowledgement to all the people who provided me their generous help in various ways during my five years at UCLA:

Special thanks should be given to my adviser, Professor Qibing Pei, for his precious advices and financial support to make my Ph.D. study happen. Not only provided me with inspiring ideas and enormous assistance in scientific research, Professor Pei also taught me to be a person with great personality. I also thank other members on my doctoral committee board: Professor Yu Huang, Professor Suneel Kodambaka, and Professor Christopher Lynch for their guidance and help. Thank Professor Ren Sun of the Department of Molecular and Medical Pharmacology for first introducing me to the greatness of University of California, Los Angeles.

Especially, I would thank Dr. Wei Yuan and Dr. Zhibin Yu for their patience in teaching me the fundamental skills in the lab, setting up experimental apparatus, and managing research projects in the early stage of my Ph.D. study; thank Dr. Paul Brochu for working together with me in the lab all the time and critical reviewing my manuscripts for publication; thank post-doctoral and visiting scholars Dr. Sungryul Yun, Dr. Hristiyan Stoyanov, Dr. Xinguo Yang, Dr. Jiajie Liang, and Dr. Lu Li for flourishing the scientific ideas in Chapter 2, 3, 4, and 5 of this dissertation, and mentoring me on scientific article writing; thank Mr. Huafeng Li, Dr. Jun Liu, Dr. Qi Chen, Dr. Chaokun Gong, Dr. Weili Hu, Ms. Wei Hu, Mr. Zhi Ren, Mr. David McCoul, Ms. Han Zhang, Mr. Antony Jan, Mr. Brandon Salazar, Ms. Ruby Leo, Mr. Christopher Lai, Mr. Dustin Chen, all other previous and current lab members, and my research collaborators from all over the world for sharing with me their valuable experience and knowledge to make all my research work come true.

VITA

2008	B.S., Polymers Science & Engineering Zhejiang University, Hangzhou China
2010	M.S., Materials Science & Engineering University of California, Los Angeles
2010-2013	Ph.D. Candidate Materials Science and Engineering University of California, Los Angeles

Chapter 1 Introduction

1.1 Overview

1.1.1 Background and mechanisms of dielectric elastomers

A lot of polymers are dielectrics or insulators with poor bulk conductivity and resist the flow of current. These polymers can survive high electric fields as they have no free charge carrier and large band gaps in their electronic structures.[1] Due to their simpler fabrication and lower cost with respect to traditional inorganic materials, polymer dielectrics are extruded into thin films or sheets, and are widely used in capacitors,[2] gate dielectrics in transistors,[3] electrical cable wraps,[4] microelectronic encapsulation,[5] etc.

When a high electric field is applied on a dielectric polymer film, opposite charges accumulate on both surfaces of the dielectric film. An electrostatic attraction force builds up between the opposite charges. Meanwhile, like charges on the same electrode repel each other. The synergistic effect of the two forces presses the polymer film in the direction of the electric field and stretches in the orthogonal directions, causing it to shrink in thickness and expand in area. The phenomenon was firstly discovered and named after James Clerk Maxwell, as Maxwell stress or Maxwell pressure,[6,7] with the expression of:

$$P = \varepsilon_0 \varepsilon E^2 \quad (1)$$

where ε_0 is the vacuum permittivity, ε is dielectric constant of the dielectric material, and E is the electric field applied across the material thickness. This equation is only valid assuming that ε does not change in its value along with the applied electric field, the stress or strain in the material.

Maxwell pressure is a phenomenon to be avoided in traditional capacitor industries. Even slight shape changes will crack the thin film metal electrodes used in capacitors and prevent the device from functioning. Localized thinning of the dielectric sheet will lead to drastic charge and electric field localization. Ultimately the device will be shorted. The phenomenon has been found in a number of dielectrics including polyethylene and polyisobutylene.

Recently, scientists at Stanford Research Institute (SRI International) found that Maxwell pressure can be useful with the use of some special polymers.[8–10] Specifically, when a soft elastomeric dielectric polymer was used with compliant carbon grease electrodes, an electrostrictive strain as large as 32% could be achieved.[8,9] The same group further demonstrated more than 100% strain with biaxially or uniaxially prestretched polymer films.[10] Compared to less than 1% strain people previously thought the Maxwell pressure can generate,[11] there is a three orders of magnitude increase in the amount of electromechanical strain generated when soft elastic dielectrics were used.

Due to their electric field-driven nature, these polymers are given the name of dielectric elastomers (DE). Figure 1-1 shows an illustration of a common DE actuator structure, comprising of an elastomer film sandwiched between a pair of compliant electrodes. Similar with the traditional dielectrics, opposite charges are conducted to the both surfaces of the DE film through the compliant electrodes, upon the application of an electric field. A local electric field is established across the DE film and Maxwell pressure develops. The DE film is squeezed in the thickness direction and expands in area. The resilient force in DE is not large enough to balance out the Maxwell pressure, likely due to lower stiffness in DE (normally on the order of 0.1-10 MPa) than in other polymers (e.g. 250 MPa in LDPE for electrical cables[12]). Therefore the strain in DE could be considerably large, as long as no electrical or mechanical failure is present.

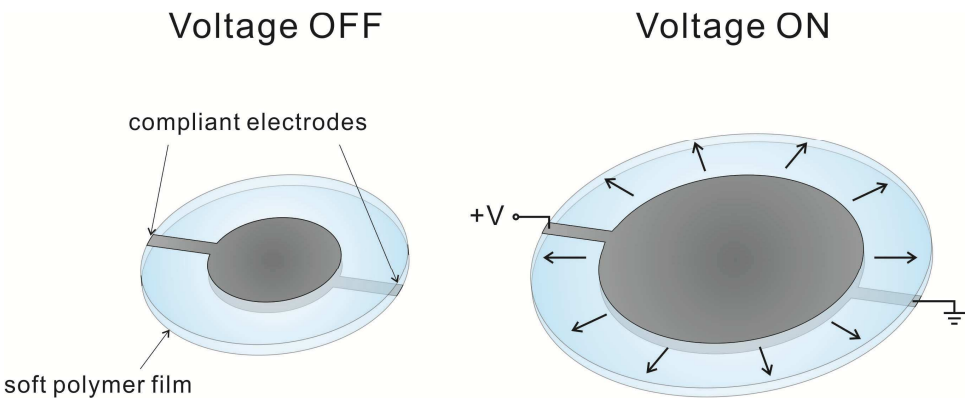

Figure 1-1. Mechanism of actuation in dielectric elastomers.

DE serves as a transducer material converting electrical and mechanical energy. With a linear storage modulus assumption, one can roughly estimate the electrostrictive strain in the thickness direction by taking the Maxwell pressure p divided by the modulus Y of the elastomer:[10]

$$s_z = -\frac{p}{Y} = -\frac{\varepsilon_0 \varepsilon E^2}{Y} = -\frac{\varepsilon_0 \varepsilon}{Y}\left(\frac{V}{d}\right)^2 \tag{2}$$

where s_z is the strain in the thickness direction, V is the voltage applied, and d is the thickness of the DE film. Assume the material is incompressible, the strain in area s_A can be calculated as:

$$s_A = \frac{1}{1+s_z} - 1 \tag{3}$$

Electromechanical energy density e is a simple but useful measure of the amount of electrical energy converted to mechanical energy per unit volume of material for one cycle:

$$e = -0.5p \ln(1+s_z) \tag{4}$$

With this equation one can compare the estimated performance of high strain DE materials to traditional low strain piezoelectrics.

However, the strain calculation is only valid with the actual strain is small, for instance, less than 20%, as Y only stays constant in that range and will change along with further increase of strain. For higher strains, non-linear strain energy functions have to be used to simulate the stress-strain behavior of the elastomer. Different strain energy functions were well developed by Ogden,[13] Yeoh,[14] and Mooney-Rivlin.[15] Electromechanical models based on these strain energy functions were further presented by physicists, taking the electrostatic force into consideration.[16–20] Recently, thermodynamics has been used to explain the non-linear electromechanical behavior in DE.[21–25] Further improvements in modeling considered mechanical viscoelasticity and electrical leakage current.[26,27]

1.1.2 Materials and compliant electrodes

Firstly, an ideal DE film must be a good insulator. The typical nominal electric field needed can be larger than 100 MV/m in order to generate strains greater than 100%.[10] True electric field can be as large as 250 MV/m, since the local thinning in the DE film has to be taken into consideration. Leakage current should be minimized to avoid local thermal failure of the DE material.[28] Typical bulk resistivity of dielectric polymers should be higher than 10^{15} ohm-cm.[29] Moreover, improvement of dielectric constant ε is also essential. It can be enhanced by means of increasing the polarization of the polymer backbone and side chains. More charges can be induced in the soft capacitor charging process, and a higher effective local electric field can be reached. The driving voltage can potentially be brought down by this means.[30]

From the mechanical point of view, low Young's modulus, high elongation at break, and low viscoelasticity are critical for DE materials. Young's modulus Y bridges electrical and mechanical responses of the material and is important in reducing electromechanical instability as discussed in Chapter 2. A lower Y and high elongation at break determine the physical limit of the electromechanical strain. Material will experience mechanical loss when actuated repeatedly because of the friction and dissipation between molecule chains. Low viscoelasticity can minimize the mechanical loss in the material, and increase its dynamic response speed and efficiency to the external field driven actuation.[30]

Compliant electrodes are needed in a wide range of applications beyond DE actuators,[31] such as in stretchable electronics.[32,33] The materials used as compliant electrodes usually have good intrinsic conductivity to ensure the conductance of charges onto the elastomer surfaces.[10,30] They must be able to keep their mechanical integrity under a large stretch, for example 100%, and still maintain a relative high conductivity. The reliability must be high upon a large number of repetitive stretches.[34] A broken electrode layer may lead to degraded maximum strain and/or respond speed. Since the compliant electrodes are bonded to the DE film and moving together, the use of compliant electrodes should not significantly increase the stiffness of the DE.[35] An ideal compliant electrode material has a high conductivity that does not change with strain, and zero stiffness. Compliant electrode is even not necessary in some cases to prevent electromechanical instability.[36] Compliant electrodes should be deposited onto designated areas of the DE film with an easy and straightforward process, as the actuator designs vary.

1.1.3 Advantages and applications

Table 1-1 indicates a detailed summary of literature reported DE actuators and other transducer technologies that converts electrical energy to mechanical energy.[30,34,37] It is easy to identify that DE is the only material with performances comparable or beyond mammalian skeletal muscles in strain, energy density, efficiency and speed.[38] Actually, DE is known as a candidate "artificial muscle" due to this similarity.

Table 1-1. Electrical-mechanical transducer technology summary

Property	Dielectric Elastomers	Mammalian Skeletal Muscles	Electromagnetic Coils	Piezoelectric Ceramics	Electrostrictive Polymers
Maximum Strain (%)	10->100	20-40	50	1.7	0.1
Maximum Pressure (MPa)	7.2	10-60	0.1	131	3.8
Electromechanical Energy Density (J/g)	<3.4	0.008-0.04	0.003	0.13	0.0013
Maximum Efficiency (%)	60-80	<40	>90	>90	-
Response Speed	Medium to Fast	Slow	Fast	Fast	Fast

DE artificial muscles enable a plurality of commercial actuator applications as shown in Figure 1-3. Danfoss Polypower A/S, a Denmark based company, developed their own silicone-based DE material in high volume roll-to-roll manufacturing.[39] Optotune AG in Switzerland used DE in electrical focus tunable lenses and laser speckle reducers, to build fast and more compact optical systems without using complex mechanical systems.[40] By applying a driving voltage, the radius of the tunable lens will change and the focus length can be controlled in milliseconds. Artificial Muscle Inc. (AMI), a spin-off of SRI International and now part of Bayer

MaterialScience, developed their first commercial haptic feedback module for consumer electronics such as smartphones, tablet computers, and gaming controllers.[41,42] The mounting actuator module shakes the whole consumer electric device, providing a perfect mimic of real object movements as seen on the screen. Another project being developed by the company is a force-feedback headphone for out-of-ear 4D sound experience.

The commercial potential of the dielectric elastomer actuators has been broadly recognized, and reflected in the attendance of over a hundred technology developers from a variety of companies and research institutes in the annual SPIE Conferences on Electro-Active Polymers Actuators and Devices (EAPAD). A number of demonstrations of prototypes have attracted significant attention of the society. In the early stage, a walking robot made from DE spring roll actuators was demonstrated by SRI.[43] (Figure 1-3(a)) The spring rolls were made so that multi-degree-of-freedom can be realized in the actuations. Also demonstrated were applications in MEMS, for example a micro cell-stretchers (Figure 1-3(b)). Multiple DE actuators were stacked to give a force output large enough to arm-wrestling with human beings.[44] (Figure 1-3(c)). Active vibration control is important in precise manufacturing and semiconductor fabrication. Vibration attenuation up to 40dB was achieved with DE technology.[45] A remote control for portable music players with haptic feedback was demonstrated in Germany.[46–48] (Figure 1-3(d)) Lately, DE materials were widely used in refreshable Braille displays. A number of prototypes were demonstrated and one of them was shown in Figure 1-3(e).[49–53] Other applications of DE actuators include inchworm robots,[54] gripper hands,[55] gear motors,[56] and linear motors.[57]

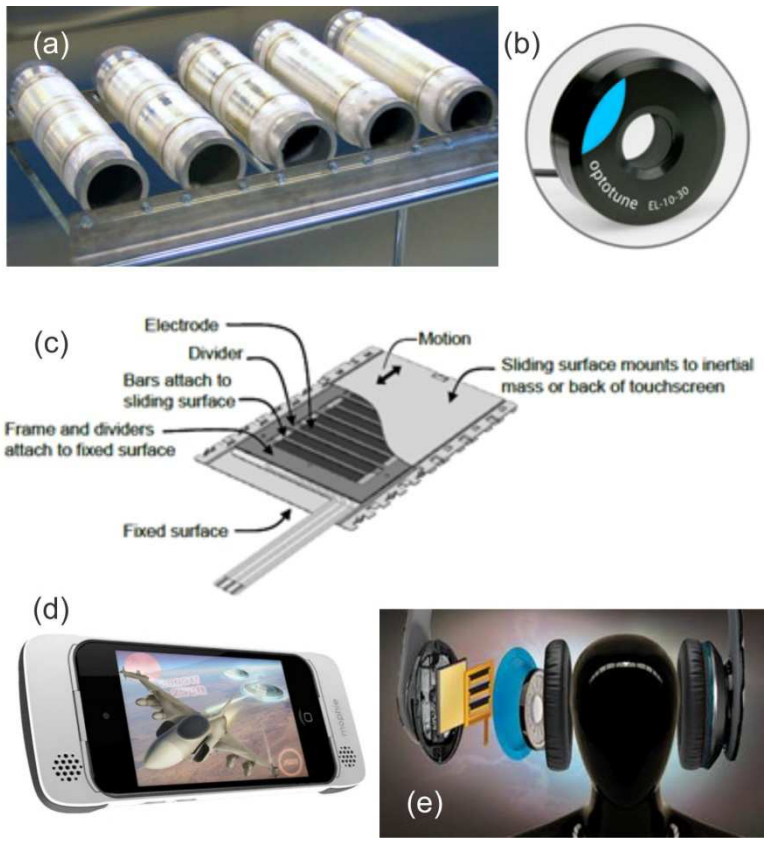

Figure 1-2. Commercialized dielectric elastomer products: (a) roll-to-roll manufactured DEAP^{TM} films made by Danfoss Polypower; (b) electronically tunable lens made by Optotune AG, Switzerland; (c) illustration of Vivitouch^{TM} haptic feedback module made by AMI; (d) Mophie Pulse^{TM} haptic feedback accessory using Vivitouch^{TM} technology; (e) illustration of 4D haptic feedback headphones using Vivitouch^{TM} technology.

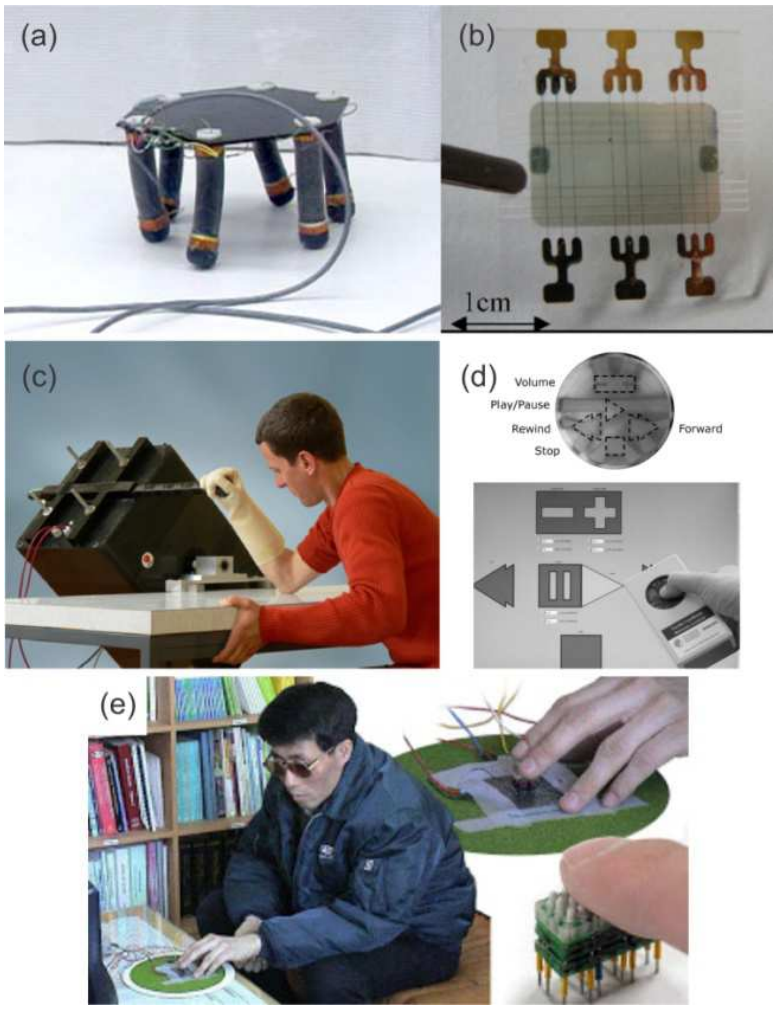

Figure 1-3. Prototypes based on dielectric elastomers that are under development: (a) a walking robot built by SRI International; (b) a cell stretcher; (c) an arm-wrestling machine; (d) a remote control of music player with tactile feedback; (e) a 3-cell refreshable Braille device.

1.2 Motivation of the thesis research

It has been more than 10 years since the debut of the first large-strain dielectric actuation concept. Researchers have made great achievements on both fundamental and application oriented research in this field. To further thrive this area, breakthroughs in the following aspects are highly desired:

- high performance dielectric elastomer materials;

- easy processing of DE materials;
- new compliant electrodes;
- innovative functionality, device structures and application concepts.

Specially designed DE materials are necessary to achieve adjustable electromechanical performances according to applications. Current DE materials on the market are originally developed for unrelated purposes. The commonly used acrylic based DE giving largest electromechanical strain and highest energy density, 3M VHB^{TM} 4905/4910, is an industrial adhesive. The reference silicone DE that has wide temperature stability and low viscoelasticity, Dow Corning HS3, is a high strength moldmaking rubber for detailed reproduction of figures and objects. The high performance of these materials as DE is indicated simply by exclusive screening tests. Further improvement of these materials is considered difficult since the chemical composition and molecular structure are unknown due to business proprietary. One motivation of this dissertation is to establish a material synthesis platform open to custom designs, with tunable electromechanical properties that can be adapted into specific applications. A design guideline or structure-property relationship should be established to keep record of effect of different components to the property.

Reliability and cost control are of great importance to make a prototype into a real product. Simple processing is essential make to reliable and low cost products. A higher yield in each processing step and a small number of total steps are always desired, especially in the conversion from a prototype to high volume production. For instance, prestretching dominates the fabrication of high performance acrylic and silicone materials, but it is at the same time a great pain to device makers. Most of the products and prototypes shown in Figure 1-2 and Figure 1-3 were fabricated with prestretched DE films. As shown in Figure 1-4(a), the equipment used for

prestretching can be bulky in size and high in fabrication cost. The prestretched films have to be held on a rigid frame to prevent them from relaxing. (Figure 1-4(b)) Tension from prestretching will cause the film to mechanically fatigue and become vulnerable in actuation. Also the mismatch in modulus between the frame and prestretched film will lead to local stress concentration at the contact edges, causing mechanical failure. To dig the full potential of DE materials, the ideal solution would be designing a material with no need of prestretching. A lot of research efforts have been given with promising results, such as acrylic IPNs and pre-swollen by solvents. However, the related fabrication processes to the alternative materials are even more complex than prestretching itself, and are not compatible with industrial production. The material system explored in this dissertation with tunable electromechanical performance will be demonstrated with industry compatible coating process with no need of prestretching.

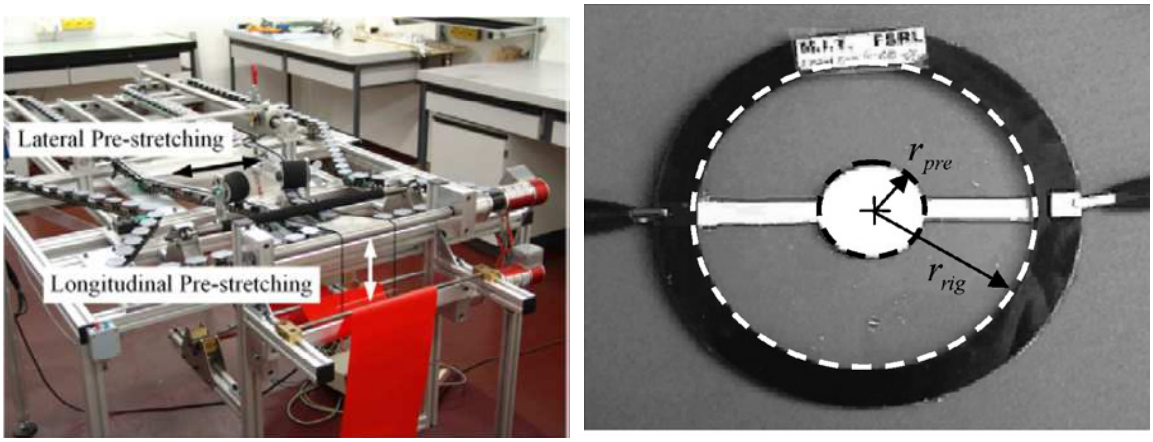

Figure 1-4. (a) A prestretching machine built in EMPA, Switzerland; (b) a prestretched VHB film attached to a rigid plastic frame (MIT).

As a novel transducer technology, DE features certain advantages to traditional technologies. How to better utilize these features in real applications is an open question to all scientists and

product development engineers. Market needs should be clearly identified by an extensive market research. The technology itself also has to be further developed and well modified to adapt into the niche market. For instance, it is recognized that there is an urgent need in the vision impaired community for a large-scale refreshable Braille display technology.[59] With this purpose in mind, this dissertation will present a novel set of solution with a new bistable electroactive polymer (BSEP), a derivate of DE. The research will focus on both material development and device integration to bring this innovative product concept to a successful demonstration.

The performance of DE actuators is highly determined by the compliant electrodes used.[31] Conductivity, stretchability, and low stiffness are the basic requirements for a compliant electrode material. The compliant electrode should also be easy to integrate into the final device structure. The candidates so far include flat and rugged thin film metal,[60,61] carbon grease and carbon black powder,[8,10,57,62] polymer paste with conductive fillers,[63–65] conducting polymers,[66] carbon nanotubes,[35,67–70] graphene,[71] implanted metal ions,[72–74] etc. Each of these candidates has its comparative advantages in some of these features. However, there is no ideal solution to cover all the aspect yet. In this dissertation a new compliant electrode material candidate is described with an emphasis on high conductivity and stretchability. It can also be applied in the BSEP material system as Joule heating electrode so that the overall device structure can be simplified.

1.3 Scope and layout of the dissertation

The dissertation is divided into seven chapters.

Chapter 1, the current chapter, gives an overview of the research field, including working mechanism of dielectric actuation, dielectric materials and electrode materials, advantages and applications of dielectric elastomers. Also covered is the motivation and layout of the dissertation.

Chapter 2 discusses the development of an open DE material system with tunable electromechanical properties. The material has suppressed electromechanical instability and simple, scalable processing.

Chapter 3 covers the invention and concept of a new multifunctional dielectric elastomer derivative, bistable electroactive polymer (BSEP). Improvement of the actuation stability of BSEP is achieved by introducing interpenetrating network into the material structure.

Chapter 4 presents prototypes of refreshable Braille display devices up to smartphone size made by BSEP. By using a polymer sheet laminate structure and a separate heater, each dot can be individually driven to a buckled ON state and refreshed to flat OFF state in a bistable way. The technology advancement made meets the urgent need of a large scale refreshable Braille display device.

Chapter 5 reports a new silver nanowires (AgNW) polymer composite material that is conductive enough for Joule heating purpose even at a large strain of 90%. It is especially suitable for BSEP devices as it provides a solution combining the actuator and the heater together in a thin film architecture.

Chapter 6 provides an outlook for future research and Chapter 7 concludes the dissertation.

Chapter 2 New Prestrain-Free DE with tunable electromechanical properties

2.1 Background of the study

2.1.1 Materials

A large number of elastomer materials were investigated, including isoprene rubber latex,[75] acrylics,[8,10,75] silicones,[10,75–77] polyurethanes,[75] fluoroelastomers,[78] thermoplastic elastomers,[63,64,79–86] and other synthetic rubbers.[87,88] Of these categories acrylics are widely used in fundamental research and proof of concept prototypes, since they provide excellent electromechanical strain and energy density. The reference material, 3M VHB series, can be driven to as large as 158% in a biaxially prestretched circular actuator and 380% in a linear actuator.[10] In some precisely controlled device structures the strain can be as high as 1692%.[89] A 3.4 J/g energy density is reported in acrylics.[10] Further improvements are considered difficult since the crosslinked elastomer network in VHB has already been formed in the commercial product.

Silicones have better performance in thermal and electrical stability, and viscoelasticity.[90] The Si-O-Si bonds have higher bond energy than C-C bonds to provide high temperature and electrical stability. Also Si-O-Si units have larger bond angels and more compliant molecular configurations, providing lower internal dissipation.[91] As a result, silicone elastomers will retain their elasticity even at -60 ^{o}C. Common silicone elastomers are supplied in one or two parts before vulcanizing from various suppliers. Some modifications can be done during this step to improve the properties, such as tuning the polymer structure,[92,93] blending with high permittivity nanofillers,[94–96] grafting with high polarity side groups,[97] etc. Due to their better processibility, silicones are used more in product development.

2.1.2 Prestretching process

A general protocol during employment of most DE materials to obtain actuation strains greater than 33% is prestretching.[9,10] It is known to suppress the electromechanical instability (EMI) of the elastomeric material when being actuated, and improve its breakdown strength and energy density.[9,23,24,98] However, prestretching complicates the device structure, limits the application, and lowers the lifetime of DEAs due to the stress relaxation and fatigue in the biaxially prestretched material, as well as the stress concentration along the rigid frame supporting the prestrain.

Attempts to modify this system include forming a second interpenetrating polymer network (IPN) to maintain the prestrain needed for good actuation performance.[99–102] These IPN films are fabricated by spray coating thermal curable multifunctional additives and initiators onto a prestretched VHB film, letting the additives diffuse into the film, and cure the additives to form a second rigid polymer network. Upon releasing from the prestretch support, the resulting film will have most of prestrain "locked-in" by the rigid second network resisting the contraction of the first VHB host. The IPN films are capable of reaching a performance similar with prestreched VHB films in both strain and energy density. Also the IPN films have a balanced internal stress state that would not lead to long time fatigue of material. Models were developed to describe the mechanical and electromechanical behaviors of the IPN films.[103–105] However fabrication of IPN is somehow cumbersome, involving prestretching, spray-coating, vacuum heating, and releasing, and is not proper for industrial production and to replace acrylics with prestrain.

Pre-swollen thermoplastic elastomer gels (TPEG) are another kind of materials that have good performance without prestretching.[63,64,79–83] The material is a triblock copolymer

(SEBS or MBM) swollen in a low-volatility rubber selective solvent (oil or plasticizer). The solvent molecules separate the rubbery chains, in analogy to prestretching the crosslinked polymer chains. The actuation strain can be 115% with a MBM copolymer.[64] However, similar with the IPN approach, fabrication of TPEGs involves a complicated process which prevents the material from being widely used.

2.1.3 Electromechanical instability and analysis

Theoretical analysis of the large electromechanical strain in DE and the effect of prestretching are of great interest to researchers. Physicists start from constructing models by derivation and numerical simulations, and then fit experimental measurements with the models to validate them, with the hope of predicting the electromechanical behavior of new materials. Starting from the basic small strain assumption, hyperelastic and viscoelastic materials are being considered in recent modeling work. Mechanical and thermodynamic approaches are both being studied and widely used in predicting behaviors of DE materials. These models are validated with most of the existing DE materials such as acrylics, silicones, and polyurethanes.

The thermodynamic theory developed by Suo et al is of special interest in explaining the electromechanical behavior during the actuation.[21–25] According to this model, dielectric elastomers can be divided into type I, II, and III, depending on their voltage-stretch curve $\Phi(\lambda)$, breakdown-stretch curves $\Phi_B(\lambda)$, and the intersections of these two curves:

$$\Phi(\lambda) = H\lambda^{-2}\sqrt{\frac{\sigma(\lambda)}{\varepsilon}} \tag{5}$$

$$\Phi_B(\lambda) = E_B H\lambda^{-2} \tag{6}$$

where λ is the stretch, H is the original thickness, $\sigma(\lambda)$ is the stress-strain relationship, and E_B is the electric breakdown strength of the material. (Figure 2-1) In type I dielectrics, such as glassy polymers or ceramics, the breakdown will not happen until the voltage mobilizes charged spices in the dielectric and creates a conductive path. The electromechanical strain is commonly small. In type II dielectrics the maximum strain is normally limited by electromechanical instability (EMI), or pull-in effect. Maxwell pressure is larger than the resilient force of the elastomer, causing the elastomer film to thin down excessively when actuated and finally fails. The intrinsic breakdown curve intersects the voltage-stretch curve in the saddle area. The model predicts the existence of a type III dielectrics, in the intrinsic breakdown curve is higher than the voltage-stretch curve, until a very large stretch. The material can survive the EMI, reach a stable state without electrical breakdown, and attain large strains. This model successfully explains the effects of prestretching,[24] prestrain-locked IPN,[23] and the giant strain under varying chamber pressures.[89]

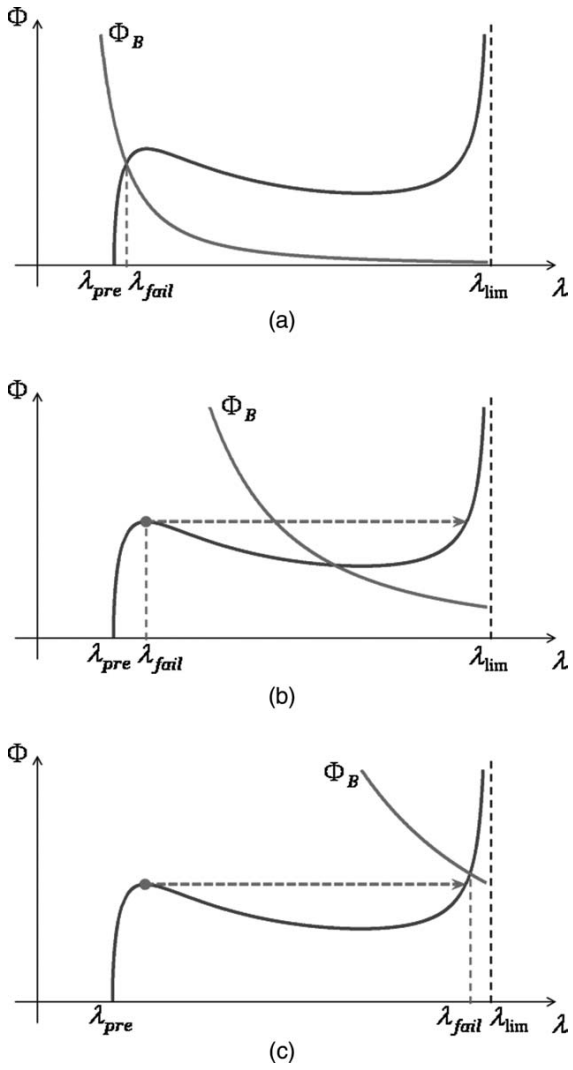

Figure 2-1. Three types of dielectrics described in Suo's model.

2.1.4 Scope

In this chapter it is reported that a series of DE materials with tunable electromechanical properties[106] were synthesized by UV curing, a technology known as an effective method for fabricating high performance coatings, inks, and adhesives.[107] No prestretching is needed to reach the best performance. EMI in the materials can be selectively suppressed with the addition of crosslinkers. Potentially the formulation of the materials can be adjusted with almost limitless possibilities to achieve materials ranging from extremely soft or gel-like elastomers, to rigid,

scratch-resist materials. Deployment of such materials can be easily accomplished by industrial thin film coating techniques such as blade coating, slot die coating, and spin coating. The form factor of cured materials (thin films with a few to tens of micrometer thickness) meets the requirement of DEs. The ability to tune the composition also allows for an adjustable adhesion between different layers of coatings which will ease the fabrication of DE devices, such as multilayer stack DEA.[57]

2.2 Experimental

2.2.1 Chemicals and Prepolymer Solutions

CN9021 (difunctional acrylic esters resin), isodecyl acrylate (IDA), isobornyl acrylate (IBOA), trimethylolpropane triacrylate (TMPTA), 1,6-hexanediol diacrylate (HDDA), and dibutoxyethoxyethyl formal (DBEF) were obtained from Sartomer Company and used as received. 2,2-Dimethoxy-2-phenylacetophenone (DMPA) and benzophenone (BP) were purchased from Acros and used as received. The acrylate monomers and a photoinitiator were mixed thoroughly by mechanical stirring to form a homogeneous prepolymer solution.

2.2.2 Elastomer Film Preparation

Two methods were used to prepare elastomer films for tensile and actuation tests. For tensile stress-strain tests, a prepolymer solution was coated on a Teflon plate with a controlled thickness by a doctor's blade. Then it was cured on a UV curing conveyor equipped with a 2.5 W cm^{-2} Fusion 300S type "H" UV curing bulb, at a speed of 6.0 feet per minute for 2 passes. (Figure 2-2) The film was gently peeled off. For actuation tests, the prepolymer solution was spin-coated onto a plastic petri dish at a speed of 800 rpm for 18 s, and then cured under the same conditions

mentioned above. Carbon grease (NyoGel 756G, Nye Lubricants Inc.) was smeared onto both sides of the films as compliant electrodes.

Figure 2-2. Auto drawdown machine and UV curing conveyer used in fabrication of UV-DE material.

The 3M VHB material was used as a reference material in our study and was referred to as VHB4905. Similarly, the modified VHB material with interpenetration polymer network was fabricated as reported previously[99] and was referred to as IPN4905.

2.2.3 Mechanical Tests

Mechanical properties of UV-DE are characterized on a TA RSA3 dynamic mechanical analyzer. For tensile tests, type IV dumbbell shape samples were made with a cutting die as defined in ISO 37, and tested at a strain rate of 3.33 mm s^{-1}. At least three repetitive samples were tested for each formulation. Dynamic mechanical properties, including loss factor (tan δ),

of the elastomer films were measured with blade-cut rectangle samples of around 0.3 mm in thickness and 10 mm in width. A 15 mm gap between the thin film grips was used when the samples were loaded onto the equipment. All tests were carried out at 1 Hz frequency, <2% strain, and a temperature ramping rate of 7 ^{o}C min^{-1}.

2.2.4 Actuation Tests

The electroded elastomer films were attached to a diaphragm chamber made of aluminum with a 10 mm circular opening onto which the thin DE films were mounted. A bias air pressure of 2.5 Torr was applied such that when the DE films were actuated, they deform out of plane to form a raised dome shape. The active area of the DE films was flat and circular with a diameter of 6.35 mm (before actuation). A high voltage power supply fabricated in house was used to drive the actuators. A digital camcorder was used to record the actuation process. The actuation strain was measured from the video frame-by-frame and calculated by an equation already reported.[99] The strain values for a particular voltage were taken after the constant driving voltage has been applied for 5 seconds. The nominal electric field was calculated by dividing the applied voltage by the initial thickness of the elastomer film. The breakdown field was calculated by dividing the applied voltage by the instantaneous thickness of the elastomer film at maximum strain. At least three repetitive samples were tested for each formulation. The whole setup is illustrated in Figure 2-3.

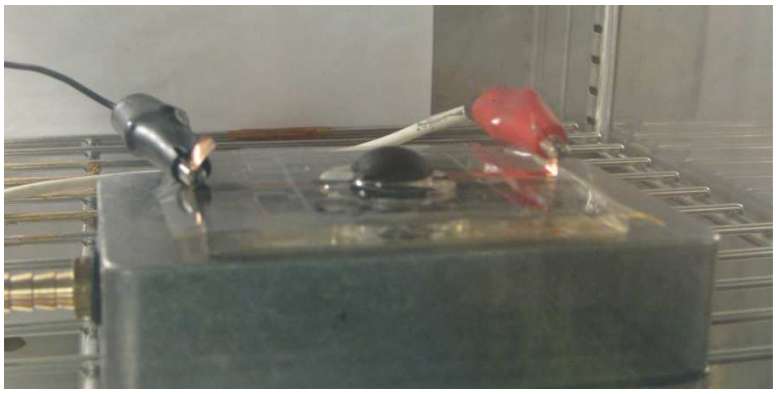

Figure 2-3. Experimental setup for actuation tests.

2.2.5 Permittivity Measurement

Elastomer films of known thickness were coated with silver grease (MGChemicals, Cat. No. 8463) to form circular electrodes with a diameter of 12.7 mm. Capacitance was measured using a GwInstek LCR-819 LCR meter at 1 V excitation and 12 Hz frequency. Relative permittivity ε of the materials was calculated by:

$$\varepsilon = \frac{Cz}{\varepsilon_0 A} \tag{7}$$

where C is the measured capacitance, z is the thickness of the elastomer film, ε_0 is the vacuum permittivity, and A is the effective area.

2.3 Design Guidelines

The electromechanical pressure and strain can be estimated with a linear assumption as in Equation (1), (2) and (3). Due to the nonlinearity of the elastomer, the modulus of the elastomer changes along with stretching. The apparent modulus of the elastomer at the actuation strain should be used to calculate the strain.

Therefore, the actual performance of DE actuators is determined by a few factors: the hyperelastic stress-strain response (stiffness-strain relationship), stretchability (elongation at break and reversibility), the macroscopic permittivity (dielectric constant) of the polymer, and dielectric breakdown strength (the maximum field applied without causing arcing). These parameters govern material selection and processing. Viscoelasticity or dynamic mechanical loss factor plays a key role in response speed and energy efficiency. Most DE materials investigated so far exhibit EMI, or pull-in failure, at an electric field much lower than the polymers' intrinsic breakdown field strength or actuation performance potential.

Table 2-1. Formulations (parts of weight) and nomenclature of prepolymer solutions and corresponding elastomer films.

Name	CN9021	HDDA	DBEF	IDA	IBOA	TMPTA	DMPA	BP
C0-P0	70	0	0	23	5	1	1	0.5
C2-P0	70	2	0	21	5	1	1	0.5
C3-P0	70	3	0	20	5	1	1	0.5
C4-P0	70	4	0	19	5	1	1	0.5
C5-P0	70	5	0	18	5	1	1	0.5
C5-P10	70	5	10	18	5	1	1	0.5
C5-P20	70	5	20	18	5	1	1	0.5
C5-P30	70	5	30	18	5	1	1	0.5

With these considerations in mind, we formulated DE precursor solutions containing a prepolymer (oligomer), reactive diluents, photoinitiators, and other additives. In general, the oligomer, or a blend of a few oligomers, is selected as the framework responsible for the basic

mechanical properties of the material system. Reactive diluents, including monofunctional and/or multifunctional acrylates, are used to adjust rheology, provide crosslinking, and precisely tune the mechanical properties of the material. Photoinitiators are used to initialize the polymerization. Additives can be added into the precursor solutions when special requirements must be met. Table 2-1 summarizes the formulations screened in this work. Here CN9021 acrylic ester resin was chosen as the oligomer. It is a urethane acrylate compound comprising a flexible polyether diol segment, a relatively flexible aliphatic diisocynate segment in its structure, and a high molecular weight. The resulting homopolymer of CN9021 has high flexibility, low modulus, and is moisture resist.[108] DMPA and BP were synergistically used as co-initiators, to achieve complete bulk and surface curing in thin films.[109] A few reactive diluents were used, including IDA to reduce the viscosity of the precursor solutions, lower the modulus of the co-polymers, and increase hydrophobicity. IBOA was used to improve the toughness, and TMPTA to provide the baseline crosslinking.[107] HDDA was used as the main crosslinker to adjust the mechanical and electromechanical properties of the material. DBEF was used as a plasticizer.

2.4 Effect of Crosslinker

Radiation polymerization is known to form a complex network structure, in a heterogeneous way with microgel formation.[110] But qualitative analysis of the crosslink density can still be performed by analyzing the equilibrium swelling ratio as well as the gel fraction of the elastomer. The swelling ratio Q is defined as cubic of the ratio of the diameter of a swollen elastomer disc to its initial diameter. The gel fraction is defined as the ratio of the mass of the deswollen elastomer over its initial mass, and measures the weight loss during swelling. Figure 2-4(a) shows such data of a series of UV-DE elastomers, with various crosslinker concentrations. C0-

P0, with no additional crosslinkers, has the largest Q of 8.37 and the smallest gel fraction of 75.7%. Q decreases drastically to 4.57 in C2-P0, and then slightly decreases along with further increases in the amount of crosslinker, to 3.11 in C5-P0 containing 5% by weight of HDDA. The gel fraction increases to 88.7% in C4-P0, and saturates after that. The high gel fractions in this series indicate that the polymer networks formed are close to ideal.[111] According to Flory-Rehner theory,[112] if the degree of swelling is large, the average molecular weight between crosslinks, M_c, can be defined as:

$$M_c = \frac{2\rho V_1 Q^{\frac{5}{3}}}{1-K} \quad (8)$$

where ρ is the density of the polymer network, V_1 is the molar volume of the solvent, and K is a constant depending on temperature, polymer, solvent, and their interaction. The crosslink density, which is inversely proportional to M_c, therefore has a negative correlation to Q. With a higher HDDA concentration, the crosslink density in the UV-DE material system is effectively increased. The oligomer and monomers have been effectively incorporated into the crosslinked network and thus will contribute to the better rubbery elasticity in such materials.

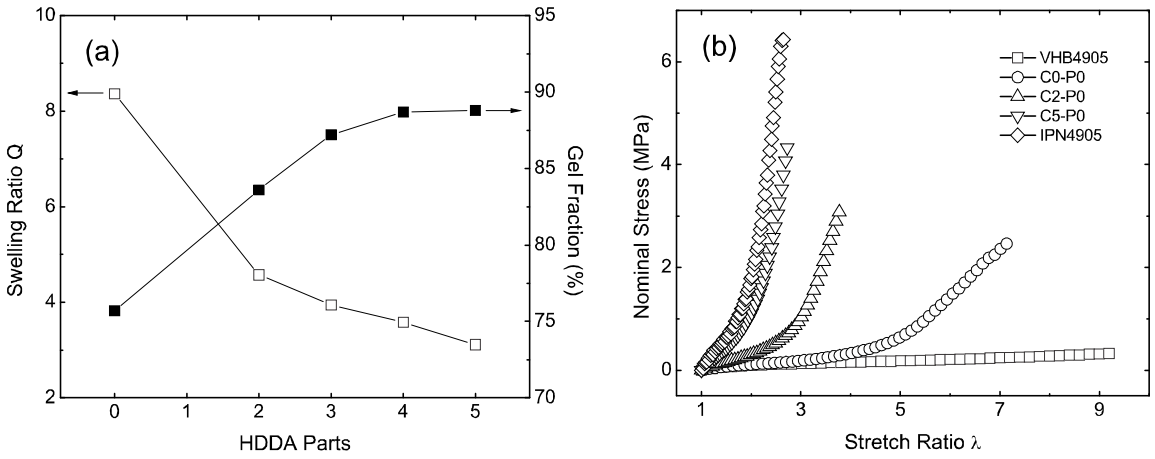

Figure 2-4. (a) Swelling ratio Q (□) and gel fraction (■) and (b) nominal stress versus stretch ratio relationship of UV-DE with different crosslinker concentrations.

Figure 2-4(b) shows the nominal stress versus uniaxial stretch curves of UV-DE materials with different crosslinker concentrations. VHB4905 and IPN4905 fabricated by a method previously reported[99] were chosen as reference materials. The tensile strength is improved from 2.46 MPa in C0-P0 to 4.38 MPa in C5-P0. The stretch ratio at break is compromised from 7.13 in C0-P0 to 2.73 in C5-P0. The modulus of the elastomer at small stretch ratios (λ<1.1) increases along with crosslink density, from C0-P0 similar to non-prestretched VHB4905, to C5-P0 similar to IPN4905. The behavior is due to additional chemical bonds between polymer chains that prevent them from shearing, which can be derived by thermodynamics and rubbery elasticity, and even used as a measurement of crosslink density.[113] Another important feature of the UV-DE is the stiffening after a critical stretch ratio. As the crosslink density increases, a smaller stretch is needed in UV-DE to drive the elastomer into its non-Gaussian region, wherein the non-crystalizable elastomer starts to have stress redistribution and causes substantial stiffening.[114–116] Such critical stretch ratio shifts to a smaller value at a higher crosslink

density, which makes the mechanical properties of the elastomer to shift from being VHB-like to IPN-like in nature.

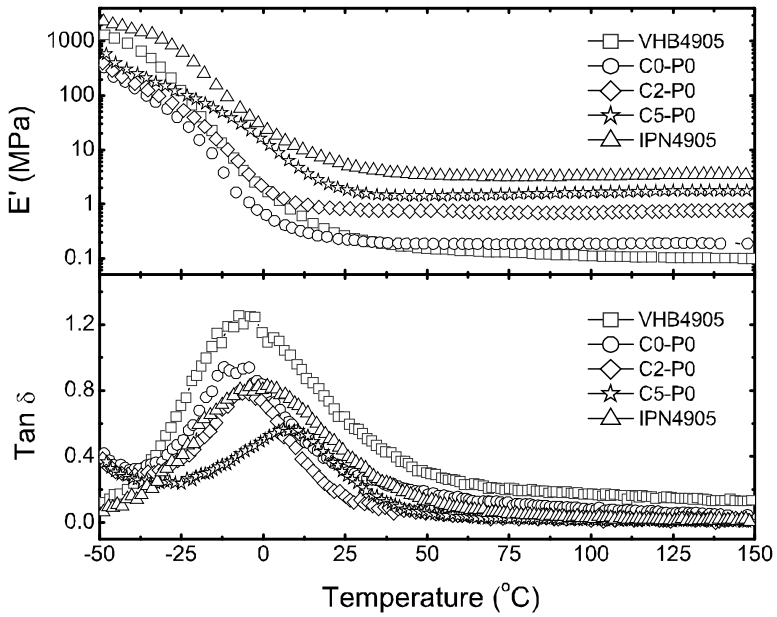

Figure 2-5. (*Top*) Storage modulus and (*Bottom*) loss factor of UV-DE with different crosslinker concentrations, compared to the reference VHB4905 and IPN4905 materials.

The modulus increase with increasing crosslink density is further demonstrated in Figure 2-5. The observed storage modulus of UV-DE varies in between the values of non-prestretched VHB4905 and IPN4905. Also observed is a higher glass transition temperature (T_g) in the highly crosslinked elastomers. A smaller free volume in higher crosslinked elastomers, which leads to a confined chain movement, is responsible for the higher T_g. Also due to this confinement, the amplitude of the chain segment movement is limited. As a result, the loss peak of highly crosslinked elastomers is flattened compared to those with lower crosslink density. Compared to non-prestretched VHB4905 ($\tan \delta = 0.642$), the UV-DE materials have up to 76% decrease in the

loss factor (C2-P0, tan δ = 0.157) at room temperature. It indicates that the material is expected to have a better electromechanical frequency response.

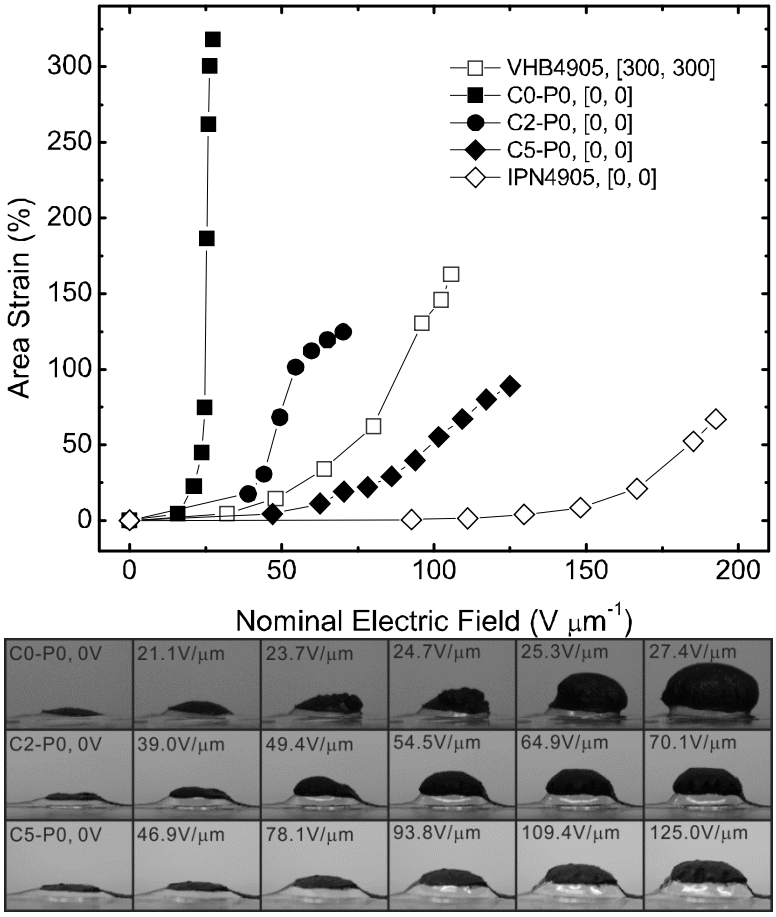

Figure 2-6. (*Top*) Electromechanical strain versus applied electric field relationships of UV-DE with different crosslinker concentrations; (*Bottom*) Pictures of the actuated elastomer films.

The electromechanical performance of UV-DE materials is compared to prestretched VHB4905 (300% by 300% biaxially) and IPN4905 in Figure 2-6. VHB4905 has a maximum strain of 163%. Very little EMI can be observed in the biaxially pre-stretched VHB material. In IPN4905, the stiffness of the second polymer network is responsible for balancing the prestrain applied to the first network, so no EMI is observed even when the material is freestanding. The

observed actuation strain is 67%. The UV-DE materials, with no prestretching applied during actuation, show various electromechanical behaviors. C0-P0 has a large maximum strain of 318%, and a significant EMI snap-through from 23% at 21.0 V μm^{-1} to 262% at 25.8 V μm^{-1}, with three intermediate states in between. This large strain snap-through is very similar to a giant strain snap-through in VHB reported recently,[89] where adjustment of chamber pressure was used to suppress EMI. The EMI is suppressed in C2-P0, where the snap-through is from 31% at 44.1 V μm^{-1} to 102% at 54.5 V μm^{-1}. The maximum strain decreases to 125%. If more crosslinker is used, as in C5-P0, the maximum strain is further reduced to 89%. No significant strain snap-through can be observed, which indicates that EMI has been completely suppressed. The similarity of C5-P0 and IPN4905 are further evidenced by the observed electromechanical properties.

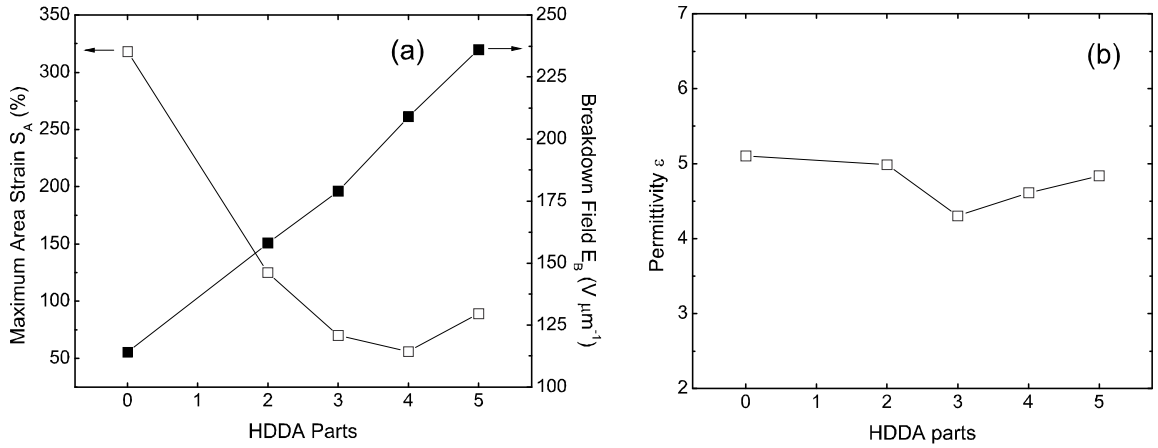

Figure 2-7. (a) Maximum electromechanical strain (□) and breakdown field (■) and (b) permittivity of UV-DE with different crosslinker concentrations.

The ultimate electromechanical behavior and permittivity have been summarized in Figure 2-7, from a full set of actuation tests of UV-DE materials with various crosslinker concentrations.

The apparent electrical breakdown field, defined by the voltage applied divided by the thickness at the maximum strain, increases monotonically, from 114 V μm^{-1} in C0-P0 to 236 V μm^{-1} in C5-P0. The increase could be explained as the synergic effect of the suppression of EMI (explained below) and improvement of the intrinsic breakdown field. On the other hand, the maximum area strain s_A shows a non-linear decrease along with increased crosslink density, from 318% in C0-P0, 125% in C2-P0, to 70% in C3-P0, a minimum of 56% in C4-P0, and then increasing to 89% in C5-P0. As seen in Figure 2-6, EMI is responsible for the large strains in the lightly crosslinked elastomers (C0-P0). A small fluctuation in electric field can thin down the elastomer by a significant amount. Although not fully suppressed, the EMI becomes less significant in materials with higher crosslink densities (C2-P0, C3-P0, and C4-P0). Larger forces are needed to initiate the strain snap-through due to the stiffening effect in such materials. If the crosslink density is further increased (C5-P0), EMI will no longer be the main electrical breakdown mechanism and intrinsic dielectric breakdown will take over. The increased intrinsic breakdown strength will allow the material to attain a higher strain.

Further explanation of the suppression of EMI in the non-prestretched UV-DE materials can be given by the model developed by Zhao and Suo.[23] Figure 2-8(a) shows the voltage-stretch curves of UV-DE materials with various crosslink densities, as well as non-prestretched VHB4905 and IPN4905. An original thickness of 50 μm and the permittivity measured by LCR have been employed as model parameters. The inset shows the true stress and uniaxial stretch relationships of these materials. VHB4905 is compliant at small stretches and does not display any significant stiffening up to λ=9.5 (limit of test equipment). As a result, its voltage-stretch curve reaches a peak, and then monotonically decreases. As such, non-prestretched VHB4905 is a typical type II dielectric, which will fail due to EMI. On the other hand, IPN materials are

reported to have a type III dielectric behavior, where the minimum on the voltage-stretch curve is eliminated by the steep stiffening of the stress-strain relationship, and is monotonically increasing.

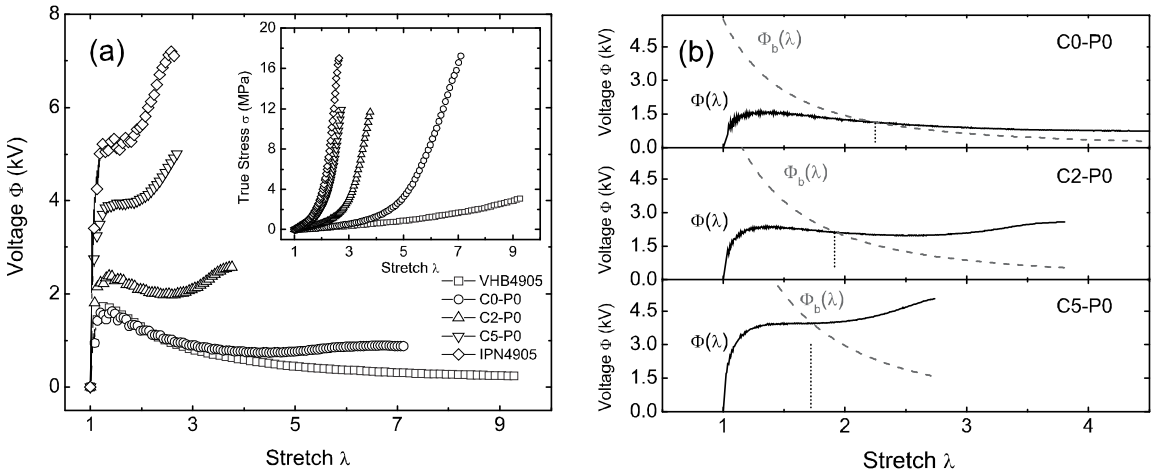

Figure 2-8. (a) Voltage versus stretch $\Phi(\lambda)$ curves and (b) intersection of $\Phi(\lambda)$ and breakdown field versus stretch $\Phi_B(\lambda)$ curves of UV-DE with different crosslinker concentrations.

The UV-DE materials show both types of behaviors, according to their different crosslinker amounts. The one with no additional crosslinker, C0-P0, has a lowest Young's modulus at small stretches (λ<1.1). It has a stiffening effect after λ=4.75 and a minimum can be found on the corresponding voltage-stretch curve. As the amount of HDDA increases, the Young's modulus of the material at small stretches increases, while the stiffening effect tends to show up earlier and steeper. The minimum on the voltage-stretch curves also shifts to a smaller stretch, and finally diminishes in C5-P0, similar with IPN4905. The Zhao-Suo model predicts that C5-P0 will have a similar electromechanical behavior as the IPN material, which matches well with the experimental observation shown in Figure 2-6. Note that no prestretching is involved during the fabrication and testing of the new DE materials.

The intersections of the voltage-stretch curves and breakdown-stretch curves in UV-DE materials can be used to fit or predict the ultimate electromechanical properties, as shown in Figure 2-8(b) The electric breakdown strengths of the materials are determined by dividing the nominal electric field at failure by the thickness strain. In C0-P0 two curves intersect at λ=2.24, which is beyond the maximum on the curve (λ=1.30), but much smaller than the minimum on the voltage-stretch curve (λ=4.75). This indicates a possible meta-stable strain snap-through along the voltage-stretch curve from the peak at λ=1.30. Therefore C0-P0 should be categorized as a type II dielectric. Similarly in C2-P0, the intersection at λ=1.92 is between the maximum (λ=1.30) and the minimum (λ=2.60), but much closer to the minimum. It is still a meta-stable type II dielectric, while the stability of the strain after snap-through is better than the C0-P0 case. In C5-P0 the intersection is at λ=1.71. Since the minimum is eliminated, it can be categorized as a type III dielectric which is able to totally suppress EMI. The theoretically predicted values deviate from the experimental strain values, but they follow the same trend. The deviation is probably due to the problematic assumption of estimating biaxial actuation strain with a uniaxial stretch in a much stiffer system.

2.5 Effect of Plasticizers

Increasing crosslink density can suppress EMI and improve breakdown field, while still allowing a useful large strain. One problem is the high modulus brought in by the high crosslink density. Although not a linear term, the modulus could be taken as a measurement of sensitivity of the material to an electric field, as explained previously in literature.[10] A lower modulus is preferred so that a lower field is needed for the material to be deformed. Although the overall viscoelasticity has been reduced, the glass transition temperature increases with higher crosslink

density, and viscoelastic behavior still limits the frequency response of the UV-DE. Plasticizers are known as an effective low molecular weight additive to plastics and rubbers that can lower the T_g and make the material more flexible.[102,117] Although the flexible monomer IDA can serve as an internal plasticizer to a certain level, we choose dibutoxyethoxyethyl formal (DBEF) as an external plasticizer of the UV-DE system due to its good low temperature performance, good compatibility with acrylate elastomers, as well as low volatility.[102,117]

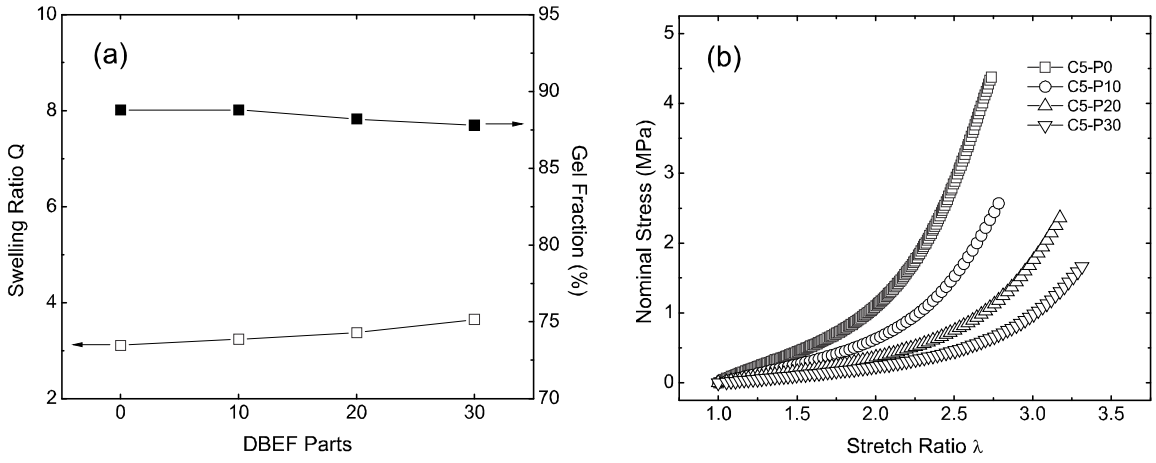

Figure 2-9. (a) Swelling ratio Q (□) and gel fraction (■) and (b) nominal stress versus stretch ratio relationship of UV-DE with different plasticizer concentrations.

Based on the highly crosslinked UV-DE (C5-P0), the effect of DBEF on the crosslink density is studied again with equilibrium swelling tests (Figure 2-9(a)). In the calculation of gel fractions, the weight of the plasticizers was excluded, as the plasticizers are small molecules without reactive functional groups and will not be incorporated into the network. As the plasticizer concentration increases, the swelling ratio increases slightly and the gel fraction decreases slightly. The reason could be the double bond concentration has been diluted by the plasticizer. Also the ether-based plasticizer has a higher chain transfer constant, which could

sacrifice the efficiency of the incorporation of double bond into the polymer network. Overall, the swelling ratio with 30 parts of DBEF is still comparable with sample with 4 parts of HDDA and no plasticizer. As such, plasticizing with DBEF has no significant effect on the network structure of UV-DE. Basic stress-strain relationships of plasticized UV-DE (Figure 2-9(b)) show that plasticized materials have a lower modulus, higher elongation, and a lower tensile strength. Plasticizers present improve the mobility of polymer chains, resulting in softening.[117] The stiffness increase with stretching is still present, although the slope decreases with higher plasticizer loading. Voltage-stretch curves of the plasticized UV-DE materials (**Fig. S2**) show similar shapes as C5-P0. A longer "necking" after the maximum at $\lambda \sim 1.3$ indicates that the suppression of EMI becomes less effective when too much plasticizer is used.

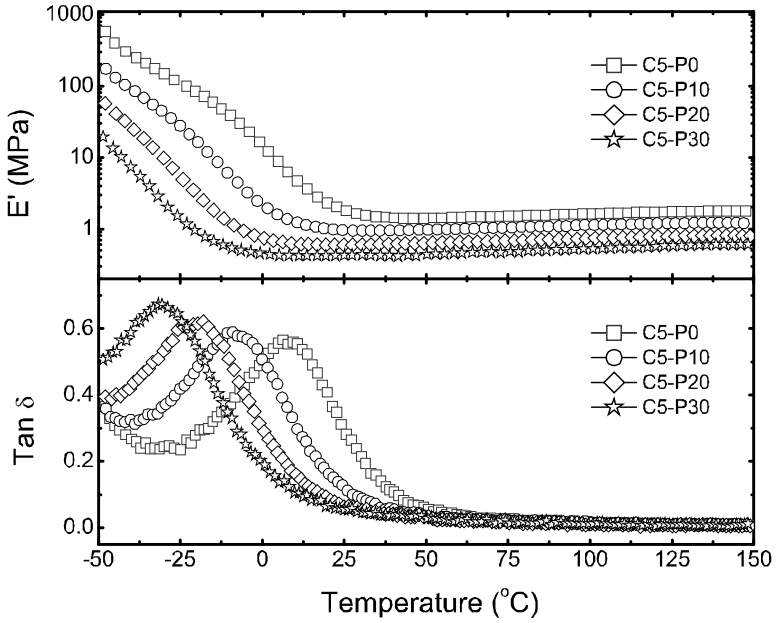

Figure 2-10. (*Top*) Storage modulus and (*Bottom*) loss factor of UV-DE with different plasticizer concentrations.

Another important improvement of using plasticizers is the lower T_g. As shown in Figure 2-10, T_g, defined by the peak of mechanical loss factor, has shifted from 7.8 ^oC for C5-P0, to -30.5 ^oC for C5-P30. Because of the free volume increase in plasticized materials with lower T_g,[117] a number of mechanical properties have been tuned. The storage modulus at 25 ^oC decreased from 1.8 MPa of C5-P0 to 0.4 MPa of C5-P30. The loss factor at 25 ^oC decreased from 0.28 for C5-P0 to 0.05 for C5-P30, which is much lower than that of VHB4905 (0.64 at 25 ^oC) and comparable with most of silicone elastomers (0.06 for CF19-2186).[10] The electromechanical frequency response is a complex process that involves the loss factor, modulus at small strains, and the non-linear modulus change as the material is stretched. Although more comprehensive studies are still being carried out, the improvement in loss factor and modulus at small strains already demonstrates that plasticizing with DBEF is promising for improving the electromechanical frequency response of UV-DE materials.

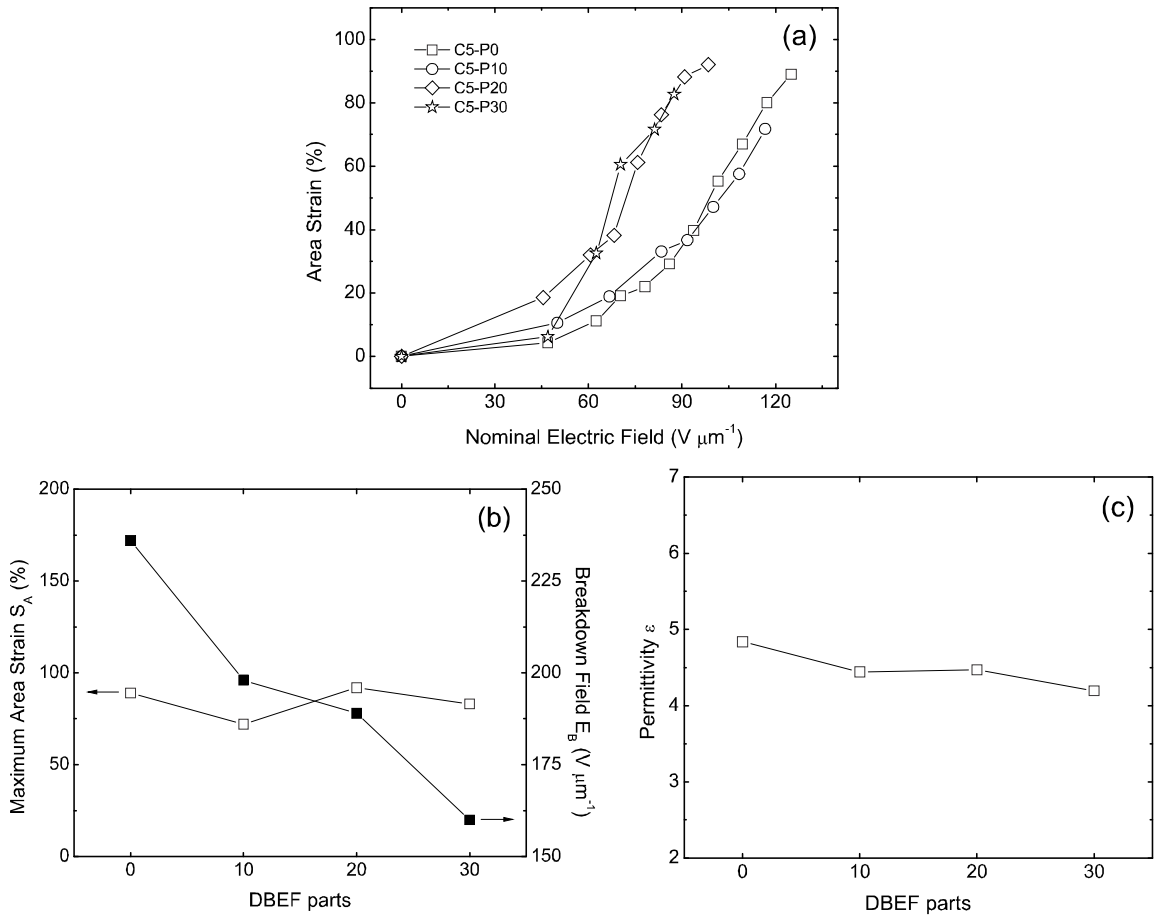

Figure 2-11. (a) Electromechanical strain versus applied electric field relationships, (b) maximum electromechanical strain (□) and breakdown field (■), and (c) permittivity of UV-DE with different plasticizer concentrations.

Figure 2-11 shows the permittivity measurement and electromechanical actuation performance of plasticized UV-DE with a high crosslink density. As the plasticizer concentration increases the permittivity is seen to decrease slightly, from 4.84 in C5-P0 to 4.19 in C5-P30. While the mobility of chain segments is improved, no overall permittivity improvement was observed, due to the non-polar nature of the network structure. A larger strain can be achieved under a given nominal electric field, especially when the plasticizer concentration is above 20 parts per 100 parts of resin. The achievable maximum area strain remains around 90%, while the

breakdown field remains high, but decreases gradually from 236 V μm^{-1} in C5-P0 to 160 V μm^{-1} in C5-P30. The lower stiffness in the plasticized materials results in a more sensitive strain response to electric field. At the same time, the small DBEF molecules also lead to a reduced resistivity in the material, which results in a higher leakage current during the actuation and a lower breakdown strength.

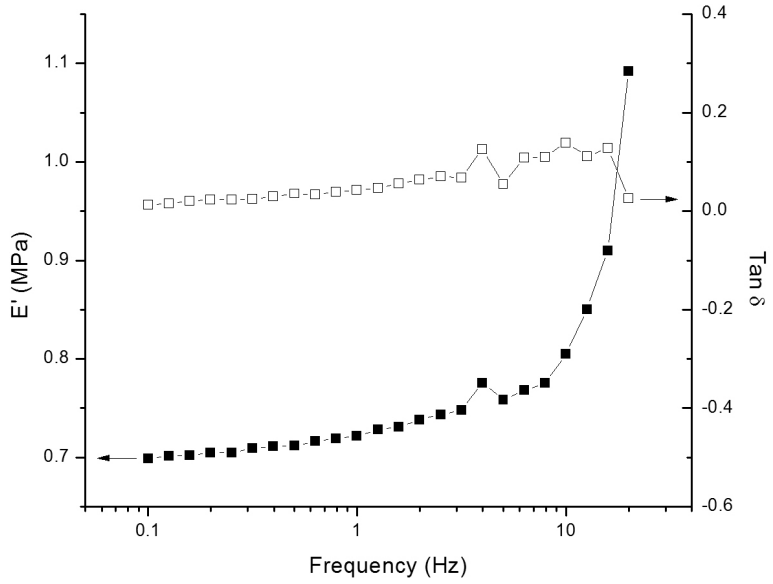

Figure 2-12. Modulus and loss factor change of C5-P20 along with frequency.

The response of the material to an externally introduced strain reflects its viscoelasticity. Figure 2-12 shows the measurement of storage modulus and loss factor changes along with frequency. The modulus of C5-P20 slightly increases from 0.7 MPa at 0.1 Hz, to around 0.8 MPa at 10 Hz. After that rapid increases can be observed. The loss factor does not change significantly over the whole range. Compared to VHB 4905 ($\delta = 0.642$ at 1 Hz), the loss factor of C5-P20 is much lower, which indicates the viscoelasticity has been reduced in C5-P20.

2.6 Energy Density

The maximum energy density of UV-DE is calculated based on the maximum thickness strain s_z, breakdown field E_B, and permittivity ε of the material,[10] as in Equation (4).**Error! Reference source not found.** To maximize the achievable energy density, an improvement in all three parameters is preferred. By increasing the crosslink density, the permittivity does not change too much, the maximum strain is limited, while the breakdown field is improved. As a result of the balancing of these parameters, the energy density shows the complex trend in Figure 2-13(a). The effects of increasing breakdown field and decreasing strain balance out in materials with up to 3 parts of HDDA. After that, the improvement of breakdown field overweighs and the energy density increases. The formulation C5-P0 stands out with a maximum energy density of 1.51 MJ m^{-3}. Note that this number is achieved with no external prestretching applied. By plasticizing, the maximum strain does not change due to the limitation of mechanical stiffening. The breakdown field decreases while the permittivity remains. The energy density generally decreases due to the sacrificed breakdown strength. (Figure 2-13(b))

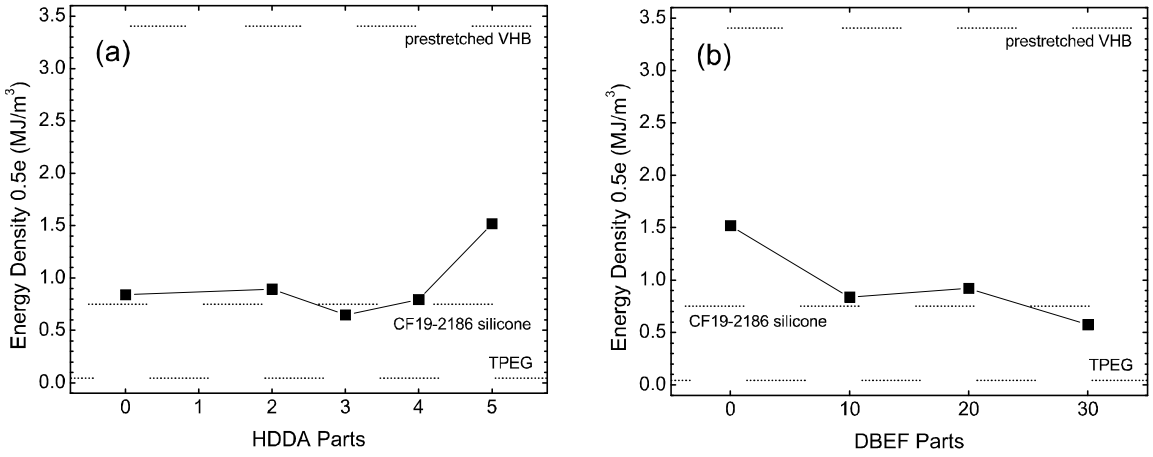

Figure 2-13. Energy density of UV-DE with different (a) crosslinker (no plasticizer) and (b) plasticizer (HDDA kept at 5%) concentrations.

2.7 Multilayer actuator demonstration

With the objective of making prestrain-free linear actuators in mind, we spin coat and cure multiple C5-P20 layers and spray coat electrodes alternatively. Figure 2-14 shows a general look of a fabricated multilayer stack actuator. It has 10 active C5-P20 layer spin coated at 800 rpm for 18 s. Two encapsulation layers were spin coated with the same material at 3000 rpm for 18 s to protect the device from scratching and arcing. The electroded area has a diameter of 3/16" and a 1/32" wide passive area is given when die-cutting the device. Electrical contacts are made from the side with aluminum foil and carbon grease. The device is then attached to a cantilever so that the laser displacement sensor can record the displacement from above. The passive area and contact with the cantilever are made minimum to avoid sacrificing the actuation strain.

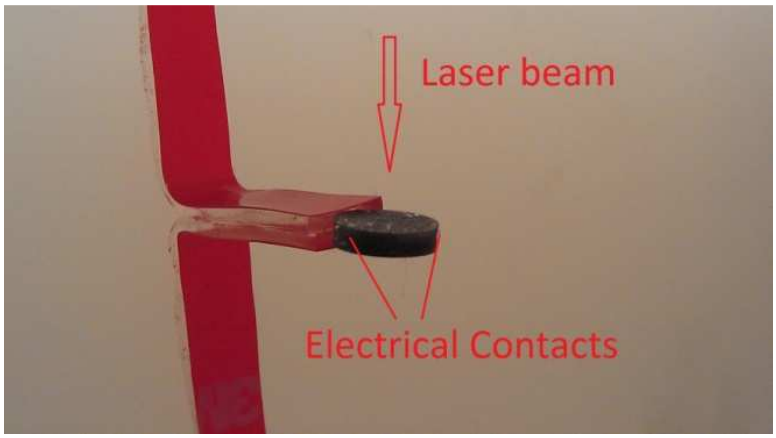

Figure 2-14. A typical multilayer stack linear actuator. The device is attached to a piece of adhesive tape to keep freestanding during the actuation strain measurement.

Actuation performance of the fabricated actuators are shown in Figure 2-15. At 0.1 Hz, a maximum displacement of 0.12 mm can be measured at 5000 V (Figure 2-15(a)). The strain can

almost relax to zero at this frequency without significant creeping. Considering the overall thickness of the device, the maximum strain at 5000 V is 11.1%. The maximum driving voltage is higher than that of the buckling type actuator, since we have to coat thicker active layers to minimize the number of defects. This problem will be resolved in future by making the devices in a cleaner environment. Similarly as in the buckling actuators, the strain increases non-linearly along with driving voltage in the linear actuators as shown in Figure 2-15(b). Note that the displacement is only measured from one side of the freestanding actuator. Ideally, the total displacement or strain should be twice as large, since both free ends can move. This will be proven in our on-going study with two laser displacement sensors measuring simultaneously from both sides.

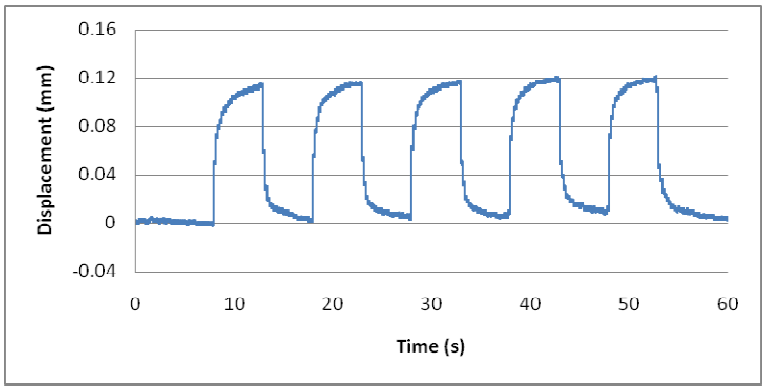

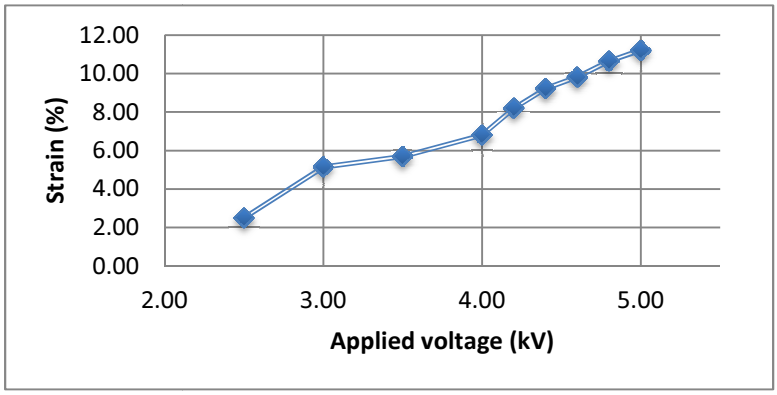

Figure 2-15. (a) Vertical displacement versus time of a 10-layer linear actuator. Tested at 5000 V, 0.1 Hz. The overall thickness of the device is measured 1.08 mm; (b) Vertical displacement versus driving voltage, 5th cycle tested at 0.1 Hz.

2.8 Conclusions

In conclusion, we have synthesized a new category of dielectric elastomers, UV-DE, via UV curing of a formulated precursor solution. By controlling the mechanical and electromechanical properties via the amount of crosslinkers, the elastomers can be customized to achieve an electromechanical strain of 314%, or a maximum breakdown field of 236 V μm^{-1} with a fully suppressed EMI. By introducing plasticizers, the T_g of elastomers is decreased making the elastomer softer and less viscoelastic for improved strain sensitivity and better frequency response. No prestretching is needed in any of these new elastomers to achieve the peak performance. The experimental results are consistent with the thermodynamic model. The stiffening of the elastomers via crosslinking is found critical in optimizing the electromechanical actuation performance. The results here should point to experimental approaches to synthesizing new, improved dielectric elastomers by design. Ease of fabrication in multilayer stack dielectric elastomer actuators can be expected with the application of this new material.

Chapter 3 Performance Improvement of Bi-Stable Electroactive Polymers

3.1 Background of the study

The ability of materials to respond to external stimulations is always considered useful and has broad applications. Dielectric elastomer falls in the "smart material" category. However, one limitation of DE is that, the low modulus of the material cannot provide enough support to the applied load. The high driving field has to be applied at all times to keep the large strain generated. Current will be constantly drain from the external power source. Also there will be safety concerns when used in consumer electronics. Bistable electroactive polymer (BSEP) is developed to provide a solution to this problem. A BSEP is a multifunctional polymer material that combines the electrically induced large strain actuation of dielectric elastomers and the bistable deformation of shape memory polymers. BSEP may find applications in tactile displays, adaptive structures, and biologically-inspired robots.[118–120]

3.1.1 Mechanism

A BSEP polymer has a glass transition temperature (T_g) above room temperature. The basic structure of a BSEP actuator consists of a BSEP thin film coated with a pair of compliant electrodes on opposing surfaces.[118,119] When heated to above T_g, it behaves as a rubbery dielectric elastomer and can be actuated to a temporary shape by Maxwell stress in a high electric field.[10] The actuation is fast and reversible at the elevated temperature. The deformed shape can be made meta-stable by cooling the polymer to below T_g while the Maxwell stress is maintained. The cooled shape is rigid and will maintain its shape whether the applied field is kept, changed, or removed, until the polymer is heated again to recover to its original shape.

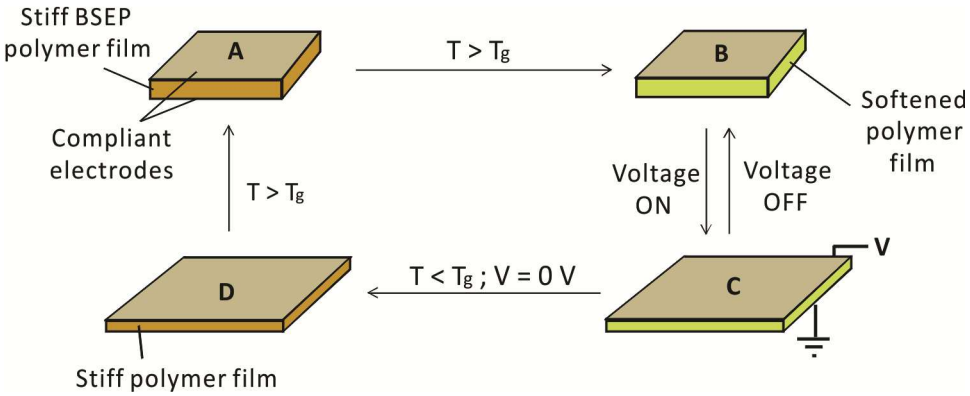

Figure 3-1. BSEP Mechanism

With BSEP rigid-to-rigid deformation can be achieved with a lower energy consumption. Assumption is made that 0.1 mm3 BSEP material is considered, with similar density and heat capacity with polyethylene terephthalate (PET), which are 1.39 g/cm^3 and 2.17 J/(g ^{o}C) separately. A common Young's modulus of the BSEP polymer is about 1 GPa at room temperature and 1 MPa at above T_g. To directly deform the BSEP material in its glassy state to 100%, the Maxwell pressure needed is around 500 MPa and the energy density is 346.6 MJ/m^3, according to Equation (1) and (4) in Chapter 1. The total energy consumed will be 36.2 mJ. Note that in practice, the rigid polymer would fracture at strains much smaller than 100%. In the case of BSEP, the material is firstly heated to above T_g, for instance 70 ^{o}C, and then actuated by Maxwell pressure at rubbery state. The energy density needed is only 0.404 MJ/m^3 and total electrical energy consumption is only 0.041 mJ. The thermal energy consumption is 13.5 mJ under a 100% heat transfer efficiency assumption. Totally, the ideal energy consumption via BSEP is less than one half of that needed to deform a rigid polymer directly.

3.1.2 Material improvements

To achieve high performance BSEP actuation, both material properties and device structures have to be investigated. Typical material properties related to BSEP include dielectric strength, modulus at rigid and rubbery state, glass transition temperature, viscoelasticity, etc. They will determine the theoretical limitation of the performance. Device structure engineering can give solutions to other practical issues such as heat transfer efficiency, stability, and so on. In this chapter fundamental material issues will be addressed. Fabrication of an efficient BSEP device will be discusses in detail in Chapter 4.

An ideal BSEP film at room temperature is rigid, with an elastic modulus greater than 100 MPa to support load as a structural material. In the rubbery state, its elastic modulus must be smaller than 10 MPa to obtain large Maxwell strain. Most dielectric elastomers have moduli on the order of 1 MPa to produce Maxwell strains as high as 100% or larger. Similar with DE, the strain is inversely proportional to modulus, and becomes non-linear at larger strains.[10,37] The BSEP film also needs to have high dielectric strength to support electric fields greater than 100 MV/m. With a typical dielectric constant of 3 for elastomers,[37] 100 MV/m produces a stress of 266 kPa. Also low viscoelasticity in the rubbery state can lower the internal friction and ensure a large number of stable actuation cycles.

Poly(tert-butyl acrylate) (PTBA) has been synthesized previously to demonstrate the concept of BSEP.[118,119] T_g of this material is around 45℃ (defined as the point where Young's modulus begins to drop). At ambient conditions it is a rigid thermoplastic and has a Young's modulus of around 1GPa. When heated to 70℃ the material behaves like a dielectric elastomer and has a Young's modulus of 0.7MPa. This transition temperature is too high for some specific applications. For example, for haptic displays users do not want to touch a device

that is at a temperature much higher than their body temperature. Additionally, a lot of energy is consumed in the heating process and the required time to heat the polymer to its elastomeric state is too long for most applications.

The actuation in linear thermoplastic PTBA is rather unstable at strains greater than 100%. Two factors were considered responsible to the instability. One stems from the thermoplastic nature of the polymer. The physical crosslinks responsible for the rubbery elasticity in PTBA above 60 °C are nanocrystalline domains of various sizes and melting temperatures around 190 ^{o}C.[119,121] As such, the modulus changes rapidly with temperature. Temperature fluctuation and non-uniformity will cause localized over-actuation and dielectric breakdown. Electromechanical instability (EMI, or pull-in effect) is another factor that often causes the breakdown field of a dielectric to appear substantially lower than its intrinsic dielectric strength, especially in dielectric elastomers without prestrain.[23,29] The origin of the pull-in effect is that, above a threshold field during constant voltage operation, a soft actuator film will be driven thinner and thinner until the local electric field exceeds the dielectric strength of the film.[37] The threshold voltage is lower than the dielectric strength and is dependent on the polymer's hyperelastic stress-strain response.

3.1.3 Scopes

Plasticizers were first added to linear thermoplastic PTBA to bring down its glass transition temperature. The amount of plasticizers is controlled so that with a lower T_g of 45 ^{o}C, the modulus at room temperature is still high enough to support the actuator to maintain its shape after a strain larger than 300%.

Another method was used to overcome the EMI in PTBA so that a stable actuation can be achieved. BSEP polymer composed of interpenetrating networks of chemically crosslinked PTBA was synthesized instead of using linear thermoplastic PTBA.[122] Elongation of the first network to overcome EMI is obtained by swelling, instead of mechanical stretching. The resulting PTBA-IPN membranes exhibit a stable modulus above the glass transition. EMI is effectively suppressed during actuation. Electromechanical strain as large as 228% in area expansion has been obtained at the rubbery state, with a breakdown field of 194 MV/m, a Maxwell stress of 2.2 MPa, and a calculated specific energy density of 2.65 MJ/m^3. The actuation is stable: no dielectric breakdown is observed during continuous application of a constant voltage at 150% strain for over 4 hours. The bistable actuation of this material has been utilized to fabricate arrays of BSEP diaphragm actuators. The technology is promising for the application of refreshable Braille readers.

3.2 Experimental

3.2.1 Chemicals

Tert-butyl acrylate (TBA), 2,2-Dimethoxy-2-phenylacetophenone (DMPA) and toluene were purchased from Sigma-Aldrich and used as received. Dibutoxyethoxyethyl formal (DBEF, SR660), CN9021 acrylic resin and ethoxylated trimethylolpropane triacrylate (SR9035) were obtained from Sartomer Company and used as received. CN9021 is a difunctional acrylic ester resin for UV/EB-cured laminating and pressure-sensitive adhesives.

3.2.2 Film Preparation

Thermoplastic PTBA was synthesized by UV initiated free radical polymerization under a 365 nm UV lamp with a 100W mercury bulb set at 3" above the monomer solution. The polymer was dissolved in toluene to make solutions with the proper viscosity to cast films of the desired thickness. DBEF plasticizer was added into the solution in different weight percentages (0%, 2%, 5%, and 10%) to adjust the glass transition temperature of the polymers. Films were drop-cast on clean, leveled glass substrates. After the solvent evaporated, the polymer films on glass substrates were annealed at 80℃ overnight. The polymer films were peeled off with care from the glass substrates and dried before use.

PTBA-IPN films were fabricated in a different way. A typical procedure for the preparation of PTBA-IPN-50 is as follows: A first monomer solution consisting of 100 parts (by weight) of TBA, 15 parts of CN9021, 3 parts of SR9035, and 1 part of DMPA was prepared. The solution was coated on a glass substrate and covered with a second sheet of glass. A spacer was used to define the thickness of the liquid layer. The monomer solution was cured under a 365 nm UV lamp with a 100W mercury bulb set at 3" above the monomer solution. After 15 min exposure, the cured membrane (first network) was peeled off and immersed in the second monomer solution consisting of 100 parts of TBA, 3.5 parts of SR9035, 1 part of DMPA, and 50 parts of toluene. After 60 min of soaking, the swollen membrane was sandwiched between two glass sheets and cured with the same UV lamp setup for 45min. The cover glass was then removed. The IPN membrane was post-cured on a hot plate at 130℃ for 60min. The resulting membrane, PTBA-IPN-50, was allowed to cool down to room temperature, and then peeled off of the glass substrate as a freestanding thin rigid sheet. The fabricated films are referred to as PTBA-IPN-X,

wherein X is the parts by weight of toluene in the second monomer solution relative to 100 parts of tert-butyl acrylate.

3.2.3 Mechanical Tests

Mechanical properties of the membranes were tested on a TA Instruments RSAIII dynamic mechanical analyzer. Samples for dynamic tests had a dimension of 10 mm width, 80 μm thickness and 25 mm total length. Dynamic temperature ramp test was done at 5℃/min, 1Hz frequency and 1% strain. Samples for tensile tests at 70℃ were 6 mm long and 5 mm wide and had various thicknesses. The extension rate for tensile test was 1 mm/s.

3.2.4 Actuation Tests

Actuation tests were carried out on a diaphragm chamber with an air pressure of 5 Torr (0.1 psi). The active areas when flat (before actuation) was circular with 0.25” diameter. Carbon grease was smeared on as the compliant electrodes. An environmental chamber from Thermotron was used to control the temperature between ambient and 70°C. A high voltage power supply fabricated in house was used to drive the actuators. A power resistor with 10MOhm, 5W was connected in serial. A digital camcorder was used to record the actuation process. The actuation strain was measured from the video frame-by-frame. The area strain was calculated by the equation already reported.[99] The steady-state strain values after 1 min of actuation at a constant voltage was recorded as the strain for that voltage and the calculated electric field. In lifetime tests, a Keithley 2000 digital multimeter was connected in serial to record the current.

3.2.5 Dielectric Tests

The capacitance of the actuators was measured with an LCR meter at 1kHz and used to calculate the materials' dielectric constants.

3.3 Thermoplastic linear polymers with plasticizers

3.3.1 Mechanical property

Figure 3-2 shows the storage moduli and loss factors measured as a function of temperature for the BSEP samples with different plasticizer content. One can clearly observe that the glass transition temperature (defined by both the onset of the storage modulus drop and the loss factor peak) shifts towards a lower temperature with an increase in the amount of DBEF plasticizer. The high moduli around 1GPa in all five samples at low temperatures suggest that the plasticizer has a limited effect on the rigid glassy state of PTBA. In other words, as long as the temperature is below Tg, no matter how much plasticizer there is in the polymer, the BSEP will retain its rigidity and shape bistability. On the other hand, the moduli in the rubbery states are lowered significantly by the addition of plasticizer. This means that, if actuated at this temperature without dielectric breakdown, the stain of PTBA with 5% DBEF will be 100% larger than intrinsic PTBA. The addition of the plasticizer has the additional benefit of allowing us to tune the stiffness of the polymer over a relatively wide temperature range. If we assume the ideal storage modulus to actuate the BSEP is 0.7MPa, then we can tune the amount of plasticizer to obtain different operating temperatures that meet the requirements of a particular application.

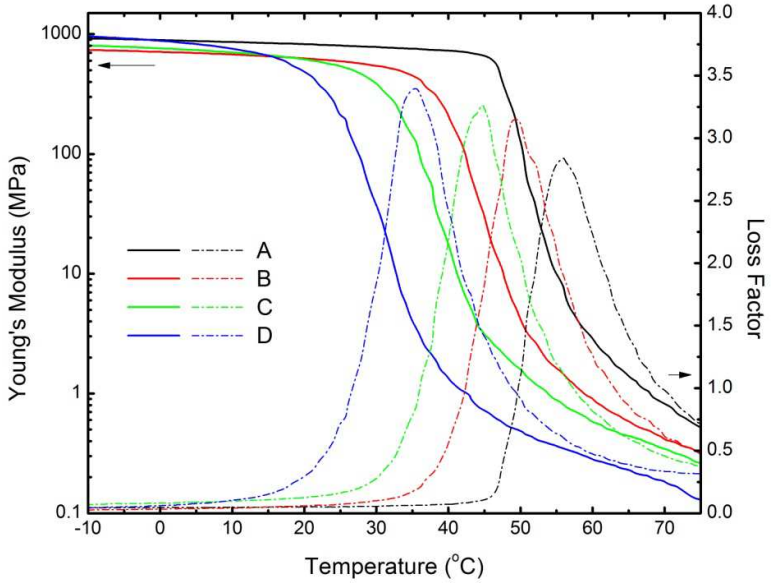

Figure 3-2. DMA results of plasticized PTBA: (A) 0%, (B) 2%, (C) 5%, (D) 10%. Solid lines show Young's moduli and dash dot lines show loss factors of various samples.

3.3.2 Field-Strain

Figure 3-3 shows the dielectric actuation of plasticized PTBA at a particular temperature of 45℃ Materials were actuated to high strain levels and made bistable by cooling down to room temperature quickly with a fan and subsequently removing the driving voltage. The largest strain around 560% of sample D at 145V/μm is shown in the lower left inset. The shape fixities of all samples were close to 100%, which means no significant shrinkage occurred after the removal of the actuation voltage. The experimental results follow a parabolic fit as expected from Maxwell force induced actuation. Data points at high strain levels are offset from the parabolic fits primarily due to the discontinuity of the compliant carbon grease electrode and the increased modulus of materials at high strain levels. At this temperature, because of the tuned Tg values of the plasticized films, Young's moduli of these materials show significant differences. Pure PTBA remains rigid and shows negligible E-field induced strain at very high electric fields while

PTBA with 10% DBEF plasticizer can expand to 200% strain at only 50V/μm. Note that the strain is bistable in all cases. This tunable actuation capability provides a potential method to produce a smart system that possess several bistable states, allowing the device to transition between shapes at various temperatures with shape changes localized to one or more regions depending on the temperature.

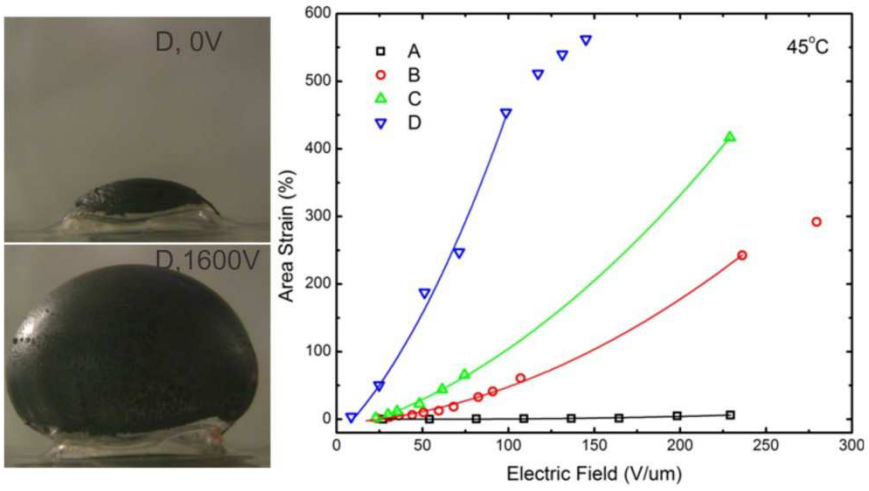

Figure 3-3. (*Left*) When heated up above Tg, the BSEP film with 10% DBEF plasticizer (73μm thick) can be actuated to 580% strain at 1600V (*bottom*) from initial state (*up*) and maintain that shape after sequentially cooling the film to ambient temperature and removing the actuation voltage. When reheated to above Tg, the thin film recovers its originally shape.; (*Right*) Dielectric actuation of DBEF plasticized PTBA thin films at 45℃: (A) 0%, (B) 2%, (C) 5%, (D) 10%. Solid lines show parabolic fittings of experimental results.

3.4 BSEP interpenetrating networks

3.4.1 Methodology

The fabrication process of the PTBA-IPN is illustrated in Figure 3-4. In a typical procedure, a crosslinked PTBA membrane, the first network, was prepared by UV initiated free radical bulk polymerization of a liquid membrane consisting of tert-butyl acrylate, a crosslinker, and a

photoinitiator. The cured membrane was immersed in a solution containing tert-butyl acrylate monomer, crosslinker, photoinitiator, and toluene as the solvent. After the membrane had swollen to a gel-like state, it was placed on a glass substrate and cured under UV exposure. The membrane was then thermally annealed to remove residual monomer and solvent, and to increase the crystallinity of the polymer to enhance mechanical rigidity at room temperature and elasticity in the rubbery state. The resulting PTBA-IPN membrane was peeled off from the glass substrate. We refer to the resulting membranes as PTBA-IPN-X wherein X is the parts by weight of toluene in the second monomer solution relative to 100 parts of tert-butyl acrylate. Formation of the second network can be confirmed by a weight increase of 380% in PTBA-IPN-0, 371% in PTBA-IPN-10, 263% in PTBA-IPN-50, and 157% in PTBA-IPN-100.

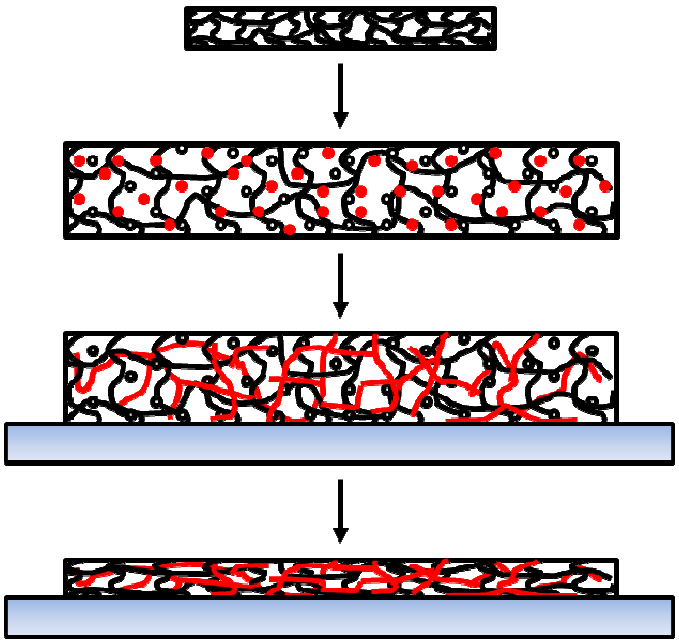

Figure 3-4. Schematic illustration of fabrication process of a PTBA-IPN membrane. The first UV-cured PTBA network is swollen in a second monomer solution with solvent. The second monomer is then UV cured, followed by thermal annealing on a glass substrate.

3.4.2 Swelling Characterization

Figure 3-5(a) shows the geometrical changes of a PTBA-IPN-50 in the various steps of the fabrication process. The membrane was first isotropically swollen by 228% in area and 80% in thickness. The swelling ratio *Q*, defined as the swollen volume divided by the original volume, was 5.9. The swelling ratio is determined by the chemical crosslinking density of the polymer and remains the same for good solvents and their mixtures.[113] After the formation of the second network, the membrane was anisotropically dried and annealed, with the change of the in-plane area being constrained due to adhesion between the membrane and glass substrate, while the thickness was relatively free to contract. The thickness shrank by 25% largely due to the removal of solvent. After the membrane was peeled off the substrate, no in-plane shrinkage was observed. Reheating the free-standing PTBA-IPN membrane caused slight area shrinkage (-15%) and thickness expansion (18%). Overall, the free-standing membrane is composed of a highly tensioned first network (176% in area, 62% in thickness) and compressed second network (-16% in area and -12% in thickness). The two networks are internally balanced, similar to the IPN dielectric elastomers we previously reported.[89] The existence of stress balance inside the IPN was further evidenced by the wavy surface morphology formed in cases where the second network was only partially cured..

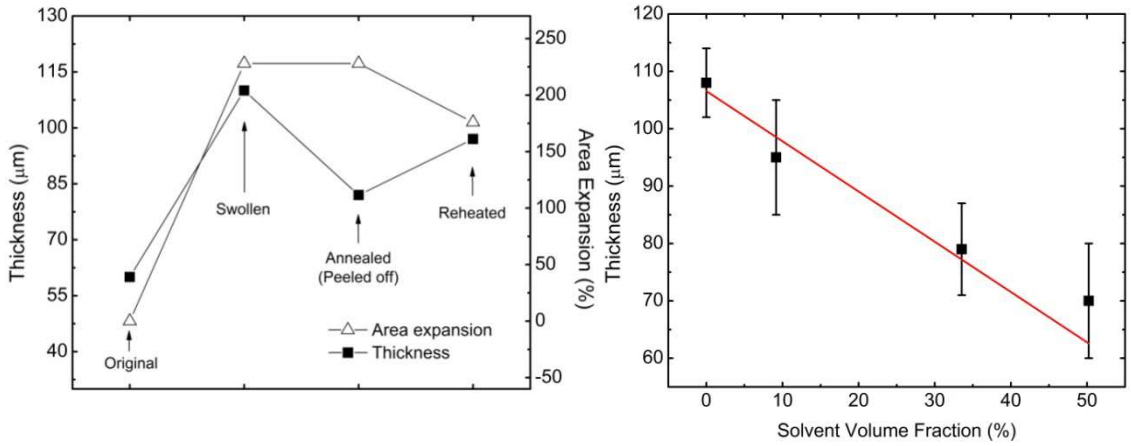

Figure 3-5. (a) Thickness and area of a PTBA-IPN-50 membrane during the various fabrication stages; (b) Thicknesses of PTBA-IPN membranes after annealing as a function of the volume fraction of toluene in the swelling solvents. Solid line is derived from Equation (1).

If one assumes that mixing of solvent occurs without an appreciable change in the total volume of the gel,[113] the final thickness of the PTBA-IPN membrane is correlated to the solvent concentration as:

$$t_a = t_0 Q^{\frac{1}{3}} - t_0 \left(Q^{\frac{1}{3}} - Q^{-\frac{2}{3}} \right) x \qquad (9)$$

where t_a is the thickness of the annealed membrane, t_0 the thickness of the first network before swelling, Q the swelling ratio, and x the volume fraction of the solvent. This linear relationship is shown in Figure 3-5(b), wherein the experimental data are in good agreement with the theoretical predictions. The loss of both the monomer and solvent due to evaporation can cause a slight variation of the experimental results. This equation can also be used to control the thickness of the resulting membranes during experimental designs.

3.4.3 Shape Memory Behavior

The PTBA-IPN membranes are rigid at room temperature and optically clear. The shape memory property is shown in Figure 3-6 for a freshly prepared PTBA-IPN-50, being heated, stretched to 100% linear strain then cooled down, and reheated. The material exhibits a shape fixity of 100% and shape recovery >98%.

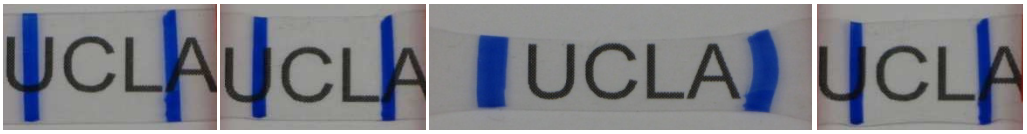

Figure 3-6. (a) A PTBA-IPN-50 membrane freshly made (distance between the blue markers are 25 mm) , (b) heated at 70°C, (c) stretched by 100% in the horizontal direction and then cooled to room temperature, and (d) reheated for 10s at 70°C.

3.4.4 Mechanical Property

Dynamic mechanical analysis shows that PTBA-IPN-50 is glassy up to 45 °C, with a room temperature storage modulus of approximately 1 GPa. (Figure 3-7) The glass transition occurs in the temperature range of 45-70 °C. The peak of the loss factor (tan δ), the ratio of loss modulus to storage modulus, is at 52 °C. This T_g is slightly lower than that of PTBA likely due to the presence of the crosslinker co-monomer (Sartomer CN9021) which forms a soft sticky polymer on its own when cured. The rubbery state exhibits a relatively stable storage modulus, 0.8-1.0 MPa from 70 to 120 °C. The stable modulus is considered to be the combined results of ideal rubber behavior whose shear moduli increases proportionally with absolute temperature and the continuous melting of nanocrystalline domains of PTBA which lowers the modulus with temperature. For comparison, PTBA has a rapidly descending storage modulus in the rubbery

state, being 0.8 MPa at 70 °C, 0.25 MPa at 100 °C and 0.1 MPa at 120 °C. The tan δ of PTBA-IPN in the rubbery region is substantially lower than that of PTBA, indicative of lower viscoelasticity and faster actuation response. Samples with different solvent compositions (X values) have very similar dynamic mechanical responses.

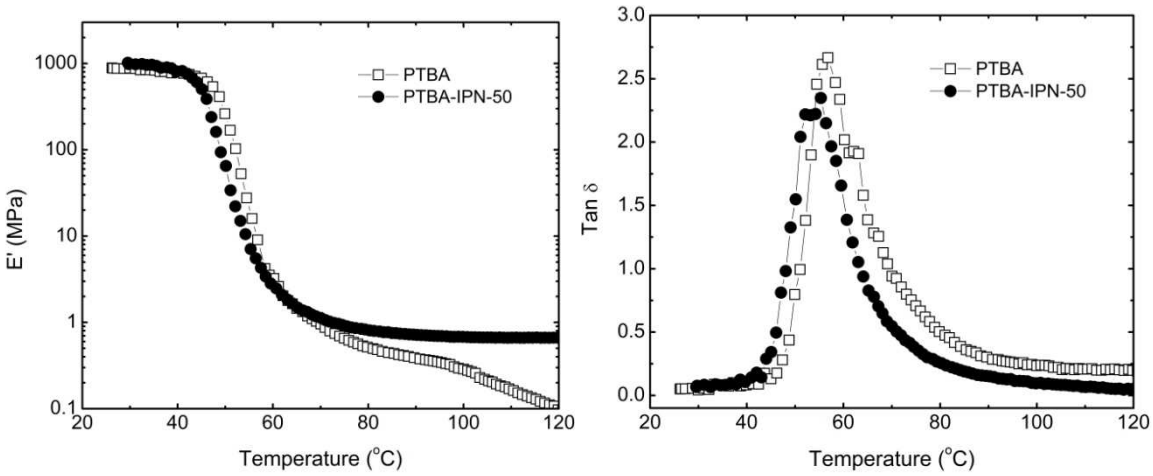

Figure 3-7. (a) Storage modulus versus temperature and (b) loss factor versus temperature of PTBA and PTBA-IPN-50 membranes.

The hyperelasticity of PTBA-IPN at the rubbery state was characterized via uniaxial stretch tests at 70°C. (Figure 3-8) The control sample, PTBA, has a maximum elongation of more than 1100% in the rubbery state (not shown in the figure), though its tensile strength at break is only 0.68 MPa. It lacks the rapid rise of stiffness at high strains to suppress EMI. Chemically crosslinked PTBA membranes consisting of only the first network has an improved tensile strength of 2.2 MPa and a reduced tensile elongation at break of 307%. PTBA-IPNs exhibit even higher tensile strengths while maximum elongations are further lower. The tensile strength and elongation at break are 5.8 MPa, 284% and 5.7 MPa, 215% for PTBA-IPN-0 and PTBA-IPN-50, respectively. The first order derivative of the stress with respect to strain measures how fast the

stress increases with strain, i.e. the "pseudo" Young's modulus at specific hyperelastic strains.[99] At the tensile break point, the pseudo Young's modulus is 0.03, 2.95, 3.21, and 6.06 MPa for PTBA, crosslinked PTBA, PTBA-IPN-0, and PTBA-IPN-50, respectively. Introducing the interpenetrating polymer network enhances the stiffness of the polymers. In the case of PTBA-IPN-50, the pseudo Young's modulus increases from 0.80 MPa at 1% strain, to 1.05 MPa at 100%, 5.10 MPa at 150%, and 6.06 MPa at 215%. The rapid rise of stiffness in the strain range of 100-150% is particularly interesting for overcoming the EMI during large-strain actuation.[23,37,99] The stiffness increase in PTBA-IPN can be explained by the slip-tube model suggested by Robinstein and Panyukov. [115,116] Chemical crosslinking and the addition of the second network increase the entanglement between chain segments, leading to a limited chain slippage and increased stiffness. The removal of solvent in PTBA-IPN-X during the formation of IPN morphology anisotropically compresses (or deswells) the network in the thickness direction. The extra chain length in thickness direction will be pushed out into the in-plane direction and further increases the stiffness in the in-plane direction. Another reason for the stiffness increase in anisotropically deswollen networks could be the alignment of network strands during solvent evaporation that makes the system easier to crystallize.[123]

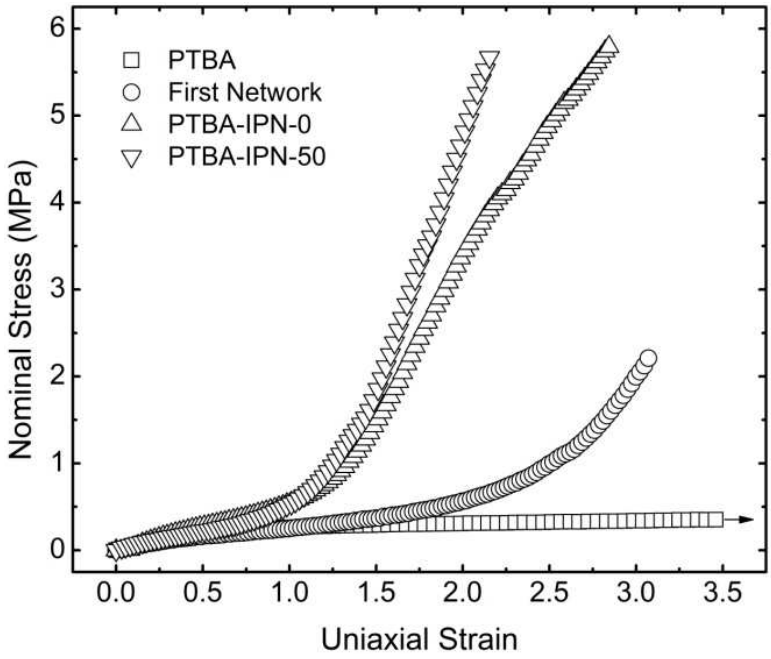

Figure 3-8. Tensile stress-strain response of PTBA and PTBA-IPN membranes till break at 70°C.

3.4.5 Field-Strain

As a good BSEP material, the PTBA-IPN membranes must be able to generate large strains under an external electric field. This large strain should be stable at the instant when a driving voltage is applied and endure when the high field is kept on. Figure 3-9 shows the strain-field curve of PTBA-IPN-50 in comparison with PTBA. The maximum area strain is 228% at a breakdown field of 194 MV/m, while PTBA break down above 50% strain and 45 MV/m. This observed breakdown field of PTBA is considerably lower than that of prestrained PTBA.[118] PTBA-IPNs with various solvent compositions show similar dielectric actuation characteristics. This could be due to the similar total crosslink densities combining both chemical and physical crosslinking in these materials. No significant strain snap-through or ballooning[89] was observed during constant voltage actuation. All intermediate strain states below the maximum strain can be stably obtained. The actuation is fully reversible and repeatable.

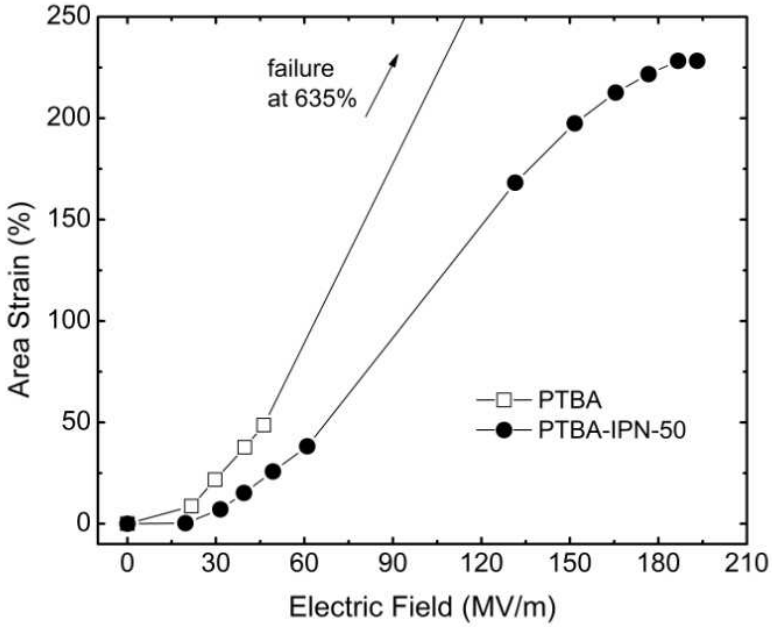

Figure 3-9. Actuation strain vs applied field for PTBA and PTBA-IPN-50 membranes at 70°C.

3.4.6 Actuation current

Figure 3-10 shows the current and strain profiles during the actuation of PTBA-IPN-50 and PTBA membranes at constant driving voltages. The PTBA membrane is driven by a constant voltage to produce an initial electric field of 34 MV/m. The strain gradually increases with time, a viscoelastic behavior, and snaps through after strain reaches 50% at 0.45min. The active area rapidly expands up to 427% strain while the actuation current spikes. The membrane momentarily dielectrically breaks and mechanically ruptures. This is a characteristic EMI behavior.[124] The PTBA-IPN-50 membrane is driven at an initial electric field of 50 MV/m. The strain gradually increases with time, from 75% to 165% in 3 min. Thereafter, the strain is fairly stable, with slight decreases after 10 min until 240 min when the membrane ruptures. The strain at breakdown is 147%. The lifetime (240 min) is more than 500 times longer than that of

PTBA (0.45min). PTBA-IPN-50 membranes do not exhibit snap-through, or EMI instability. The actuation current during the actuation is less than 2μA before it spikes at breakdown.

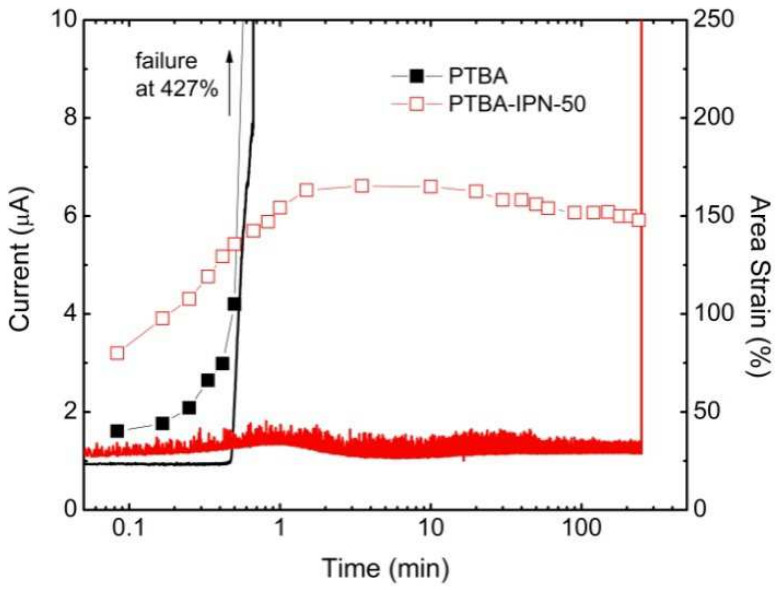

Figure 3-10. Actuation current and area strain during continuous actuation at constant voltages.

3.4.7 Energy density

Actuation energy density directly measures how much work an actuator can perform in each cycle. Table 3-1 lists the calculated energy density, along with other important properties of PTBA-IPN-50 in comparison with selected dielectric elastomers. The permittivity of PTBA-IPN-50 in the rubbery state (ε=6.6@1kHz) is higher than at room temperature (ε=4.5@1kHz). This is likely caused by eased dipole orientation of polar bonds and chain segments at elevated temperature.[125] The large permittivity, as well as the relatively high breakdown field, leads to a large Maxwell stress of 2.2 MPa. The calculated specific energy density is 2.65 MJ/m^3, which is lower than VHB 4910 but higher than most of the other dielectric elastomers.

Table 3-1. Material properties of PTBA-IPN in comparison with common dielectric elastomers

System	Storage Modulus [MPa]	Max. Areal Strain [%]	Max. Thickness Strain [%]	Breakdown Field [MV/m]	ε [1kHz]	Maxwell Stress [MPa]	Energy Density [MJ/m^3]
VHB 4910 [10]	1-3	158	61	412	4.8	7.2	3.4
HS3 silicone [10]	0.2	93	48	110	2.8	0.3	0.098
CF19-2186 silicone [10]	1	64	39	350	2.8	3	0.75
SEBS161 (30%) [80]	0.163	30	22	109	2.2	0.231	0.151
PTBA-IPN-50 (70 ^{o}C)[122]	1	228	70	194	6.6	2.2	2.65

3.5 Conclusions

In conclusion, DBEF plasticizer was added to linear thermoplastic PTBA to reduce the glass transition temperature without damaging other shape memory or electromechanical properties. Interpenetrating network structure was introduced into BSEP. Swelling has been shown to be an effective approach to synthesizing interpenetrating networks of chemically crosslinked PTBA composed of two internally balanced tension-compression networks. The IPN system formed after deswelling exhibits a hyperelastic stress-strain response with rapid rise of stress in the 100-150% strain range. The rapid stiffening is necessary to overcome electromechanical instability

and obtain stable large actuation strains. The IPN preserves the shape memory property of neat PTBA with a slightly reduced glass transition temperature due to the introduced crosslinking chain. The PTBA-IPN membranes exhibit a high breakdown electric field of 194 MV/m and stable actuation strains as large as 228% at 70°C. The electrically induced strains can be preserved, or "frozen" when the membranes are allowed to cool to ambient temperature, with 97% strain fixity.

Chapter 4 Design of a refreshable Braille electronic reader based on BSEP polymers

4.1 Background

4.1.1 Urgent need of large scale refreshable Braille display device

Vision impairment greatly limits a person's ability to communicate, receive education, and travel to new locations. According to the World Health Organization, there are an estimated 285 million people worldwide who are vision-impaired, including 39 million blind people and 1.4 million blind children (15 and under).[126,127] Based on data in early 1990s and 2000s, in the United States, the figures are 19 million vision-impaired,[128] 1.3 million who are legally blind, and about 53,600 children and adolescents.[126] Braille has been the only means to teach blind children literacy. There has been a decline in literacy for blind children in the US: in 1960, 50% of blind children read Braille, as of 2009, the number has dropped to only 10%.[129] This declining literacy rate is caused by the rapid advancement of audio devices, which cannot teach literacy, whereas most Braille devices, such as Braille paper, use century-old technologies. Graphics and math equations, two powerful tools for education and communication, have been extremely difficult to teach to blind children. 75 times more paper have to be used to fully illustrate a mathematics book in Braille, compared to a Braille novel. Current resources and technologies are limited to teach these effectively to vision impaired students. There is an urgent need to employ modern electronic technologies and develop low cost analogous devices to assist learning and communication for blind people.

4.1.2 Current technologies and their limitations

Other than the old-fashion Braille books embossed on paper and text-to-speech audio devices, Focus 14/40/80 (previous Braille Lite M20/M40 series) made by Freedom Scientific is one of the widely used refreshable Braille display product on the market.[130] It is based on individual electromechanical cells made from piezoelectric ceramic bimorph actuator arrays. Figure 4-1 shows a Braille Lite device capable of showing one line of 40 characters. Drawbacks of this product include size, weight, and cost. The ceramic bimorphs in the actuators are so long and heavy that only up to 2 lines of the actuators can be integrated. Also due to the high fabrication cost, a Braille Lite with 40 characters will cost more than $5,000 to purchase which is not affordable for common users. Lacking a revolutionary actuation technology, there are no portable electronic devices that can display more than two lines of refreshable Braille characters or graphics with a reasonable size and cost.

Figure 4-1. Braille Lite M40, a refreshable Braille display capable of displaying one line of text (*Left*) and the transducers (8 piezoelectric bimorphs) under a Braille cell (*Right*).

4.1.3 Advantages of BSEP

BSEP can provide large, bistable rigid-to-rigid deformations. It is well suited for refreshable Braille display in a thin film form factor. BSEP thin film stacked with patterned carbon black powder electrodes and a few other polymer laminates can be actuated into an array of raised dots.

The deformation is stable until the display is refreshed with heat. No bulky bimorphs or other appending structures are needed, other than the polymer laminates, to form the Braille dots. The bistability also provides a way to reduce the energy consumption .

4.2 Prototyping and characterization

Structures of the prototyped refreshable Braille device and the characterization setup are illustrated in Figure 4-2. Each Braille dot has a diameter of 1.5mm, and will rise nominally 0.5mm when fully actuated. In our design one refreshable Braille dot consists of an actuator unit and a heater unit. To test the electromechanical and bistable performance, a characterization unit can be attached additionally. The actuator unit is made of polymer laminates of BSEP thin film, constraint polymer layer, and compliant electrodes (not shown in the figure). BSEP in the active area defined by the constraint polymers is patterned with carbon black powder or single wall carbon nanotube (SWNT) compliant electrodes.[35] With the existence of constraint layers, the boundary condition of the electroactive polymer changes from a free boundary to a confined boundary. The strain will be buckling up instead of expanding in area. Ni/Cr alloy was sputtered with a Denton Discovery 550 sputter to coat on a dicyclopentadiene substrate as Joule heating element. After fabrication, the actuator and heater units are laminated together with a heat resistant foam tape. Characterization setup for the refreshable Braille dots includes a laser displacement sensor (Acuity AR 200-6, Schmitt Industries, Inc., OR), a K-type thermocouple, a Keithley 2000 digital multimeter, and NI USB-6009 and USB-9219 DAQ system. High driving voltage is supplied by a Trek Model 10/10B-HS amplifier and Joule heating power is supplied by an adjustable DC power source.

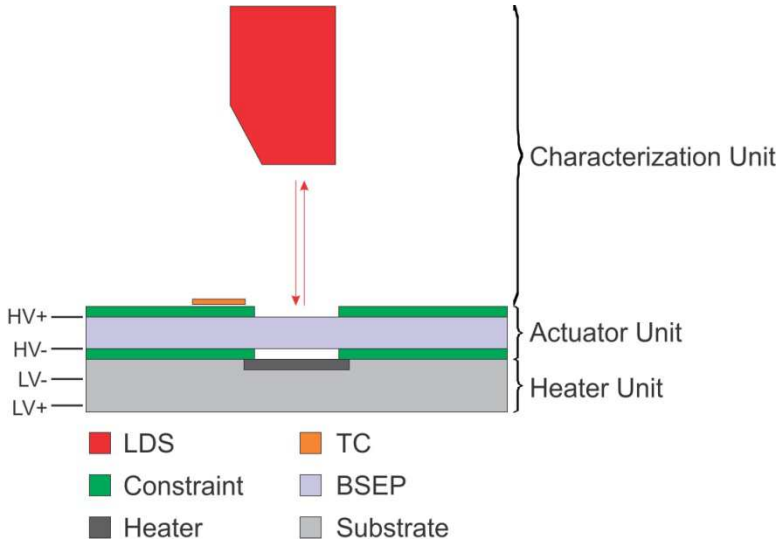

Figure 4-2. Device structure and characterization. For illustration only and scale is not accurate.

4.3 Actuator unit

Rigid-to-rigid actuated deformation of a typical diaphragm is displayed in Figure 4-3 during a bistable actuation cycle.[122] Starting with the BSEP membrane at room temperature and OFF state, the diaphragm has a rigid flat surface. It is heated up by the incorporated heater for 10 s. Then the actuation voltage is turned on and the heater is turned off. The device is allowed to cool down for 10 s and then the actuation voltage is removed. The out-of-plane displacement (raised Braille dot height) with the actuation voltage ON reaches a peak height of 0.594 mm and decreases to 0.577mm after removal of actuation voltage. The corresponding strain fixity is 97%. The raised dot height decreases to 0.005 mm when the device is heated up again. The out-of-plain strain recovery is 99%.

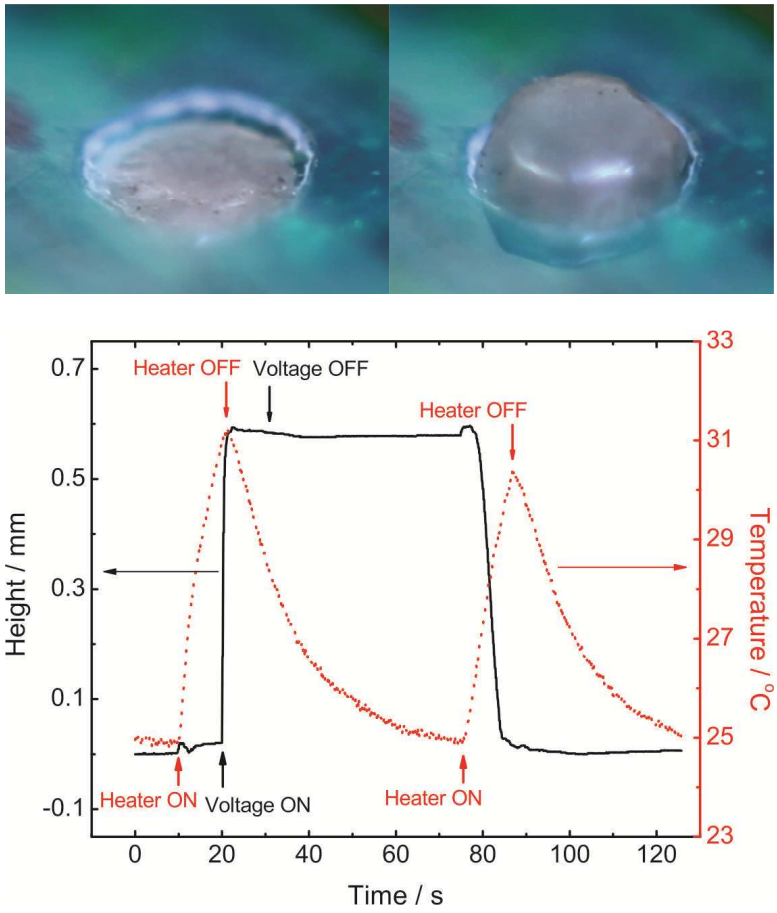

Figure 4-3. (a) Braille 1 dot; (b) Raised height and temperature of a Braille dot as a function of time during a bistable actuation cycle. 100MV/m

Figure 4-4(a) shows ten actuation cycles of actuation after 1,000 cycles of actuation during a prolonged continuous actuation cycle test at 0.1Hz frequency at 70 °C. The vertical displacement around 0.6 mm is stable and repeatable. In a longer driving run, the raised dot height increases from 0.594 mm to 0.669 mm in the first 150 cycles (Figure 4-4(b)). This increase is believed to be due to a break-in effect, a phenomenon commonly observed in rubbery elastomers, e.g. a rubber balloon is difficult to blow up for the first time and becomes much easier in subsequent attempts. After the peak height was reached the height is observed to decrease gradually, reaching 0.340 mm after 4,000 cycles of actuation.

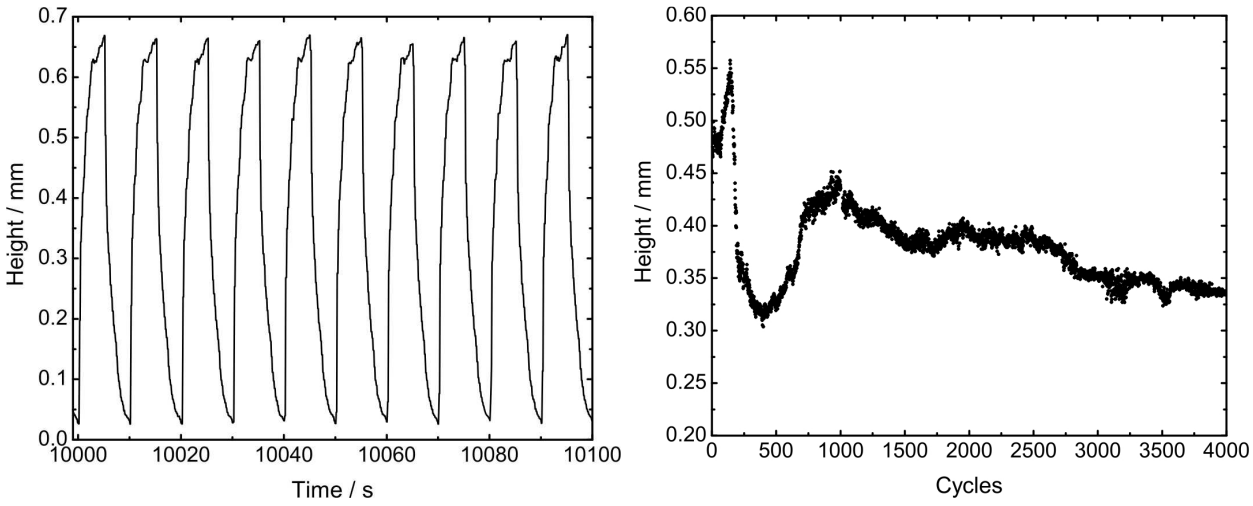

Figure 4-4. (*Left*) Raised height of a Braille dot during 1001st-1010th cycles during a repeated actuation cycle test at 70°C; (*Right*) Raised height of a Braille dot with the number of actuation cycles during the cycle test.

The capability of the Braille dots in supporting pressing forces at the tip of the dome force is shown in Figure 4-5 where the raised height of a Braille dot at the ON state is plotted with the force applied. The active PTBA-IPN-50 membrane has a calculated thickness of 28 μm at the ON state. To lower the height by 0.1 mm, the force applied is 24 grams, which is higher than the suggested force support of >10-15 g for Braille applications.[131] In separate experiments to measure the bistability of the actuation, raised Braille dots were left at ON state for 3 months in ambient condition without any external voltage or stress bias. No height change was observed.

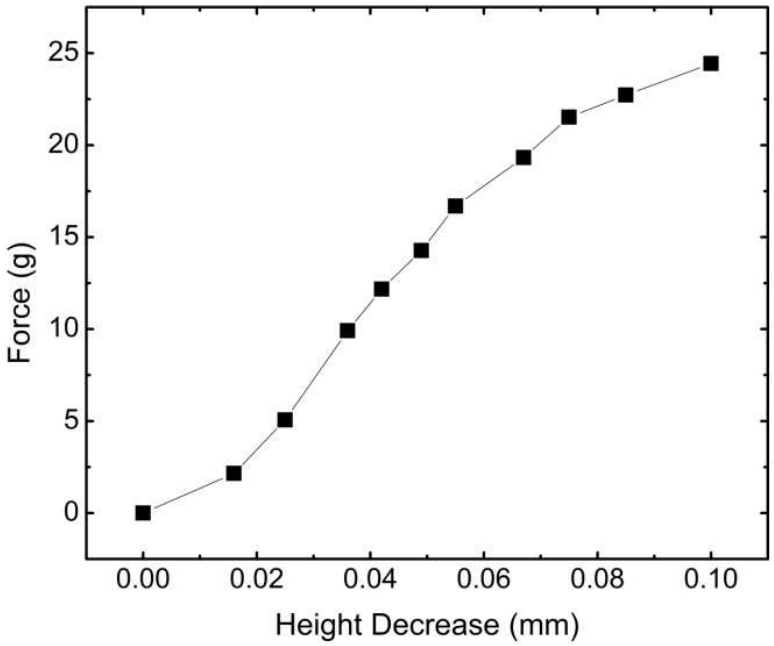

Figure 4-5. Supported force of a Braille dot actuator at the ON state as a function of the amount of height reduced as a result of the applied force.

4.4 Heater unit

The actuation of the BSEP material at its rubbery state is fast (normally less than 5s). The response speed of the whole device is greatly determined by the layout, efficiency, and operation time of the heater unit. Under a fixed heater layout (uniform heating pad) and a constant driving power (close to 150 mW), Figure 4-6 and Figure 4-7 showed some preliminary relationships between the actuation height and the heating and cooling time. The device is first heated up for t_h seconds. A constant high driving voltage is applied and heating is turned off, cooling for t_c seconds, and then the driving voltage is removed. After a 30s hold, the heating voltage is reapplied. The steps are repeated for five times and the height change is recorded.

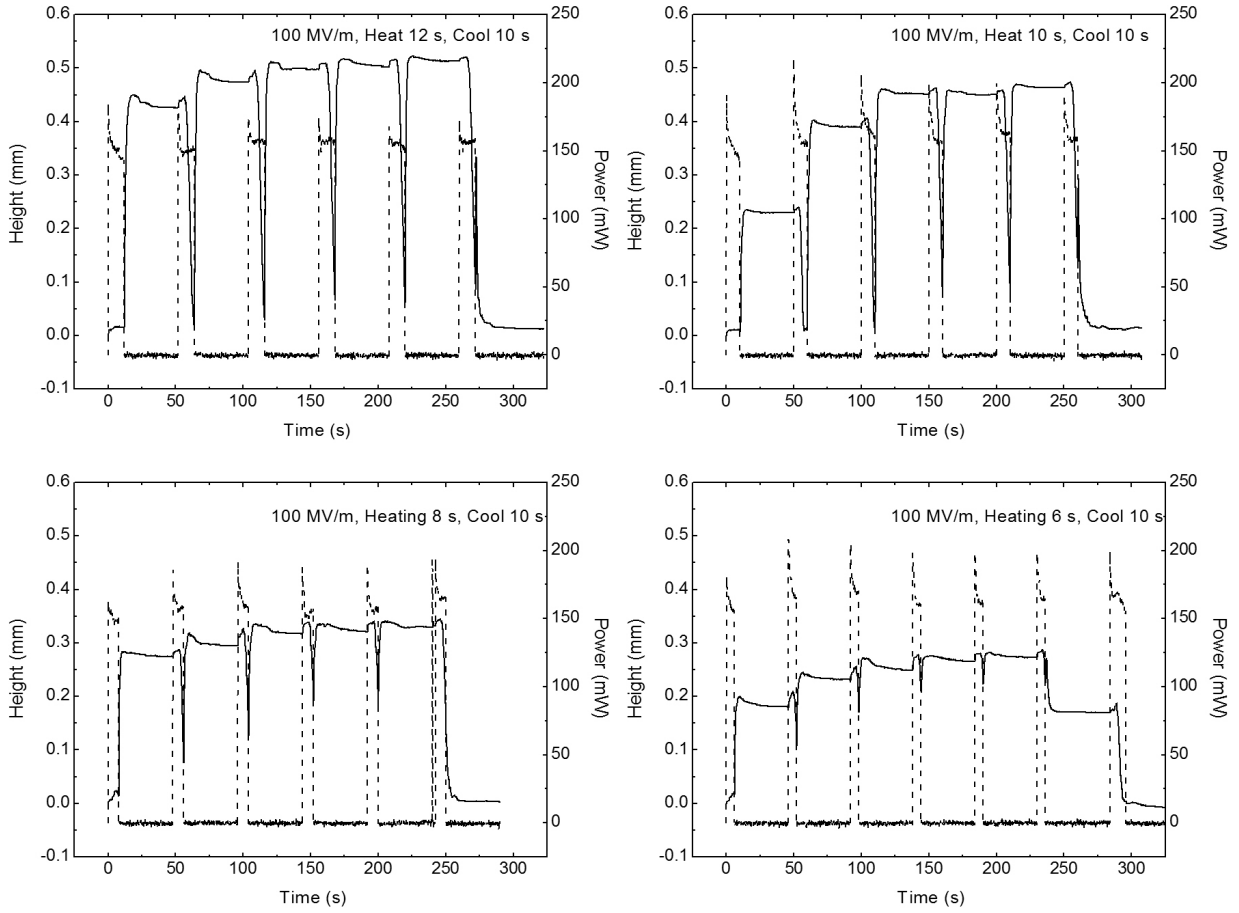

Figure 4-6. Relationship between heating time t_h and actuator vertical displacement.

In Figure 4-6(a) it shows that when t_h = 12 s, the actuator can be driven to a maximum height of 0.5 mm. Along with t_h decreases to 10, 8, and 6 s, the maximum height can be reached decreases to 0.47 mm, 0.33 mm, and 0.28 mm. In the case of t_h = 6 s, the heat generated by the heater unit is not even enough to fully reset the BSEP. A secondary heating has to be applied to reach its original flat shape. The discrepancy in the first two cycles may be due to the local temperature difference at the time when the actuator is driving. The size ratio of heater to actuator is so small that the whole device is very sensitive to temperature fluctuation. A heating time of 12 s or even 10 s would be good enough to drive the actuator to close to the nominal

height of 0.5 mm with the current driving voltage. However, the number can be further reduced if a more efficient heater layout or a higher heating power is used.

Figure 4-7 shows the effect of reducing t_c. In each cycle the height has a slight decrease after the cooling period. This represents the strain fixity due to the shape memory nature of BSEP polymer. 10 s is long enough for the BSEP to cool down to allow only a 0.02 mm height decrease. The residual resilient force can be balanced out by the material rigidity at that temperature. Further deducing tc will bring down the strain fixity, from -0.02 mm in t_c = 10 s, to -0.03 mm in t_c = 7 s, -0.05 mm in t_c = 5 s, and a significant -0.1 mm in t_c = 3s.

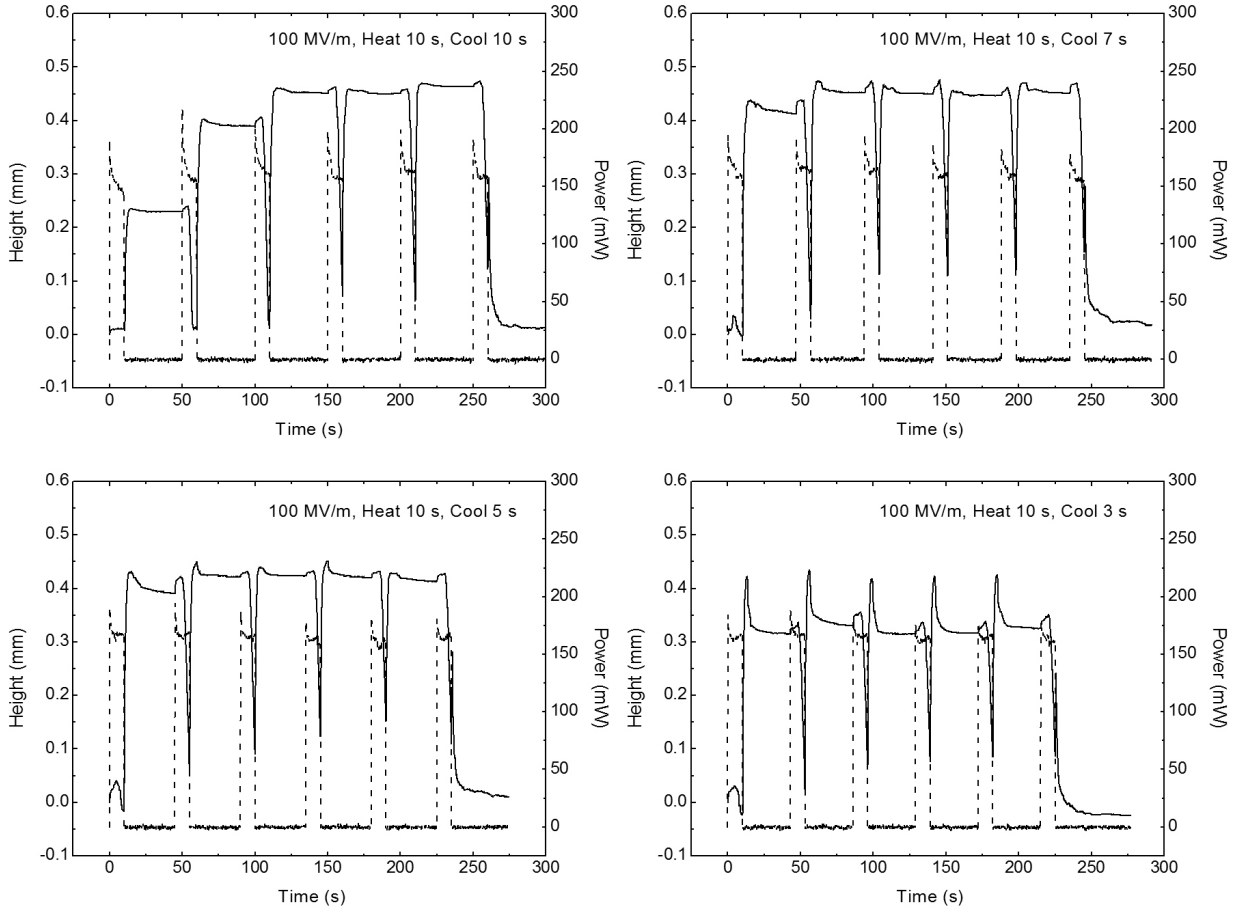

Figure 4-7. Relationship between cooling time t_c and actuator vertical displacement.

4.5 Scaling-up

The ultimate objective of this research is to fabricate a low cost, portable, large scale refreshable Braille electronic reader. The device should have the potential to display graphics and equations as well. A standard Braille character consists of a 3 by 2 Braille dot array, with a diameter of 1.5 mm and a height of 0.5 mm in each dot, and a 2.5 mm center to center distance in adjacent dots. Distance between adjacent cells is 7.5 mm within the same line and is 10.0 mm between two lines. With the dimensions in mind we first designed the 1-cell and 2-cell refreshable Braille devices shown in Figure 4-8. The whole device in total has a size of one square inch to realize the alignment of actuator unit, heater unit, and related wiring. The active layer has a total thickness of 2 mm, mounted on a base of half an inch thickness for pin connectors to the driver interface. A display box was made with all custom-made control circuitry embedded. It is able to apply driving voltage on individual dots and heating up the whole device. High voltage and heating voltage are all from external power sources. All control functionalities are realized by custom-made computer software and the communication is done through the serial port.

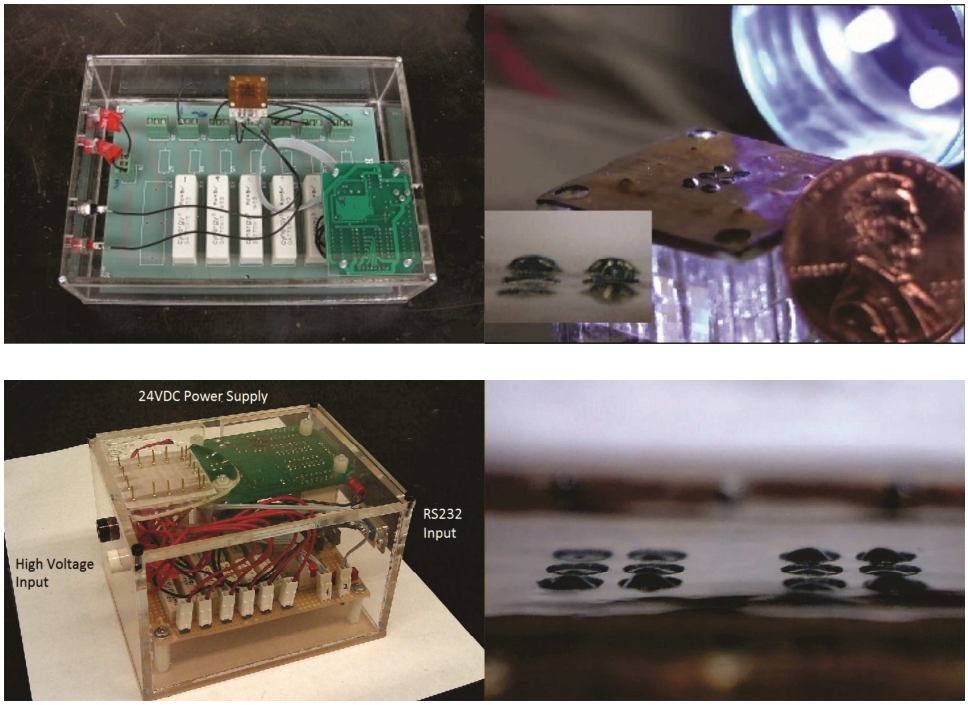

Figure 4-8. (*Up*) 1-cell and (*Down*) 2-cell Braille cell with custom-made control system.

High voltage relays sustaining up to 7kV (Cynergy^3 DAT70510) were used to switch the driving voltage on and off in the 1-cell device. The dimension of such relays are too big for this design to scale up. We fabricated thinner BSEP-IPN films to reduce the driving voltage to below 3kV, and replaced the bulky HV relays with much smaller 5kV relays (Cynergy^3 SAR90505). This design saves more than 75% of the space than the 1-cell device, and had heating power source integrated as well. However, the overall size for the control circuitry is still big. The interference issue between individual dots is very significant due to the high electromagnetic field when high voltages are switched on and off.

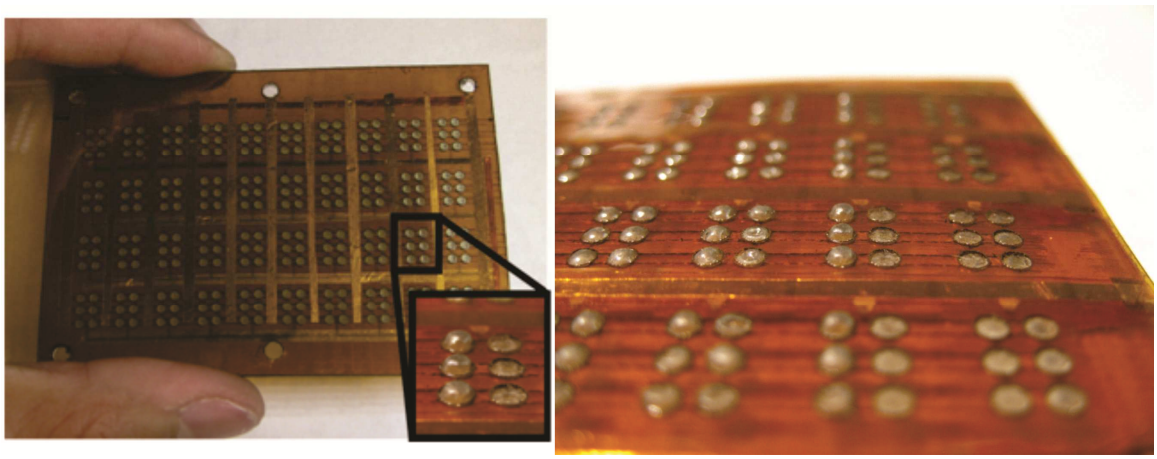

Figure 4-9. Photograph of a refreshable Braille display panel made of PTBA-IPN-50, the blow-up of one cell with 3 left dots raised to display the letter “L”.

In the most recent design we adapted a different control strategy in large size refreshable Braille devices. Instead of high voltage, heating voltage is being controlled on individual dots to provide local heating of BSEP. The high voltage over all dots are applied with one high voltage relay at the same time. Individual control of a matrix of low voltage, high current signals can be realized with standard IC designs. It reduces the size of control circuitry, simplifies the design, and avoided the interference issue. Figure 4-9 shows a smartphone size prototype with part of the dots actuated. The actuator stability is improved by employing reformulated BSEP material processed by precise coating and UV curing method. Further improvement of heater unit stability is still under development.

4.6 Conclusions

The membranes are a suitable electroactive material for the fabrication of smartphone-size refreshable Braille displays which, once commercialized, could profoundly improve the education of blind children and the quality of life of blind adults. The commercialization of the

technique still requires further development of the materials to reduce the glass transition temperature such that actuation can be done at a more comfortable temperature such as 50°C. The devices also require high-voltage active matrix control circuitry which is currently unavailable.

Chapter 5 Silver nanowires as compliant electrodes for actuation and Joule-heating

5.1 Background

Stretchable electronics promise a wide range of devices capable of reproducing the functions of many biological systems, such as artificial eyes, skin, and noses.[132,133] These applications require compliant electrodes that have low mechanical impedance (modulus), low electrical impedance (remain highly conductive even under large stains), and are durable (no degradation of mechanical and electrical properties after numerous deformation cycles). Another promising bio-inspired technology, artificial muscles, particularly dielectric elastomer actuators (DEA) require compliant electrodes that possess rubbery elasticity and maintain high conductivity at strains as large as 100%.[10,37] Shape memory polymers (SMPs) are another category of smart material with large strain actuation. The shape memory operation requires a means of heating which could be performed by resistive Joule heating for control convenience.

For BSEP, which is a combination of DE and SMP, its operation requires a compliant electrode that can support strains greater than 100%, and a Joule heating electrode sustaining similarly high strains.[118] Ideally, a single compliant electrode can cover both high actuation strain and Joule heating. Here, we report the synthesis of a new compliant electrode based on a silver nanowire (AgNW)-polymer composite that meets this requirement.[134] The composite electrodes consist of an ultrathin layer of AgNW buried in the surfaces of poly(*tert*-butyl acrylate-co-acrylic acid) poly(TBA-co-AA) films, a BSEP polymer. The surfaces of the films are highly conductive (R_s: as low as 10 Ω/sq) and remain low (R_s: $10^2 \sim 10^3$ Ω/sq) at strains as high as 140%. The electrodes are also capable of being used for Joule heating; composite films can be actuated up to 68% area strain using Joule heating. The combination of the AgNW composite

electrodes and BSEP materials allows for the demonstration of repeated bistable electrically-induced actuation and relaxation in a thin film architecture.

5.2 Experimental

AgNWs were synthesized by following the process reported in references.[135–137] AgNW dispersed in methanol (2 mg/mL) were drop cast onto a glass substrate, dried and annealed on a hotplate for 30 min at 200 ^{o}C. To make the conductive composites, a monomer solution containing 100 parts of tert-butyl acrylate (Sigma-aldrich), 0.5 parts of SR9035 crosslinker (Sartomer company sample), 0.5 parts of 2,2-dimethoxy-2-phenylacetophenone photo initiator (Sigma-Aldrich), and various amounts of acrylic acid (Sigma-aldrich) was drop cast onto the glass substrate coated with AgNW. A cover glass was placed on top of the monomer solution using spacers to control the film thickness, and the monomer was photo-crosslinked by UV irradiation (power: 100 W, wavelength: 365 nm) for 20 min with a distance of 3 inches from the lamp. The sample was further annealed at 80 ^{o}C for 10 hours before peeling it from the glass substrates. SEM surface and cross-sectional microscopic images of the AgNW composite transferred into PTBA-co-AA were taken by a JEOL JSM-6701F scanning electron microscope. Transmittance spectra of the AgNW composites were collected by a Shimadzu UV-1700 spectrophotometer.

For the Rs profile measurements, the conductive composite was cut into strips 300 mm long and 10 mm wide. 100 nm gold electrodes were sputtered on both ends of the surface of the AgNW composite, leaving only a 1 mm uncovered span in the middle. Conductive copper tape was attached on the sputtered gold to act as the leads. Electrically insulating Kapton tape was used to insulate the sample from the equipment. The sample was loaded into a TA RSA III

dynamic mechanical analyzer (DMA) with sample holders on both ends, leaving only the central non-sputtered area (1 mm long, 10 mm wide). A linear strain signal was applied to test the change in Rs with uniaxial stretching after heating to 80 ^{o}C. The resistance was measured using a Keithley 2000 digital multimeter. The Rs was calculated using the original dimension of the sample (10 mm wide, 1 mm long). To test the R_s profile under cyclic stretching/releasing, the same protocol was used except that a repeated triangular strain signal was used instead of a linear one.

For actuation testing, the AgNW-poly(TBA-co-AA) composite was made into circular diaphragm actuators. A circular top electrode and dog-bone shaped bottom electrode were both transferred using the method described above. A small positive pneumatic pressure (0.1 psi) was applied to the diaphragm to prevent the active area from wrinkling during the actuation test. The deformation of the active area in response to electric field was monitored with a digital camera. Active area strain was calculated from geometric relations.

5.3 Results

The preparation of the composite electrodes is illustrated in Figure 5-1(a). AgNWs with an average diameter of about 60 nm and an average length of about 20 μm were dispersed in methanol and drop cast on a glass substrate. The resulting thin AgNW coating was annealed to form a fused interconnected network.[138] The R_s and optical transparency of the nanowire coating depends on the density of AgNWs (mg per square meter as surface area). Higher AgNW density leads to lower Rs but higher optical loss.

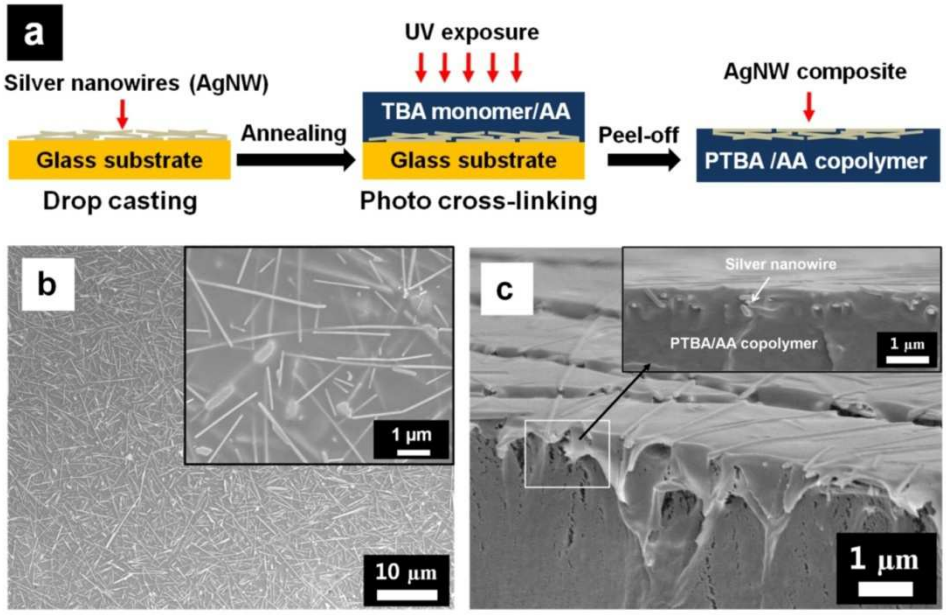

Figure 5-1. Fabrication method and structure of the AgNW/polymer composite electrode material.

The thin AgNW coatings were transferred and embedded inside a copolymer of tert-butyl acrylate (TBA) and acrylic acid (AA) (poly(TBA-co-AA)) by in-situ photopolymerization. This photo-polymerization and transfer process preserves the AgNW network that is interpenetrated within the polymer matrix. Low surface resistance can be obtained at extremely low AgNW loadings. The conductive surface was subjected to repeated adhesion and peeling tests with Scotch tape. No degradation of surface conductivity was observed. Figure 5-1(b) and (c) shows scanning electron microscope (SEM) images of the conductive surface and cross-sections of the AgNW composite electrode. The AgNW network is clearly shown on the surface of the composite that was in contact with glass as well as embedded in the thin layer beneath. At cross-sections, the AgNWs (588 mg/m^2) in the composite are observed as deep as 600 nm in the polymer matrix. The depth varies in the range of 200 to 600 nm depending on the coating density of AgNW on glass (147 to 588 mg/m^2).

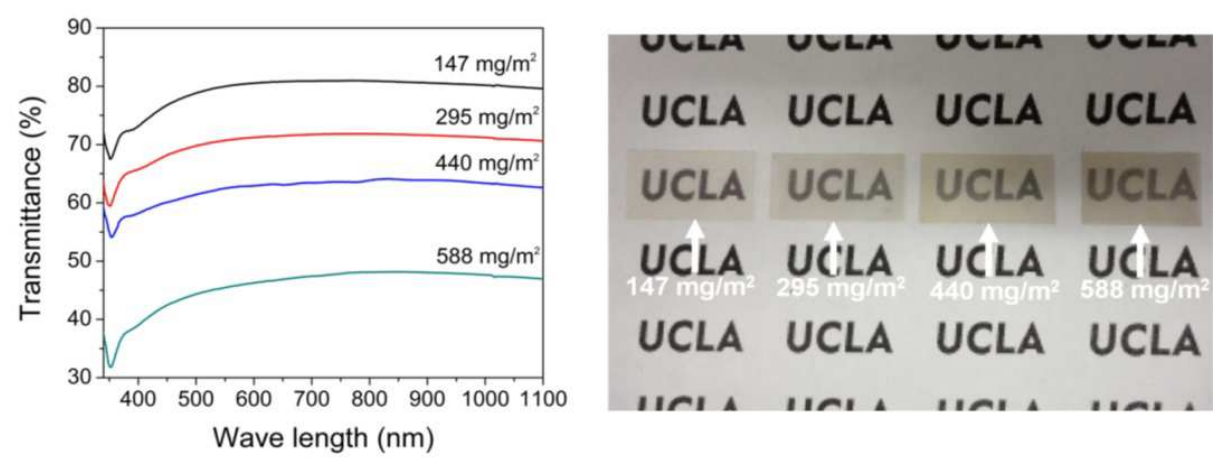

Figure 5-2. Transmittance and general look of AgNW/polymer composite electrodes with different AgNW loadings.

The optical transmittance at 550 nm decreases from 80% at an AgNW loading of 147 mg/m^2 to 45% at 588 mg/m^2 (Figure 5-2). The sheet resistance (R_s) of the conductive surface is typically 10 Ω/sq at 588 mg/m^2 and 88.6 Ω/sq at 147 mg/m^2.

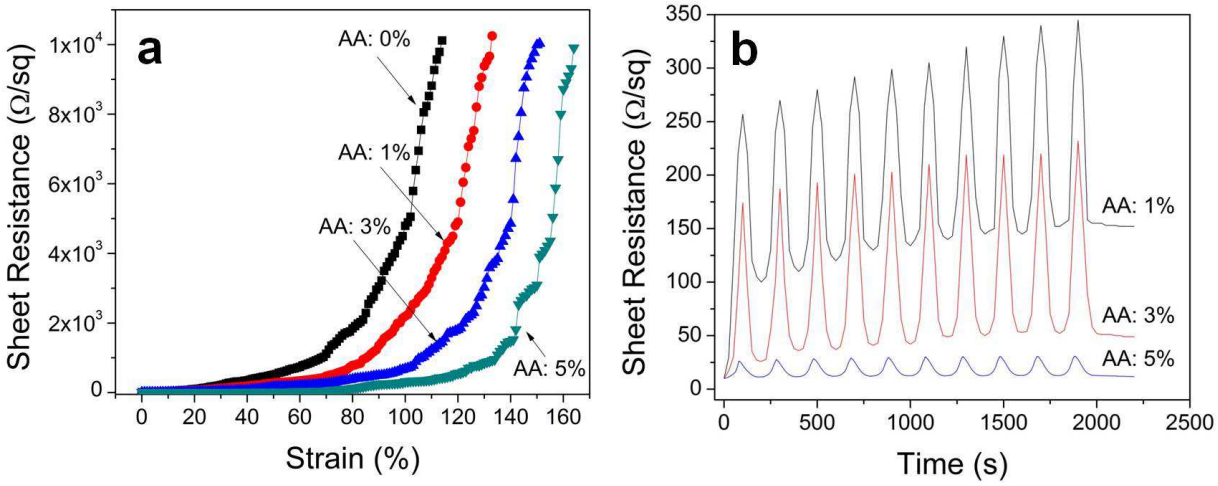

Figure 5-3. Effect of acrylic acid in the composite material to sheet resistance while stretching.

In order to test the stretchability of the conductive composites, samples containing 0 ~ 5% AA were heated to 80 ^{o}C, at which the polymers are sufficiently soft to allow large-strain deformation. The homopolymer of TBA (PTBA) has been shown to be a good shape memory material,[118] but its hydrophobicity leads to poor interface bonding with AgNWs. Addition of AA in the polymer composition can help improve the adhesion between the AgNW network and the polymer matrix. Further increasing the AA content is undesired since it would increase the actuation temperature of BSEP to a prohibitively high value. This would lead to an increase in the power consumption, longer heating and cooling times, and increased discomfort for haptic display devices. The R_s of the composites increases with strain as shown in Figure 5-3(a). The concentration of AA in the matrix plays an important role in the rate of increase of the resistance. At 5% AA, the electrode can be stretched to 160% strain while maintaining an R_s below 10 kΩ/sq. The enhanced stretchability with a small amount of AA is attributed to the increased bonding between the matrix and AgNWs via the carboxylic acid group. This bonding could prevent sliding between the AgNWs and the matrix during expansion and relaxation. The AgNW network thus stretches and relaxes with the elastic matrix.

Figure 2b shows the R_s profile of conductive composites being cyclically stretched and relaxed between 0 and 50% strain at 80 ^{o}C. All samples containing 1 ~ 5% AA maintain an R_s below 350 Ω/sq, thanks to partial anchoring of the AgNW in the elastic matrix. However, the R_s profile is a function of AA content. In the case of 1 % AA, the peak R_s gradually increases with the number of strain-relaxation cycles. The baseline R_s (at 0% strain) also shows an increasing trend. The sample containing 3% AA shows similar trends, but at a slower pace. The sample with 5% AA shows much higher compliancy of electrical conduction. The R_s at 50% strain

increases slightly from 26 Ω/sq in the first cycle to 30 Ω/sq in the tenth cycle. The resistance increase during elongation is mostly restored with R_s increasing from 10 Ω/sq to 11 Ω/sq after 10 cycles. The resistance can be completely restored after the samples are kept in the relaxed state for 1 hour, an indication that the increased baseline resistance is caused by viscoelasticity of the matrix rather than a loss of electrical conduction in the AgNW network.

The density of AgNW coatings transferred into poly(TBA-co-AA) is another important factor to realize better stretchability of the conductive composite. Samples with different AgNW density (147 to 588 mg/m^2) were made using poly(TBA-co-AA) with 5% AA. R_s versus strain curves were measured to evaluate the stretchability of the conductive composites. Higher AgNW density leads to a lower rate of increase of the R_s and higher allowable strain, as large as 160%, as shown in Figure 5-4(a). The enhancement in stretchability might be correlated to an increase of fused interconnections among AgNWs as AgNW density is increased.

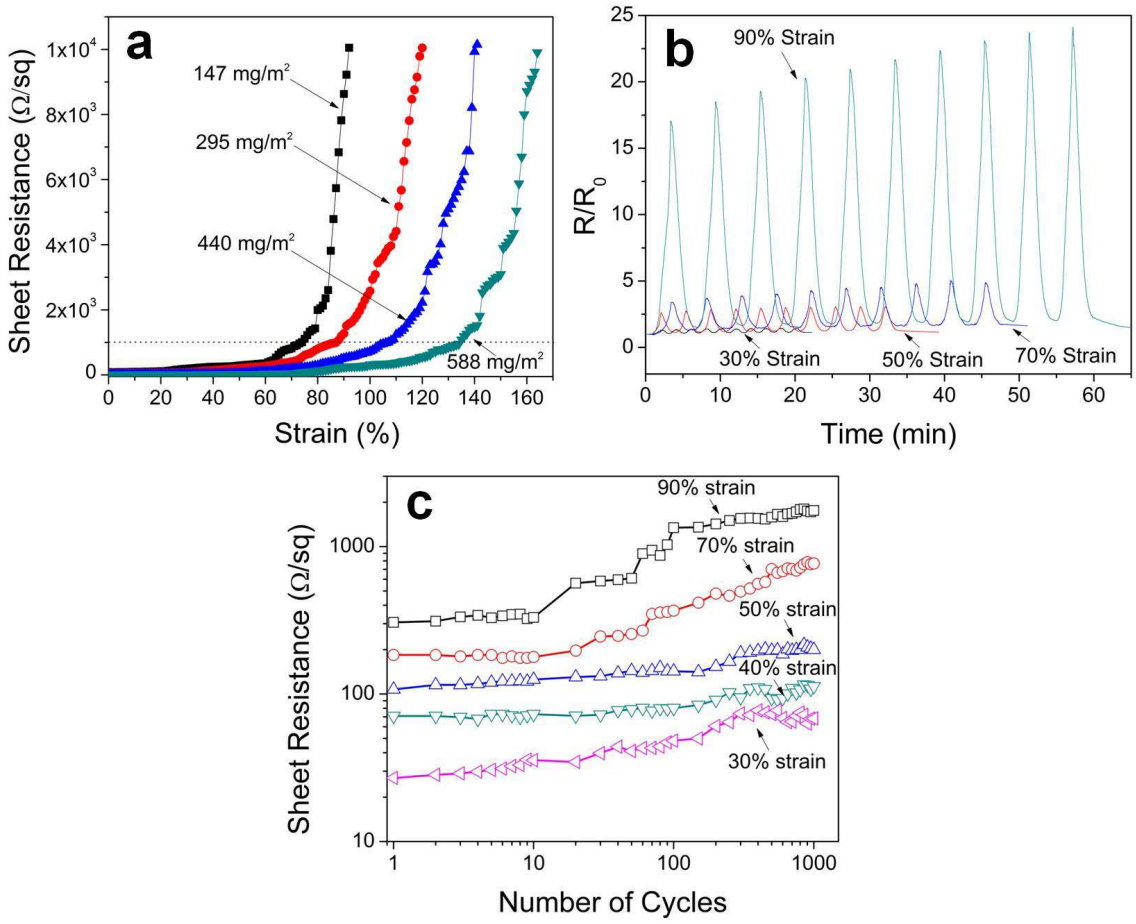

Figure 5-4. Effect of AgNW loading to sheet resistance while stretching.

Figure 5-4(b) shows the resistance change with respect to initial resistance (R/R_0) for conductive composites (AgNW density: 588 mg/m^2) being cyclically stretched to various strain values and released to 0% at 80 ^oC. After 10 loading cycles at 30% peak strain, peak resistance recovery (how much the resistance decreases upon relaxation relative to the peak value) was 98% and the peak-to-baseline resistance change (R_p/R_b) is only 1.3. Even at 70% peak strain, the peak resistance recovery was 95% with Rp/Rb below 5. The R_p/R_b increases with the number of strain cycles in the initial few cycles and then stabilizes. Increasing the amplitude of the peak strain further to 90% decreases the peak resistance recovery to 90% and R_p/R_b to around 25. The R_p/R_b

continues to increase without stabilization which can be correlated with the viscoelasticity of the host polymer matrix.[119,139] However, the composite still maintains a highly conductive network during deformation. The compliance of the conductive composite at large strains is significantly higher than not only other flexible electrodes made from metal nanowires, single walled carbon nanotube and graphene,[135,140–142] but also metal ion implanted electrodes.[73]

Figure 5-4(c) shows R_s profiles of the composite electrode during continuous repetitive cyclic loading with five different levels of peak strain corresponding to 30, 40, 50, 70 and 90%. The Rs of the composite continues to increase with the number of strain cycles and then appears to stabilize. After 5000 cycles, the Rs of the composite is still below 2 kΩ/sq. This value is still low enough so that this composite has the potential to be used as a compliant Joule heating electrode embedded in BSEP materials.

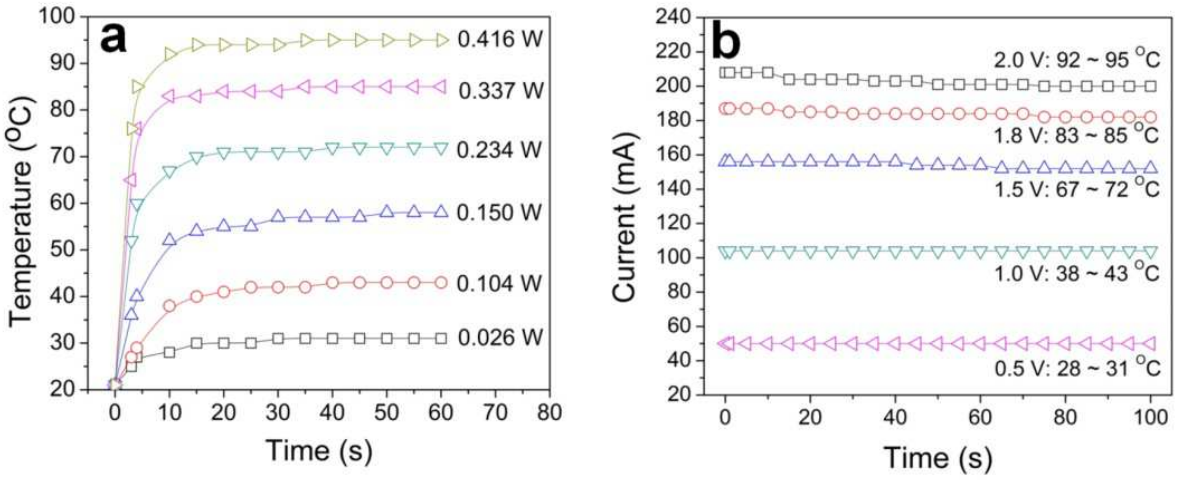

Figure 5-5. Joule heating with AgNW/polymer composite.

The AgNW composites (density of AgNW: 588 mg/m^2) were Joule heated using a DC power supply. Five different levels of electric power, ranging from 26 to 416 mW, were

individually applied to the active area (1 cm^2) of the composite. As shown in Figure 5-5(a) and (b), the temperature on the AgNW composite electrode increases sharply and saturates with time. Under an electric power of 416 mW, a temperature as high as 85 ^oC can be reached in 5 seconds; the temperature then stabilizes to 95 ^oC after an additional 10 seconds without any significant degradation of current on the composite electrode despite an increase in deformation of the softened host polymer. The heating rate and heating response to reach a steady state temperature is faster than a recently developed SWCNT film heater.[143]

Diaphragm actuators were fabricated by using poly(TBA-co-AA) with 5% AA with a thin AgNW coating embedded in both surfaces. Circular electrodes with a diameter of 5 mm were patterned with a single rectangular leads to connect to high voltage on the top and two rectangular leads on the bottom to connect to low voltage and ground. During Joule heating, the BSEP actuator can produce deformation in response to electric fields (10 ~ 45 MV/m) applied between the top and bottom electrodes. However, using this setup the deformation is uneven across the electrode and non-repeatable because the narrow leads result in an increased current density, and therefore increased Joule heating in the central region of the electrode which can easily be damaged due to undesired overheating. To overcome this issue, the Joule heating electrode was redesigned with a dog-bone shape, with larger flared leads leading toward the active electrode area. The design contributes to reducing the undesired excess heating on the circular active area.

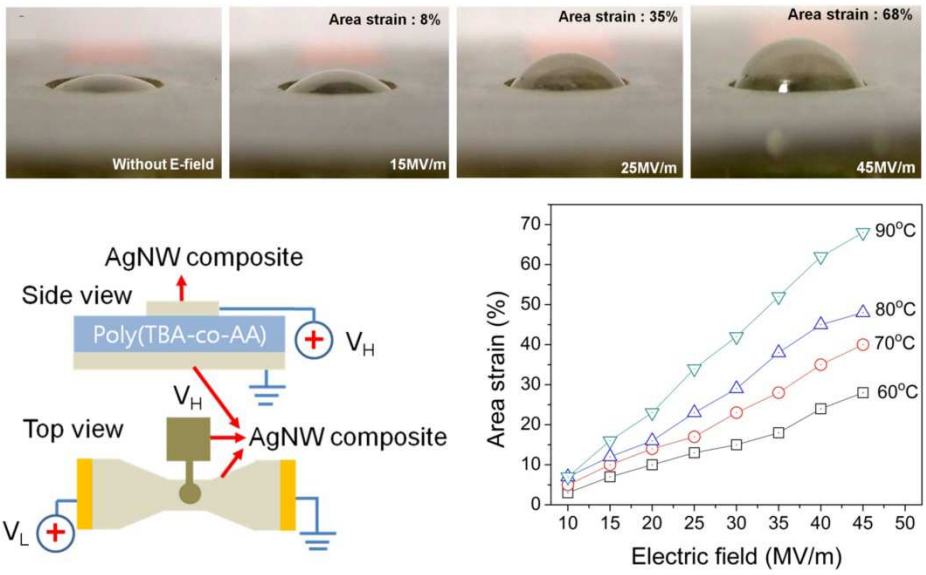

Figure 5-6. AgNW/polymer composite as Joule-heating and actuation electrodes.

Figure 5-6(a) shows photographs of the actuator deformed in response to different electric fields. The actuator produces a deformation with negligible curvature after the onset of Joule heating due to the presence of a small positive pneumatic pressure inside the chamber (very left of Figure 5-6(a)). When actuated in the heated state, the flat circular active area expands thanks to the electroactive nature of the polymer and takes on a convex dome shape. Figure 5-6(b) shows schematic illustration of the BSEP actuator. At each constant Joule heating temperature, a higher electric field leads to larger area strain. At a constant electric field, a higher Joule heating temperature contributes to higher area strain which can reach values as large as 68% at 45 MV/m as shown in Figure 5-6(c).

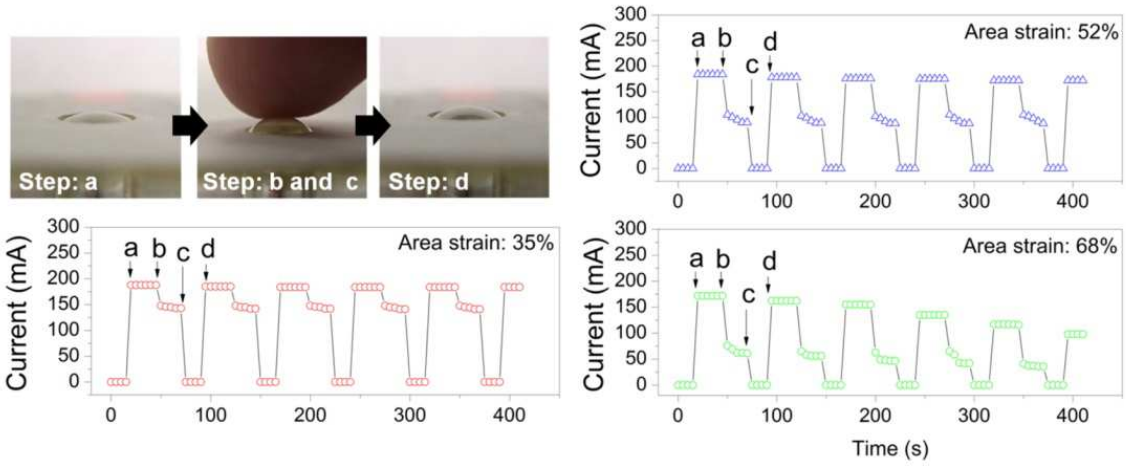

Figure 5-7. Bistable actuation under Joule heating.

The actuated shape of the active area can be locked-in by removing the Joule heating current and cooling the actuator to room temperature; the initial relaxed shape can be fully recovered by reheating the active area (upper left of Figure 5-7). A video file, included in the Supporting Information, demonstrates the shape memory characteristics of the BSEP actuator with AgNW composite electrodes. For durability testing, the current profile of the Joule heating electrode was monitored during 5 repetitive actuations using a two-terminal Keithley multimeter. The results are shown in Figure 5-7. Each actuation cycle was programmed with four steps as specified in the upper left of Figure 5-7. During the repetitive actuations with area strains as large as 52%, there is no significant degradation of the Joule heating current. On the other hand, in the case of 68% area strain, the Joule heating current exhibits a decreasing trend as the number of actuations increases and reduces to as low as 70% of the initial current.

5.4 Conclusions

In conclusion, we have developed a new compliant electrode based on a silver nanowire (AgNW) polymer composite that can be applied to smart materials. Embedding a fused AgNW network within the surface layer of a polymer matrix imparts excellent compliance, stretchability and mechanical robustness against external friction without loss of conductivity. The AgNW composite is highly conductive (R_s: as low as 10 Ω/sq) and remains conductive (R_s: $10^2 \sim 10^3$ Ω/sq) at strains as high as 140%. The composite exhibits acceptably small increases in baseline resistance under repetitive large strains as high as 90% and maintains a high level of conductivity even after 5000 continuous loading cycles with strains ranging from 30% to 90%. The composite can be Joule heated at rates as high as 17 ^{o}C/s. When the composite is employed as compliant electrodes, the BSEP actuator produces repeatable out-of-plane actuation with up to 68% area strain under Joule heating. The combination of the AgNW composite electrodes and BSEP materials allows for the demonstration of repeated bistable electrically-induced actuation and relaxation in a thin film architecture.

Chapter 6 Future Researches

Commercialization of the dielectric actuation technique of polymers requires high performance materials, easy processing steps, and innovative device structures and application ideas. A good start point for designing specific materials for actuation is the UV curable prestrain-free DE and BSEP systems described in the dissertation. However, the structure-property relationship has to be further established in these systems.

6.1 Further study in prestrain-free dielectric elastomers

Besides crosslinkers and plasticizers, there are other additives in the formulation of UV-DE precursors that are of great importance to the structure-property relationship. Photoinitiators with high oxygen resistance can be used to reduce the oxygen inhibition during UV curing. The molecular weight can be further increased and tear strength of the polymer can be increased. Thinner elastomer films can then be fabricated to reduce the driving voltage. Oligomers and monomers are to be further screened to lower the modulus at small strains and quickly stiffens the material above a certain critical strain.

The ability to tame EMI behavior through varying elastomer stiffness opens up an avenue to design new dielectric elastomers. Non-Gaussian networks containing bimodal chain lengths can be tailored to meet this requirement. An example bimodal system can be synthesized by mixing two precursors with distinct molecular weight distributions and crosslinkable functional groups on the chain ends, and crosslinking in stoichiometric proportions. The resulting elastomer would have both high elongation at break and high tensile strength, combining the advantages of short chain networks and long chain networks.

6.2 New BSEP formulations

BSEP can be formulated and UV cured in a similar fashion as the prestrain-free DE, without damaging the strain and stability performance. BSEP at rubbery state is equal to the UV-DE at room temperature, thus the design guideline developed in Chapter 2 should apply. The difference will be in glass transition temperature T_g and crosslink density. Since in random polymerization the overall T_g of the polymer is depending on that of individual components and their mole ratio, an oligomer/monomer combination should be identified to have a proper T_g for bistable actuation. The molecular weight of the oligomer(s) should be controlled to modify the basic mechanical properties of the polymer. Crosslinkers are also to be added into the formulation to adjust the stiffness along with stretching. The fabricated BSEP will have a suppressed electromechanical instability as in the UV-DE, as well as a simple, industrially comparable fabrication process.

6.3 Full-page refreshable Braille display

One of the ultimate goals of the BSEP related study is to achieve a full page size refreshable Braille display device. Currently a smartphone size device has been demonstrated with BSEP-IPN material and a partially individually controlled heater array. With a formulated BSEP material, a tablet size (18 by 18 Braille characters) actuator unit has been made with patterned carbon black powder electrodes. (Figure 6-1) However, a number of issues should be resolved before a successful full page demonstration can be made.

First of all, the efficiency of each heater dot should be improved. Currently it consumes about 150 mW per dot to thermally activate the actuator. This number have to be significant reduced or the overall energy consumption would be too high. Luckily there is still plenty of room to improve the heater efficiency. The heater layout can be designed optimally to reduce

waste of heat on the electrical contact leads. Another possible solution is to incorporate the AgNW composite electrode as the Joule heating electrode, as suggested in Chapter 5. The heater layout also has to be designed accordingly. Secondly, the stability of each heater should be further improved. Heater burn down happens frequently when the heating power is high. Poor adhesion between the heater metal layer and the plastic substrate could be the reason. A more polar heat resistant plastic other than dicyclopentadiene will be chosen as the substrate, to improve the adhesion. Thirdly, a control circuitry has to be designed to control up to 2000 channels of heating current.

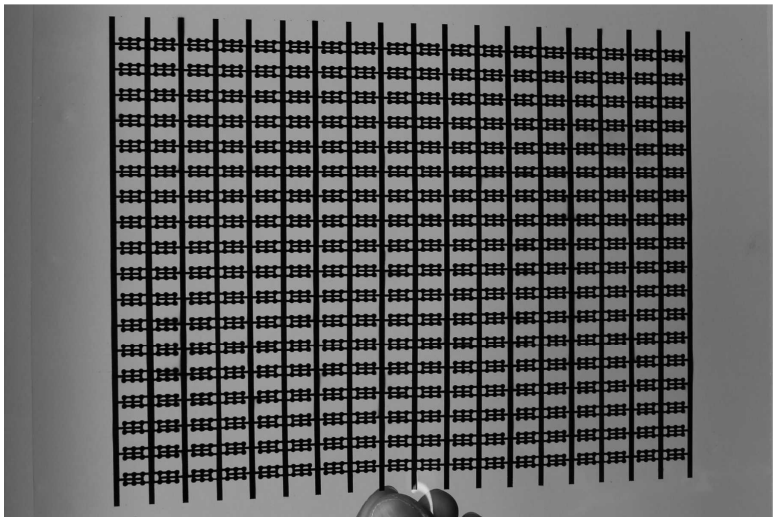

Figure 6-1. Tablet-size Braille cell with custom-made combination control system.

Chapter 7 Conclusions

This dissertation investigates several fundamental issues in the dielectric actuation of polymers, including dielectric material synthesis, processing, choice of compliant electrode, and innovative device fabrication.

A new category of UV curable DE materials (UV-DE) has been synthesized from formulated precursor solutions. The material system can be custom-designed with various thermomechanical and electromechanical properties by using crosslinkers and plasticizers. No prestretching is needed to achieve the peak performance. Electromechanical instability can be suppressed in these materials to provide long and stable actuation. The experimental results are consistent with the thermodynamic model. The stiffening of the elastomers via crosslinking is found critical in optimizing the electromechanical actuation performance. Fabrication of this new material is simplified by using coating techniques and made compatible with industrial production. Multilayer stack actuators were fabricated larger than 10% linear actuation strain.

PTBA is a proof-of-concept BSEP polymer. DBEF plasticizer was added to linear thermoplastic PTBA to reduce the glass transition temperature without damaging its shape memory or electromechanical properties. Internally balanced tension-compression interpenetrating network structure was introduced into via curing of a precursor-swollen chemically crosslinked PTBA network. The IPN system formed after de-swelling exhibits a hyperelastic stress-strain response with rapid rise of stress, which suppressed electromechanical instability, and obtained stable actuation strains larger than 100% at 70°C. The electrically induced strains can be preserved, or “frozen” when the membranes are allowed to cool to ambient temperature, with 97% strain fixity. Other properties such as leakage current and energy density of the BSEP-IPN material were characterized extensively.

The BSEP material was found to be a good candidate for large scale refreshable Braille display application. The literacy of blind children and the quality of life of vision impaired community can be significantly improved with such a device developed successfully. An actuator structure comprising of a BSEP polymer laminate was designed and tested. A separate heater unit was fabricated with a simple layout and coupled with the actuator unit to realize bistable actuation of the device. The actuator was successfully scaled up from one single dot to one Braille character, two units, and a smartphone size prototype.

An AgNW/polymer composite was nominated as a highly conductive, highly stretchable compliant electrode candidate, especially for BSEP applications. Embedding a fused AgNW network within the surface layer of a polymer matrix imparts excellent compliance, stretchability and mechanical robustness against external friction without loss of conductivity. The AgNW composite is highly conductive (R_s: as low as 10 Ω/sq) and remains conductive (R_s: $10^2 \sim 10^3$ Ω/sq) at strains as high as 140%. When used as Joule heating electrode, the material reaches a heating rate as high as 17 ^{o}C/s. The combination of the AgNW composite electrodes and BSEP materials allows for the demonstration of repeated bistable electrically-induced actuation and relaxation in a thin film architecture.

References

[1] D.I. Bower, An Introduction to Polymer Physics, Cambridge University Press, Cambridge, UK, 2002.

[2] S.A. Boggs, J. Ho, T.R. Jow, Overview of laminar dielectric capacitors, IEEE Electrical Insulation Magazine. 26 (2010) 7–13.

[3] H. Sirringhaus, Device physics of solution-processed organic field-effect transistors, Advanced Materials. 17 (2005) 2411–2425.

[4] W. Thue, Electrical Power Cable Engineering, CRC Press, Boca Riton, USA, 2012.

[5] H. Ardebili, M. Pecht, Encapsulation Technologies for Electronic Applications, William Andrew, Burlington, USA, 2009.

[6] R.M. Mcmeeking, C.M. Landis, Electrostatic forces and stored energy for deformable dielectric materials, Journal of Applied Mechanics. 72 (2005) 581–590.

[7] L.D. Landau, E.M. Lifšic, Electrodynamics of Continuous Media: Translated from the Russian by J.B. Sykes and J.S. Bell, Pergamon Press, Oxford, UK, 1963.

[8] R. Pelrine, R. Kornbluh, J. Joseph, Electrostriction of polymer dielectrics with compliant electrodes as a means of actuation, Sensors and Actuators A: Physical. 64 (1998) 77–85.

[9] R. Kornbluh, R. Pelrine, High-field electrostriction of elastomeric polymer dielectrics for actuation, Proceeding of SPIE. 3669 (1999) 146–161.

[10] R. Pelrine, R. Kornbluh, Q. Pei, J. Joseph, High-speed electrically actuated elastomers with strain greater than 100%, Science. 287 (2000) 836–839.

[11] M. Zhenyi, J.I. Scheinbeim, J.W. Lee, B.A. Newman, High field electrostrictive response of polymers, Journal of Polymer Science Part B: Polymer Physics. 32 (1994) 2721–2731.

[12] SABIC Europe, SABIC LDPE 2102TX00 Datasheet, (2010).

[13] R.W. Ogden, Large deformation isotropic elasticity - On the correlation of theory and experiment for incompressible rubberlike solids, Proceedings of the Royal Society of London A: Mathematical and Physical Sciences. 326 (1972) 565–584.

[14] O.H. Yeoh, Characterization of elastic properties of carbon-black-filled rubber vulcanizates, Rubber Chemistry and Technology. 63 (1990) 792–805.

[15] M. Mooney, A theory of large elastic deformation, Journal of Applied Physics. 11 (1940) 582–592.

[16] G. Kofod, Dielectric Elastomer Actuators, The Technical University of Denmark, 2001.

[17] M.T. Wissler, Modeling Dielectric Elastomer Actuators, Swiss Federal Institute of Technology in Zurich, 2007.

[18] M. Wissler, E. Mazza, Modeling of a pre-strained circular actuator made of dielectric elastomers, Sensors and Actuators A: Physical. 120 (2005) 184–192.

[19] M. Wissler, E. Mazza, Modeling and simulation of dielectric elastomer actuators, Smart Materials and Structures. 14 (2005) 1396–1402.

[20] N. Goulbourne, E. Mockensturm, M. Frecker, A nonlinear model for dielectric elastomer membranes, Journal of Applied Mechanics. 72 (2005) 899–906.

[21] X. Zhao, W. Hong, Z. Suo, Electromechanical hysteresis and coexistent states in dielectric elastomers, Physical Review B. 76 (2007) 134113.

[22] X. Zhao, Z. Suo, Electrostriction in elastic dielectrics undergoing large deformation, Journal of Applied Physics. 104 (2008) 123520.

[23] X. Zhao, Z. Suo, Theory of dielectric elastomers capable of giant deformation of actuation, Physical Review Letters. 104 (2010) 178302.

[24] S.J.A. Koh, T. Li, J. Zhou, X. Zhao, W. Hong, J. Zhu, et al., Mechanisms of large actuation strain in dielectric elastomers, Journal of Polymer Science Part B: Polymer Physics. 49 (2011) 504–515.

[25] X. Zhao, Z. Suo, Method to analyze electromechanical stability of dielectric elastomers, Applied Physics Letters. 91 (2007) 061921.

[26] C.C. Foo, S. Cai, S. Jin, A. Koh, S. Bauer, Z. Suo, Model of dissipative dielectric elastomers, Journal of Applied Physics. 111 (2012) 034102.

[27] W. Hong, Modeling viscoelastic dielectrics, Journal of the Mechanics and Physics of Solids. 59 (2011) 637–650.

[28] T.A. Gisby, S.Q. Xie, E.P. Calius, I.A. Anderson, Leakage current as a predictor of failure in dielectric elastomer actuators, (2010) 764211–764213.

[29] L.A. Dissado, J.C. Fothergill, Electrical degradation and breakdown in polymers, Peter Peregrinus, Stevenage, UK, 1992.

[30] F. Carpi, D. De Rossi, R. Kornbluh, R.E. Pelrine, P. Sommer-Larsen, Dielectric Elastomers as Electromechanical Transducers: Fundamentals, Materials, Devices, Models and Applications of an Emerging Electroactive Polymer Technology, Elsevier Science, Amsterdam, The Neitherlands, 2011.

[31] S. Rosset, H. Shea, Flexible and stretchable electrodes for dielectric elastomer actuators, Applied Physics A. 110 (2013) 281–307.

[32] T. Someya, Stretchable Electronics, John Wiley & Sons, Weinheim, Germany, 2012.

[33] S. Wagner, S. Bauer, Materials for stretchable electronics, MRS Bulletin. 37 (2012) 207–213.

[34] W. Yuan, Novel Electrode-Elastomer Combinations for Improved Performance and Application of Dielectric Elastomers, University of California Los Angeles, 2010.

[35] W. Yuan, L. Hu, Z. Yu, T. Lam, J. Biggs, S.M. Ha, et al., Fault-tolerant dielectric elastomer actuators using single-walled carbon nanotube electrodes, Advanced Materials. 20 (2008) 621–625.

[36] C. Keplinger, M. Kaltenbrunner, N. Arnold, S. Bauer, Rontgen's electrode-free elastomer actuators without electromechanical pull-in instability, Proceedings of the National Academy of Science of the United States of America. 107 (2010) 4505–4510.

[37] P. Brochu, Q. Pei, Advances in dielectric elastomers for actuators and artificial muscles., Macromolecular Rapid Communications. 31 (2010) 10–36.

[38] S. Ashley, Artificial muscles, Scientific American. (2003) 53–59.

[39] PolyPower DEAP materials, DanFoss PolyPower A/S. (2012).

[40] M. Blum, M. Büeler, C. Grätzel, M. Aschwanden, Compact optical design solutions using focus tunable lenses, Proceeding of SPIE. 8167 (2011) 81670W.

[41] S.J. Biggs, R.N. Hitchcock, N.M. Ave, Artificial muscle actuators for haptic displays: System design to match the dynamics and tactile sensitivity of the human fingerpad, Proceeding of SPIE. 7642 (2010) 76420I.

[42] Artificial Muscle Inc., ViviTouch Brochure, (2012).

[43] Q. Pei, R. Pelrine, S. Stanford, R. Kornbluh, M. Rosenthal, K. Meijer, et al., Multifunctional electroelastomer rolls and their application for biomimetic walking robots, Proceeding of SPIE. 4698 (2002) 246–253.

[44] G. Kovacs, P. Lochmatter, M. Wissler, An arm wrestling robot driven by dielectric elastomer actuators, Smart Materials and Structures. 16 (2007) S306–S317.

[45] R. Sarban, R.W. Jones, B. Mace, E. Rustighi, Active vibration control of periodic disturbances using a DEAP damper, Proceeding of SPIE. 7642 (2010) 76422Q.

[46] M. Matysek, P. Lotz, K. Flittner, H.F. Schlaak, Vibrotactile display for mobile applications based on dielectric elastomer stack actuators, Proceeding of SPIE. 7642 (2010) 76420D.

[47] P. Lotz, M. Matysek, H.F. Schlaak, Fabrication and application of miniaturized dielectric elastomer stack actuators, IEEE/ASME Transactions on Mechatronics. 16 (2011) 58–66.

[48] M. Matysek, P. Lotz, H.F. Schlaak, Lifetime investigation of dielectric elastomer stack actuators, IEEE Transactions on Dielectrics and Electrical Insulation. 18 (2011) 89–96.

[49] M. Matysek, P. Lotz, H.F. Schlaak, Tactile display with dielectric multilayer elastomer actuators, Proceeding of SPIE. 7287 (2009) 72871D.

[50] S. Lee, K. Jung, J. Koo, S. Lee, H. Choi, J. Jeon, et al., Braille display device using soft actuator, Proceeding of SPIE. 5385 (2004) 368–379.

[51] I.M. Koo, K. Jung, J.C. Koo, J. Nam, Y.K. Lee, H.R. Choi, Development of soft-actuator-based wearable tactile display, IEEE Transactions on Robotics. 24 (2008) 549–558.

[52] T. Levard, P.J. Diglio, S.-G. Lu, C.D. Rahn, Q. Zhang, PVDF core-free actuator for Braille displays: design, fabrication process, and testing, Proceeding of SPIE. 7976 (2011) 797611.

[53] T. Levard, P.J. Diglio, S.-G. Lu, C.D. Rahn, Q. Zhang, Core-free rolled actuators for Braille displays using P(VDF–TrFE–CFE), Smart Materials and Structures. 21 (2012) 012001.

[54] H.-R. Choi, K. Jung, S. Ryew, J.-D. Nam, J. Jeon, J.C. Koo, et al., Biomimetic soft actuator: design, modeling, control, and applications, IEEE/ASME Transactions on Mechatronics. 10 (2005) 581–593.

[55] G. Kofod, W. Wirges, M. Paajanen, S. Bauer, Energy minimization for self-organized structure formation and actuation, Applied Physics Letters. 90 (2007) 81916.

[56] I.A. Anderson, T.A. Gisby, T.G. Mckay, B.M.O. Brien, E.P. Calius, Multi-functional dielectric elastomer artificial muscles for soft and smart machines, Journal of Applied Physics. 041101 (2012) 1–20.

[57] G. Kovacs, L. Düring, S. Michel, G. Terrasi, Stacked dielectric elastomer actuator for tensile force transmission, Sensors and Actuators A: Physical. 155 (2009) 299–307.

[58] J.-S. Plante, S. Dubowsky, Large-scale failure modes of dielectric elastomer actuators, International Journal of Solids and Structures. 43 (2006) 7727–7751.

[59] National Braille Press, Leveraging Braille technology for future generations, (n.d.).

[60] G.-K. Lau, S.C.-K. Goh, L.-L. Shiau, Dielectric elastomer unimorph using flexible electrodes of electrolessly deposited (ELD) silver, Sensors and Actuators A: Physical. 169 (2011) 234–241.

[61] S. Hsien Low, L. Lynn Shiau, G.-K. Lau, Large actuation and high dielectric strength in metallized dielectric elastomer actuators, Applied Physics Letters. 100 (2012) 182901–182904.

[62] G. Kofod, R. Kornbluh, R. Pelrine, P. Sommer-larsen, Actuation response of polyacrylate dielectric elastomers, 4329 (2001) 141–147.

[63] R. Shankar, T.K. Ghosh, R.J. Spontak, Dielectric elastomers as next-generation polymeric actuators, Soft Matter. 3 (2007) 1116–1129.

[64] P.H. Vargantwar, A.E. Özçam, T.K. Ghosh, R.J. Spontak, Prestrain-free dielectric elastomers based on acrylic thermoplastic elastomer gels : A morphological and (electro)mechanical property study, Advanced Functional Materials. 22 (2012) 2100–2113.

[65] M. Kujawski, J. Pearse, E. Smela, PDMS/graphite stretchable electrodes for dielectric elastomer actuators, Proceeding of SPIE. 7642 (2010) 76420R.

[66] T. Lam, H. Tran, W. Yuan, Z. Yu, S. Ha, R. Kaner, et al., Polyaniline nanofibers as a novel electrode material for fault-tolerant dielectric elastomer actuators, Proceeding of SPIE. 6927 (2008) 69270O.

[67] W. Yuan, T. Lam, J. Biggs, L. Hu, Z. Yu, S. Ha, et al., New electrode materials for dielectric elastomer actuators, Proceeding of SPIE. 6524 (2007) 65240N.

[68] W. Yuan, L. Hu, S. Ha, T. Lam, G. Grüner, Q. Pei, Self-clearable carbon nanotube electrodes for improved performance of dielectric elastomer actuators, Proceeding of SPIE. 6927 (2008) 69270P.

[69] W. Yuan, P. Brochu, S.M. Ha, Q. Pei, Dielectric oil coated single-walled carbon nanotube electrodes for stable, large-strain actuation with dielectric elastomers, Sensors and Actuators A: Physical. 155 (2009) 278–284.

[70] H. Stoyanov, P. Brochu, X. Niu, C. Lai, S. Yun, Q. Pei, Long lifetime, fault-tolerant freestanding actuators based on a silicone dielectric elastomer and self-clearing carbon nanotube compliant electrodes, RSC Advances. 3 (2013) 2272–2278.

[71] K. Min, J.Y. Jung, T.H. Han, Y. Park, C. Jung, S.M. Hong, et al., Graphene electrodes for artificial muscles, Molecular Crystals and Liquid Crystals. 539 (2011) 260–265.

[72] S. Rosset, M. Niklaus, P. Dubois, H.R. Shea, Large-stroke dielectric elastomer actuators with ion-implanted electrodes, Journal of Microelectromechanical Systems. 18 (2009) 1300–1308.

[73] S. Rosset, M. Niklaus, P. Dubois, H.R. Shea, Metal ion implantation for the fabrication of stretchable electrodes on elastomers, Advanced Functional Materials. 19 (2009) 470–478.

[74] H.R. Shea, Miniaturized EAPs with compliant electrodes fabricated by ion implantation, Proceeding of SPIE. 7976 (2011) 79760R.

[75] R. Pelrine, R. Kornbluh, J. Joseph, R. Heydt, Q. Pei, S. Chiba, High-field deformation of elastomeric dielectrics for actuators, Materials Science and Engineering: C. 11 (2000) 89–100.

[76] F. Carpi, D. De Rossi, Dielectric elastomer cylindrical actuators: Electromechanical modelling and experimental evaluation, Materials Science and Engineering: C. 24 (2004) 555–562.

[77] G. Kofod, P. Sommer-larsen, Silicone dielectric elastomer actuators: Finite-elasticity model of actuation, Sensors and Actuators A: Physical. 122 (2005) 273–283.

[78] Q.M. Zhang, V. Bharti, X. Zhao, Giant electrostriction and relaxor ferroelectric behavior in electron-irradiated poly(vinylidene fluoride-trifluoroethylene) copolymer, Science. 280 (1998) 2101–2104.

[79] P.H. Vargantwar, T.K. Ghosh, R.J. Spontak, Novel thermoplastic elastomeric gels as high performance actuators with no mechanical pre-strain, Proceeding of SPIE. 7287 (2009) 72871T.

[80] R. Shankar, T.K. Ghosh, R.J. Spontak, Electroactive nanostructured polymers as tunable actuators, Advanced Materials. 19 (2007) 2218–2223.

[81] R. Shankar, T.K. Ghosh, R.J. Spontak, Mechanical and actuation behavior of electroactive nanostructured polymers, Sensors and Actuators A : Physical. 151 (2009) 46–52.

[82] R. Shankar, A.K. Krishnan, T.K. Ghosh, R.J. Spontak, N. Carolina, Triblock copolymer organogels as high-performance dielectric elastomers, Macromolecules. 41 (2008) 6100–6109.

[83] R. Shankar, T.K. Ghosh, R.J. Spontak, Electromechanical response of nanostructured polymer systems with no mechanical pre-strain, Macromolecular Rapid Communications. 28 (2007) 1142–1147.

[84] H. Stoyanov, M. Carthy, M. Kollosche, G. Kofod, Dielectric properties and electric breakdown strength of a subpercolative composite of carbon black in thermoplastic copolymer, Applied Physics A. 94 (2009) 25–27.

[85] H. Stoyanov, M. Kollosche, D.N. McCarthy, G. Kofod, Molecular composites with enhanced energy density for electroactive polymers, Journal of Materials Chemistry. 20 (2010) 7558–7564.

[86] H. Stoyanov, M. Kollosche, S. Risse, D.N. Mccarthy, G. Kofod, Elastic block copolymer nanocomposites with controlled interfacial interactions for artificial muscles with direct voltage control, Soft Matter. 7 (2011) 194–202.

[87] K. Jung, J. Lee, M. Cho, J.C. Koo, J. Nam, Y. Lee, et al., Development of enhanced synthetic elastomer for energy-efficient polymer actuators, Smart Materials and Structures. 16 (2007) S288–S294.

[88] D. Yang, M. Tian, H. Kang, Y. Dong, H. Liu, Y. Yu, et al., New polyester dielectric elastomer with large actuated strain at low electric field, Materials Letters. 76 (2012) 229–232.

[89] C. Keplinger, T. Li, R. Baumgartner, Z. Suo, S. Bauer, Harnessing snap-through instability in soft dielectrics to achieve giant voltage-triggered deformation, Soft Matter. 8 (2012) 285–288.

[90] S. Michel, X.Q. Zhang, M. Wissler, C. Loewe, G. Kovacs, A comparison between silicone and acrylic elastomers as dielectric materials in electroactive polymer actuators, Polymer International. 59 (2010) 391–399.

[91] A.K. Bhowmick, H. Stephens, Handbook of Elastomers, 2nd Ed., Marcel Dekker, New York, USA, 2000.

[92] D.M. Opris, M. Molberg, C. Walder, Y.S. Ko, B. Fischer, F.A. Nueesch, New silicone composites for dielectric elastomer actuator applications in competition with acrylic foil, Advanced Functional Materials. 21 (2011) 3531–3539.

[93] A.G. Bejenariu, L. Yu, A.L. Skov, Low moduli elastomers with low viscous dissipation, Soft Matter. 8 (2012) 3917–3923.

[94] M. Molberg, D. Crespy, P. Rupper, F. Nueesch, J.-A.E. Manson, C. Loewe, et al., High breakdown field dielectric elastomer actuators using encapsulated polyaniline as high dielectric constant filler, Advanced Functional Materials. 20 (2010) 3280–3291.

[95] H. Stoyanov, P. Brochu, X. Niu, E. Della Gaspera, Q. Pei, Dielectric elastomer transducers with enhanced force output and work density, Applied Physics Letters. 100 (2012) 262902.

[96] F. Carpi, D. De Rossi, Improvement of electromechanical actuating performances of a silicone dielectric elastomer by dispersion of titanium dioxide powder, IEEE Transactions on Dielectrics and Electrical Insulation. 12 (2005) 835–843.

[97] S. Risse, B. Kussmaul, H. Krüger, G. Kofod, Synergistic improvement of actuation properties with compatibilized high permittivity filler, Advanced Functional Materials. 22 (2012) 3958–3962.

[98] J.-S. Plante, S. Dubowsky, On the properties of dielectric elastomer actuators and their design implications, Smart Materials and Structures. 16 (2007) S227–S236.

[99] S.M. Ha, W. Yuan, Q. Pei, R. Pelrine, S. Stanford, Interpenetrating polymer networks for high-performance electroelastomer artificial muscles, Advanced Materials. 18 (2006) 887–891.

[100] S.M. Ha, M. Wissler, R. Pelrine, S. Stanford, G. Kovacs, Q. Pei, Characterization of electroelastomers based on interpenetrating polymer networks, Proceeding of SPIE. 6524 (2007) 652408.

[101] S.M. Ha, W. Yuan, Q. Pei, R. Pelrine, S. Stanford, Interpenetrating networks of elastomers exhibiting 300% electrically-induced area strain, Smart Materials and Structures. 16 (2007) S280–S287.

[102] H. Zhang, L. Düring, G. Kovacs, W. Yuan, X. Niu, Q. Pei, Interpenetrating polymer networks based on acrylic elastomers and plasticizers with improved actuation temperature range, Polymer International. 59 (2010) 384–390.

[103] A. Schmidt, A. Bergamini, G. Kovacs, E. Mazza, Mechanical modeling of interpenetrating polymer network reinforced acrylic elastomer, Proceeding of SPIE. 7642 (2010) 76421O.

[104] A. Schmidt, A. Bergamini, C. Jordi, G. Kovacs, E. Mazza, T. Empa, Electro-mechanical modeling of dielectric elastomer transducers with micro-structured electrodes, Proceeding of SPIE. 7976 (2011) 79760L.

[105] A. Schmidt, A. Bergamini, G. Kovacs, E. Mazza, Multiaxial mechanical characterization of interpenetrating polymer network reinforced acrylic elastomer, Experimental Mechanics. 51 (2011) 1421–1433.

[106] X. Niu, H. Stoyanov, W. Hu, R. Leo, P. Brochu, Q. Pei, Synthesizing a new dielectric elastomer exhibiting large actuation strain and suppressed electromechanical instability without prestretching, Journal of Polymer Science Part B: Polymer Physics. 51 (2013) 197–206.

[107] P. Carroy, C. Decker, J.P. Dowling, P. Pappas, B. Monroe, Chemistry & Technology for UV & EB Formulation for Coatings, Inks & Paints: Vol. 2 Prepolymers & Reactive Diluents, 2nd Ed., John Wiley & Sons, Weinheim, Germany, 1997.

[108] Sartomer USA LLC., CN9021 Technical Datasheet, (n.d.).

[109] J. V. Crivello, K. Dietliker, Chemistry & Technology for UV & EB Formulation for Coatings, Inks & Paints: Vol. 3 Photoinitiators for free radical and cationic polymerisation, 2nd ed., SITA, London, UK, 1991.

[110] R. Schwalm, UV Coatings: Basics, Recent Developments and New Applications, Elsevier Science & Technology Books, 2007.

[111] P. Martens, K.S. Anseth, Characterization of hydrogels formed from acrylate modified poly(vinyl alcohol) macromers, Polymer. 41 (2000) 7715–7722.

[112] P.J. Flory, J. John Rehner, Statistical mechanics of cross-linked polymer networks II. Swelling, The Journal of Chemical Physics. 11 (1943) 521–526.

[113] P.J. Flory, Principles of polymer chemistry, Cornell University Press, 1953.

[114] T.L. Smith, Strength of elastorners—a perspective, Polymer Engineering & Science. 17 (1977) 129–143.

[115] M. Rubinstein, S. Panyukov, Nonaffine deformation and elasticity of polymer networks, Macromolecules. 30 (1997) 8036–8044.

[116] M. Rubinstein, S. Panyukov, Elasticity of polymer networks, Macromolecules. 35 (2002) 6670–6686.

[117] G. Wypych, Handbook of Plasticizers, ChemTec Publishing, 2004.

[118] Z. Yu, W. Yuan, P. Brochu, B. Chen, Z. Liu, Q. Pei, Large-strain, rigid-to-rigid deformation of bistable electroactive polymers, Applied Physics Letters. 95 (2009) 192904.

[119] Z. Yu, X. Niu, P. Brochu, W. Yuan, H. Li, B. Chen, et al., Bistable Electroactive Polymers (BSEP): Large-strain actuation of rigid polymers, Proceeding of SPIE. 7642 (2010) 76420C.

[120] X. Niu, P. Brochu, B. Salazar, Q. Pei, Refreshable tactile displays based on bistable electroactive polymer, Proceeding of SPIE. 7976 (2011) 797610.

[121] M.L. Miller, C.E. Rauhut, Crystalline poly(tert-butyl acrylate), Journal of Polymer Science. 38 (1959) 63–72.

[122] X. Niu, X. Yang, P. Brochu, H. Stoyanov, S. Yun, Z. Yu, et al., Bistable large-strain actuation of interpenetrating polymer networks., Advanced Materials. 24 (2012) 6513–6519.

[123] S.T. Kim, H. Finkelmann, Cholesteric liquid single-crystal elastomers (LSCE) obtained by the anisotropic deswelling method, Macromolecular Rapid Communications. 22 (2001) 429–433.

[124] J. Zhou, W. Hong, X. Zhao, Z. Zhang, Z. Suo, Propagation of instability in dielectric elastomers, International Journal of Solids and Structures. 45 (2008) 3739–3750.

[125] C.A. Daniels, Polymers: Structure and Properties, Technomic Publishing Company, 1989.

[126] Lighthouse International, Prevalence of Vision Impairment, (2012).

[127] Visual impairment and blindness, WHO Fact Sheet No. 282. (2012).

[128] M. Lethbridge-Cejku, D. Rose, J. Vickerie, Vital and Health Statistics, Series 10, No. 228: Summary Health Statistics for U.S. Adults: National Health Interview Survey, 2004, 2006.

[129] National Federation of the Blind, The Braille Literacy Crisis in America: Facing the Truth, Reversing the Trend, Empowering the Blind, (n.d.).

[130] Freedom Scientific, Focus Blue Braille Display, (n.d.).

[131] N. Runyan, D. Blazie, EAP actuators aid the quest for the "Holy Braille" of tactile displays, Proceeding of SPIE. 7642 (2010) 764207.

[132] J.A. Rogers, T. Someya, Y. Huang, Materials and mechanics for stretchable electronics, Science. 327 (2010) 1603–1607.

[133] T. Sekitani, T. Someya, Stretchable, large-area organic electronics, Advanced Materials. 22 (2010) 2228–2246.

[134] S. Yun, X. Niu, Z. Yu, W. Hu, P. Brochu, Q. Pei, Compliant silver nanowire-polymer composite electrodes for bistable large strain actuation., Advanced Materials. 24 (2012) 1321–1327.

[135] Z. Yu, Q. Zhang, L. Li, Q. Chen, X. Niu, J. Liu, et al., Highly flexible silver nanowire electrodes for shape-memory polymer light-emitting diodes., Advanced Materials. 23 (2011) 664–668.

[136] L. Hu, H. Kim, J. Lee, P. Peumans, Y. Cui, Scalable coating and properties of transparent, flexible, silver nanowire electrodes, ACS Nano. 4 (2010) 2955–2963.

[137] Y. Sun, B. Gates, B. Mayers, Y. Xia, Crystalline silver nanowires by soft solution processing, Nano Letters. 2 (2002) 165–168.

[138] A.R. Madaria, A. Kumar, F.N. Ishikawa, C. Zhou, Uniform, highly conductive, and patterned transparent films of a percolating silver nanowire network on rigid and flexible substrates using a dry transfer technique, Nano Research. 3 (2010) 564–573.

[139] M.G. Urdaneta, R. Delille, E. Smela, Stretchable electrodes with high conductivity and photo-patternability, Advanced Materials. 19 (2007) 2629–2633.

[140] Z. Yu, X. Niu, Z. Liu, Q. Pei, Intrinsically stretchable polymer light-emitting devices using carbon nanotube-polymer composite electrodes., Advanced Materials. 23 (2011) 3989–3994.

[141] K.S. Kim, Y. Zhao, H. Jang, S.Y. Lee, J.M. Kim, K.S. Kim, et al., Large-scale pattern growth of graphene films for stretchable transparent electrodes, Nature. 457 (2009) 706–710.

[142] V.C. Tung, L.-M. Chen, M.J. Allen, J.K. Wassei, K. Nelson, R.B. Kaner, et al., Low-temperature solution processing of graphene−carbon nanotube hybrid materials for high-performance transparent conductors, Nano Letters. 9 (2009) 1949–1955.

[143] T.J. Kang, T. Kim, S.M. Seo, Y.J. Park, Y.H. Kim, Thickness-dependent thermal resistance of a transparent glass heater with a single-walled carbon nanotube coating, Carbon. 49 (2011) 1087–1093.